Adaptive Control Design with Guaranteed Margins for Nonlinear Plants

by

Jinho Jang

B.S., Seoul National University (2003)
S.M., Massachusetts Institute of Technology (2005)

Submitted to the Department of Mechanical Engineering
in partial fulfillment of the requirements for the degree of

Doctor of Philosophy in Mechanical Engineering

at the

MASSACHUSETTS INSTITUTE OF TECHNOLOGY

February 2009

Author .....
Department of Mechanical Engineering
February, 2009

Certified by .....
Anuradha M. Annaswamy
Senior Research Scientist
Thesis Supervisor

Accepted by .....
David E. Hardt
Professor of Mechanical Engineering
Chairman, Department Committee on Graduate Students

Adaptive Control Design with Guaranteed Margins for Nonlinear Plants

by

Jinho Jang

Submitted to the Department of Mechanical Engineering
on November 18, 2008, in partial fulfillment of the
requirements for the degree of
Doctor of Philosophy in Mechanical Engineering

Abstract

Adaptive control is one of the technologies that improve both performance and safety as controller parameters can be redesigned autonomously in the presence of uncertainties. Considerable research has been accomplished in adaptive control theory for several decades and a solid foundation has been laid out for stability and robustness of adaptive systems. However, a large gap between theory and practice has been an obstacle to transition theoretical results into applications and it still remains. In order to reduce the gap, this thesis presents a unified framework for design and analysis of adaptive control for general nonlinear plants.

An augmented adaptive control architecture is proposed where a nominal controller is designed in the inner-loop with an adaptive controller in the outer-loop. The architecture is completed by addressing three separate problems. The first problem is the design of adaptive control in the presence of input constraints. With a rigorous stability analysis, an algorithm is developed to remove the adverse effects of multi-input magnitude saturation. The second problem is the augmentation of adaptive control with a nominal gain-scheduling controller. Though adaptive controllers have been employed with gain-scheduling to various applications, no formal stability analysis has been developed. In the proposed architecture, adaptive control is combined with gain-scheduling in a specific manner while stability is guaranteed. The third problem is the development of analytic stability margins of the closed-loop plant with the proposed adaptive controller. A time-delay margin is derived using standard Lyapunov stability analysis as an analytic stability margin.

The overall adaptive control architecture as well as the analytically derived margins are validated by a 6-DoF nonlinear flight dynamics based on the NASA X-15 hypersonic aircraft. Simulation results show that the augmented adaptive control is able to stabilize the plant and tracks desired trajectories with uncertainties in the plant while instability cannot be overcome only with the nominal controller. The time-delay margins are validated based on a generic transport model and they are compared with margins obtained from simulations studies. We utilize numerical methods to find less conservative time-delay margins.

Thesis Supervisor: Anuradha M. Annaswamy
Title: Senior Research Scientist

Acknowledgments

I am deeply indebted to my research adviser, Anuradha M. Annaswamy, for her patient guidance and support for this thesis in the form of ideas, financial support, and moral support. She offered me the opportunity to carry out this research in the area that motivated me most. With a busy schedule, she has been always responsive and supportive to my requests, and always provided great ideas about my research. She has read each chapter with great care, often under extreme time pressure and made this thesis possible by her comments.

My sincere appreciation also goes to Eugene Lavretsky, John J. Leonard, and Jonathan P. How for being my thesis committee members and for their research advice, thorough readings, and corrections. I am really grateful for the particular help of Zachary T. Dydek in implementing the nonlinear simulation model of NASA X-15. I am grateful to many of lab colleagues, in particular, Yildiray Yildiz, Travis E. Gibson, and Megumi Matsutani for sharing research ideas. Great thanks need to go to all graduate students and research scientists in Active Adaptive Control Laboratory who gave me helpful feedback on my studies: Jeajeen Choi, Himani Jain, Paul A. Ragaller, Manohar B. Srikanth, Seunghyuck Hong, Chun Yang Ong, and Hanbee Na.

All my love and thanks sincerely goes to families and parents for believing in me and supporting me. They has always encouraged me to try my best and to achieve what I have dreamed. Particularly, I would like to thank my dearest Sunwoo Kim for her love, patience, and understanding from the bottom of my heart. My daughter, Jennifer Jang, gave me luck as well as high motivation to complete my study. And, last but not least, I have to thank God for giving me the second chance to study at MIT. I would not had this special chance without Him, and could not have made without Him.

Contents

1 Introduction **17**

1.1 Motivation 17

1.2 Research Objectives 20

1.3 Research Approach 21

1.4 Organization 23

2 Background **25**

2.1 Adaptive Control: Theory & Applications 25

2.1.1 Adaptive control in Magnitude Saturation 26

2.1.2 Stability Margins in Adaptive control 27

2.2 Gain-scheduling 27

3 Adaptive Control in the Presence of Multi-input Magnitude Saturation **29**

3.1 Problem Statement 30

3.1.1 Plant with Uncertainties 30

3.1.2 Augmentation with Integral Action 30

3.1.3 Multi-input Saturation 31

3.2 Adaptive Controller 33

3.2.1 Nominal Controller and Reference Model Design 33

3.2.2 Adaptive Controller design 34

3.2.3 Proof of Bounded Tracking - Elliptical Saturation 37

3.2.4 Proof of Bounded Tracking - Rectangular Saturation 46

3.3 Simulation 51
3.3.1 Nominal Controller Design 51
3.3.2 Adaptive Controller Design 53
3.3.3 Simulation Results 54
3.4 Summary 59

4 Adaptive Gain-scheduled Controller **61**
4.1 Problem Statement 62
4.1.1 Linear Time-varying System 62
4.1.2 Augmentation with Integral Actions 66
4.2 Adaptive Controller 67
4.2.1 Reference Model and Baseline Controller Design 67
4.2.2 Adaptive Controller Design 68
4.3 Stability Analysis 70
4.4 Simulation 74
4.4.1 Nominal Controller Design 75
4.4.2 Adaptive Controller Design 79
4.4.3 Simulation Results 79
4.5 Summary 83

5 Stability Margins for Adaptive Control in the Presence of Time-delay **87**
5.1 Problem Statement 88
5.2 Adaptive controller 90
5.2.1 Nominal controller and reference model design 90
5.2.2 Adaptive controller design 91
5.3 Delay Margins 92
5.3.1 (1,1) Pade approximation 93
5.3.2 (n,n) Pade approximation 102
5.4 Simulation 103
5.4.1 Delay Margins in the NASA X–15 103

5.4.2 Delay Margins in First Order Plants 107
5.4.3 Time delay and the Pade approximations 113
5.4.4 Delay Margins in a Generic Transport Model (GTM) 117
5.5 Summary 118

6 Summary and Future Work **121**
6.1 Summary 121
6.2 Future Work 123

A NASA X-15 Hypersonic Aircraft **127**
A.1 History 127
A.2 X-15 Flight Dynamics Model 128
A.2.1 Equations of Flight Dynamics 128
A.2.2 Aerodynamic Data 130
A.2.3 Actuators and Sensors 133

B Proofs and Constants **135**
B.1 Proof of Proposition 4.1 135
B.2 Constants for Theorem 5.2 137

List of Figures

1-1 The illustration of the X-43A: A hypersonic and scramjet-powered research aircraft [4]. 19

3-1 Elliptical and rectangular multi-input saturation functions 34

3-2 A schematic of the level set B and the region of attraction A. 40

3-3 The control input, $\bar{u}$, saturated by the rectangular saturation can be decomposed into u_d and $\tilde{u}$. 49

3-4 The block diagram of the reference model and the overall control architecture in nonlinear simulation. 55

3-5 Response of angle of attack, pitch rate, and vertical acceleration of reference (ref), adaptive (ad), and nominal (nom) systems under Λ_1. . 56

3-6 Response of angle of attack, pitch rate and vertical acceleration of reference, adaptive, and nominal systems under Λ_2. 57

3-7 Response of angle of attack, pitch rate, and vertical acceleration of reference, adaptive, and nominal systems under Λ_3. 59

3-8 Control inputs transmitted to the aircraft. 60

4-1 A block diagram of a multi-rate plant. Fast states and slow states are controlled separately. 62

4-2 A schematic of trim points inside the operating envelope in the X_g space. 63

4-3 This figure illustrates the construction of desired states, $X^*(t)$. 64

4-4 Gain-scheduling strategy: linear mapping from online mearsurement of $X_g(t)$ to the offine gain table. 69

4-5 Trim points and commands (h_{cmd}, V_{cmd}) on the $V - h$ space. 76

4-6 Profiles of altitude and velocity commands 77
4-7 Poles of the open-loop plants and the reference models 78
4-8 Velocity and altitude command-following in the presence of the uncertainty, Λ. 80
4-9 State variables of the closed loop systems and the reference model . . 81
4-10 Control surfaces of the closed loop systems and the reference model . 82
4-11 State variables of augmented and non-augmented adaptive control . . 84
4-12 Control surfaces of augmented and non-augmented adaptive control . 85

5-1 Time-delay approximation 89
5-2 Two mutually exclusive cases in the cubic polynomial $f(z)$ 100
5-3 The cubic polynomial, $f(z)$, with $\tau > \tau_m$, $\tau = \tau_m$, and $\tau < \tau_m$. 102
5-4 Analytically guaranteed and simulation-based margins with $\lambda = 0.5$, $\lambda_\alpha = 0.4$, and $\lambda_q = 1$. 106
5-5 Analytically guaranteed and simulation-based margins with $\lambda = 0.5$, $\lambda_\alpha = -0.2$, and $\lambda_q = 1$. 107
5-6 Multipliers 110
5-7 Bounded (left) and unbounded (right) sets of attraction. 111
5-8 The region where $G(e, \tilde{\theta}, \eta) \geq 0$ is shaded in blue. A bounded set of attraction exists when $\tau = 0.081$ (left) but there is no bounded set for $\tau = 0.082$. 112
5-9 The region where $\dot{V}(e, \tilde{\theta}, \eta) \geq 0$ is shaded in blue. A bounded set of attraction exists when $\tau = 0.15$ (left) but there is no bounded set for $\tau = 0.16$. 112
5-10 Phase plot of time-delay and the Pade approximations. 114
5-11 Phase plot of time-delay and $(1, 1)$ Pade approximation ($\tau = 0.15$). . 115
5-12 Control input signal (above) with the delay ($\tau = 0.15$) and the amplitude spectrum of the control input (below) 116
5-13 Planform of the C-5A aircraft [11] 117

A-1 NASA X-15 hypersonic aircraft [3] 128

A-2 The full nonlinear X-15 aircraft model 129
A-3 Planfrom of the X-15 hypersonic aircraft [12]. 131
A-4 Lift and drag coefficients [13]. 132

List of Tables

3.1 Trim conditions and inputs. 52

5.1 Analytic and simulation-based margins for the first order plant when $\gamma = 0.5,\ 1,\ 2,\ 5$ and $\sigma = 0.5$. 113

5.2 Analytic margins with the Pade approximation. departing frequencies, and dominant frequencies in control input 116

5.3 Analytic and simulation-based margins for the short period dynamics of C-5A when $\gamma = 2,\ 3,\ 4,\ 5,\ 10$ and $\sigma = 0.5$. 118

A.1 Nomenclature 129

Chapter 1

Introduction

1.1 Motivation

Control design and analysis for systems with static and dynamic uncertainties, while operating in the presence of environmental disturbances and other unknown factors, present significant challenges. A classical fixed-gain controller can handle plant parameter variations and disturbances to a certain degree. There exists an assortment of fixed control design methodologies and analysis tools for a physical system whose model is properly known. However, mathematical models of physical systems are generically imprecise and quite often simplified. In order to accommodate a larger class of uncertainties and to achieve higher performance, it is necessary to design advanced active control algorithms. This need becomes especially important for safety critical applications whose performance requirements are steeper and more stringent.

Another instance which mandates advanced controllers is in the context of unmanned autonomous flight systems, where the need for accurate performance is emphasized because the human operator is not directly in the control loop and action through remote operators may not be sufficiently swift. Recent years have witnessed a variety of autonomous systems in both civilian and military applications that need to cope with unexpected situations without remote assistance. The application of adaptive control to those systems has been sought after in order to obtain benefits in safety, survivability, and performance as an enabling technology. However, one of

the early attempts at implementations of adaptive approaches in flight control led to an accident [13] which is due to a lack of understanding of adaptive systems and an implementation based on empirical rather than a theoretically validated design. This triggered an extensive investigation of a fundamental adaptive control theory.

Aside from plant uncertainties and safety requirements, most of dynamic systems are generically nonlinear. Unlike linear systems, nonlinear systems possess more complexities, one of which is the possible existence of multiple equilibrium points. In a high performance vehicle such as the X-43A (Figure 1-1), this characteristic becomes more dominant with the vehicle exhibiting different dynamic characteristics over multiple equilibrium points. In addition, the equilibrium points are distributed over a large operating envelope. It is safe to say that while a general method exists for the control of linear plants, no universal method exists for the control of nonlinear plants. Therefore, it is not surprising that the level of success of a given nonlinear control method, which in turn is predicated on certain assumptions, depends on how reasonable the assumptions made are in a given application. In this thesis, the nonlinear control method used is based on gain-scheduling. An adaptive controller is augmented with the gain-scheduling controller, which enables us to handle both uncertainty and nonlinearity concurrently. The augmented adaptive control is, therefore, expected to enhance the tracking performance.

In the application of adaptive control, important issues arise due to constraints on the plant inputs, such as actuator magnitude saturation. While performing aggressive and safety-required missions, input constraints can impair the overall performance of adaptive control and potentially cause instability in the closed-loop system. Particularly, in the presence of uncertainties, the adverse effects of input constraints tend to grow such that instability can occur in closed-loop adaptive systems while adaptation is actively performed on uncertain parameters. This necessitates a formal method to compensate input saturation in adaptive control design and a stability analysis.

While improving the performance in the presence of uncertainties, the augmented adaptive control should also maintain its robustness with respect to perturbations. It is well known that an adaptive system is in the most vulnerable situation when the

Figure 1-1: The illustration of the X-43A: A hypersonic and scramjet-powered research aircraft [4].

adaptation is actively processed. For example, adaptation can cause divergence of the adaptive parameters when disturbances are present. To prevent instability and enhance the robustness of the adaptive control, significant efforts and, hence, principal achievements in the robust adaptive control theory were made in 1980s [27], which include modifications of the adaptive law and persistent excitation of the reference input. Unfortunately, no formal link has been developed between the robust adaptive control theory and its application to a specific problem such as aircraft control. In order to utilize the adaptive control scheme to realistic applications, it is necessary to develop analytical tools to measure and quantify its robustness. Furthermore, effects of design parameters in the adaptive controller on its robustness should be investigated extensively to transition the adaptive control theory to realistic applications. It is therefore highly required to develop analytic margins for adaptive systems to be aware of the level of perturbations that the adaptive systems are guaranteed to be stable.

1.2 Research Objectives

The research objective of this thesis is to provide a unified framework for the design and analysis of adaptive control architectures for nonlinear plants which are susceptible to parametric as well as non-parametric uncertainties, and deliver improved performance. The proposed research will concentrate on control design, stability / robustness analysis, as well as the development of Verification and Validation (V&V) methods, while using high fidelity 6-DoF nonlinear aircraft models. Specific problems that we shall address are:

- *Adaptive control in the presence of multi-input saturation*

  Control of plants with constrained inputs is a theoretically challenging problem and one of paramount practical importance since actuator subject to saturation is ubiquitous in control applications. Constrained actuators can degrade performance and potentially lead to instability if they are not taken into account in control design. In particular, adaptive control technique can destabilize the overall system especially when "adaptation" is carried out on saturation error. As a remedy to prevent instability due to saturation, compensation methods have been introduced and we extend this method to multi-input case where the adaptive control is placed in an augmentation with the nominal controller that includes integral action. The first problem in this thesis is to develop a compensation method for multi-input saturation in adaptive control design.

- *Adaptive control for nonlinear plants via integration of gain-scheduling*

  Significant characteristics of high performance nonlinear plants is that (i) they have multiple equilibrium points over a large operating envelope and (ii) they are generally multi-rate systems whose states have a broad spectrum of convergent or divergent rates. Obviously, characteristics of a nonlinear plant can vary considerably between equilibrium points. To achieve desired performance uniformly across operational envelope, a gain-scheduling controller can be constructed on nominal parameters by employing slow-rate states as gain-scheduling variables

[32, 26]. In order to maintain the performance in the presence of uncertainties, we propose to augment the gain-scheduling controller with an adaptive controller. The second specific problem is to arrive at a set of formal sufficient conditions that guarantee closed-loop stability and uniform performance.

- *Analytical stability margins equivalent to linear concepts*

  Even though adaptive systems have been extensively studied over the past 40 years, their transient performance and robustness properties remain an open problem. What is needed here are theoretically verifiable techniques to analyze and predict sensitivity to various uncertainties for systems with adaptive controllers. Currently, the chief obstacle to transitioning adaptive controllers into safety-critical applications is a lack of formal methods to assess stability / robustness margins with respect to static uncertainties, and unmodeled dynamics, such as time-delays. The third problem dealt in this thesis is to develop formal methods for calculation of stability / robustness margins for nonlinear systems operating with adaptive controllers in the loop. This will contribute to Verification and Validation (V&V) techniques for adaptive systems.

1.3 Research Approach

The approach adopted in this thesis to control a nonlinear plant in the presence of uncertainties is composed of the following three major steps:

The first step is the characterization and modeling of plausible uncertainties in nonlinear plants. Aside from numerous "unknown" uncertainties in reality, "known" uncertainties in such plants include control failures, sensor failures, input saturation, and unmodeled dynamic such as actuator dynamics, structural vibration, time-delay, and so on. They should be modeled and incorporated to the plant in a physical sense to replicate the real ones. In this step, we will form the overall plant model to be controlled in this research.

The second step is the design of the proposed controller. In the design, an adaptive

controller is augmented with a nominal controller. The reason is that there is always some prior information available, and this information can be used such that stability and uniform performance are obtained in the absence of uncertainties. The next component in the proposed architecture is the inclusion of gain-scheduling. In order to accommodate a range of equilibrium points, the nominal controller is designed using gain scheduling. This is accomplished by designing the fixed controller at each equilibrium point, resulting in a family of fixed controllers for an entire operating envelope. The gain scheduling is carried out using slow variables such as the velocity and height of the aircraft. In the outer loop of the nominal controller, the adaptive controller is included to accommodate uncertainties. The structure of the adaptive controller is determined so as to accommodate both parametric and non-parametric uncertainties.

In the third step, stability and robustness analysis of the complete closed-loop controller that consists of the gain-scheduled nominal controller in the inner-loop and the adaptive controller in the outer-loop is carried out. In the presence of both parametric and nonparametric uncertainties, the stability of the closed-loop system is analyzed. Computable measures of robustness margins where stability is guaranteed are also provided in the thesis.

To demonstrate performance of the proposed controller in simulation studies, a 6-DoF nonlinear model of the hypersonic aircraft (NASA X-15) is utilized to demonstrate performance of the proposed controller. To reconstruct the model fully, we will collect aerodynamic design and data from the literature, which will be incorporated into nonlinear flight dynamic equations. For controller design purposes, we will linearize the nonlinear flight dynamics and obtain a family of operating points for which linearized dynamics are defined. Once the controller designed, it will be tested with the nonlinear model. In order to examine performance of the proposed controller extensively, a great deal of uncertainties and unmodeled dynamics will be tested with a set of different free parameters of the adaptive controller. Through simulation and suitable analytical studies, we will quantify the worst uncertainties for a given controller and specified commands.

1.4 Organization

This thesis is divided into six chapters. The contents of chapters are summarized as followed:

- Chapter 1, *Introduction*, motivates the research effort, and introduces the research objectives as well as specific problems delivered. It also describes the research approaches adopted in this thesis.

- Chapter 2, *Background*, discusses previous works dealing with adaptive control theories and applications. In this chapter, the review of gain-scheduling methods and its applications are also stated.

- Chapter 3, *Adaptive Control in the Presence of Multi-input Magnitude Saturation*, discusses a stable method to compensate saturation of multiple inputs in the adaptive control design.

- Chapter 4, *Adaptive Gain-scheduled Controller*, addresses the problem of controlling a nonlinear system in the presence of parametric uncertainties. The proposed adaptive controller includes a nominal controller which is based on gain-scheduling to accommodate dynamic characteristic changes over multiple equilibrium points.

- Chapter 5, *Stability Margins for Adaptive Control in the Presence of Time-delay*, presents an analytical tool to quantify robustness margins of the adaptive controller with guaranteed stability.

- Chapter 6, *Conclusion*, discusses the results and summarizes the thesis work. The topics for future works are proposed based on these conclusions accordingly.

Chapter 2

Background

This chapter presents the theoretical background on adaptive control and explains its applications to dynamic systems. It then reviews the related previous works of adaptive flight control when adaptive control inputs are constrained in magnitude. Literatures on gain-scheduling are also reviewed.

2.1 Adaptive Control: Theory & Applications

One of the main characteristics than generally distinguishes adaptive control from earlier control architectures is that the former monitors the performance of the overall plant and uses the information obtained to update the control law automatically and on-line so as to improve performance. This fundamental idea underlying adaptive control dates back to mid-1950s when flight control was a source of driving force. In 1960s, several adaptive control schemes were developed an they include self-oscillating adaptive system (SOAS), model reference adaptive control (MRAC), and self-turning regulator (STR). The SOAS designed by Honeywell has been tested on the NASA X-15 hypersonic aircraft, resulting in a catastrophic result in November, 1967 [13]. Due to the crash of the test flight, interest in the adaptive control moved to stability analysis and from late 1970s to early 1980s, a systematic theory with guaranteed stability and performance emerged, and this resulted in outgrowth of publications and several books [28, 1, 15, 33, 23, 39] by the mid 1990s. Along with stability analyses,

the robustness of adaptive control was extensively studied in 1980s since nonparametric uncertainties could destabilize adaptive systems [6, 14]. Several robust adaptive control methods were developed to improve the performance of adaptive controllers in the presence of disturbances and unmodeled dynamics [28, 15]. Extensions to nonlinear control methods have been addressed extensively in [36, 22].

Aligned with theoretical achievements, in various engineering applications such as ships, automotive systems, robot manipulators, and power systems, process controls, adaptive control architectures have been utilized and proved to be suited for performance improvement. It is interesting to note that an adaptive controller was designed for a tailless fighter research aircraft, the X-36, and a test flight was carried out in 1998 [41], resulting in satisfactory performance and guaranteed stability.

2.1.1 Adaptive control in Magnitude Saturation

Adaptive control approaches for plants with constrained inputs in magnitude have been developed and introduced in [19, 2, 5, 38, 17, 24]. In [19], Karason and Annaswamy introduced a saturation compensation method for direct-adaptive control and showed that for a single input plant with output feedback, bounded trajectories can be guaranteed for a range of initial conditions whether the open-loop plant is stable or not. Cheng and Wang in [5] reviewed the current methods to compensate magnitude saturation in adaptive control. Most of those methods relied on the assumption that the open-loop plant is stable. Strategies for input saturation in indirect adaptive control were discussed in [38] for open-loop stable plants. In [17], Johnson and Calise developed a method to compensate limitation on the plant inputs when neural network adaptive control is designed. Recently, in [34], these results were extended to the case of a multi-input plant where an elliptical multi-input saturation function is employed. This results showed that boundedness of all signals in the closed-loop system is bounded when initial conditions lie in a compact set. In [24], Lavretsky presented a modification of [19] such that stable adaptation is achieved without hard actuator saturation. Instead of the artificial saturation function where inputs are constrained elliptically, a realistic multi-input saturation function was uti-

lized in [24].

2.1.2 Stability Margins in Adaptive control

Though adaptive systems have been extensively studied over the past three decades as we mentioned above, it should be noted that theoretically justifiable Verification and Validation (V&V) techniques for adaptive systems are absent. Current V&V techniques are subject to the constraint that the underlying control design is linear [10], which is inadequate for adaptive flight control systems. This may be a demanding task because adaptive systems are generically nonlinear. For example, there is no technique to quantify the level of time-delays that adaptive systems can withstand. Similarly, there is no tool to determine how far or close adaptive systems are situated from instability conditions. Absence of analytical technique for stability / robustness margins has been an obstacle to applying adaptive control theory to safety critical applications such as flight control.

2.2 Gain-scheduling

One of the promising methods for nonlinear control design is gain-scheduling [32, 26] which extends design-via-linearization approach to a range of equilibrium points [20]. It has been used in a wide range of applications including flight control [29], chemical process control [30], and wind-turbine control [25] since 1950s. Historically, gain scheduling has been considered as a "practitioner's" technique. It is therefore not surprising that most of the literature in this area, before 1990s, dealt with practical applications. Theoretical approaches to gain scheduling in terms of design, analysis, and implementation has commenced thereafter [35, 18, 31].

The main idea behind the gain-scheduling approach is to decompose the nonlinear control design task into a family of linear control design methods and scheduling this family of linear controllers based on the command signal so as to ensure that the original nonlinear system is suitably controlled. One or more measurable variables, called gain-scheduling variables, are utilized to determine what operating region the

system is currently in and to enable the appropriate linear controller designed for that region. When gain-scheduling variables are slowly varying, stability results of almost time-invariant systems can be called upon to establish the stability of the underlying linear time-varying system and therefore the closed-loop system that involves the original nonlinear system [32, 26]. The attractive feature of gain-scheduling is that it simply uses linear design tools to nonlinear systems so that a diversity of linear design methodologies can be employed. However, there are still several ad-hoc processes in designs and problem formations which are acceptable in simple applications, but troublesome in complicated ones.

The design of gain-scheduled controller can be broadly partitioned into four steps [32]. In the first step, a linear model parametrized by gain-scheduling variables needs to be obtained. The most common method is based on Jacobian linearization on a family of equilibrium points, particularly called trim points in flight control. This generates a family of linearized plants. The second step is to design linear controllers for those linearized plants such that for each frozen value of gain-scheduling variable, the closed-loop system with the corresponding linear controller shows satisfactory performance. Then, the off-line table of controller gains is built based on the gain-scheduling variables. In the third step, the gain-scheduling is executed so that the controller gain is varied based on the current value of the gain-scheduling variables. Historically, an interpolation process has been used to schedule the controller gains. The fourth step is stability analysis and performance test which is subject to simulation studies.

In an aircraft flight control system, the altitude (or dynamic pressure) and Mach number (or velocity) have been used as scheduling variables conventionally, which are slowly varying variables compared to aero-angles and rates [32, 26].

Chapter 3

Adaptive Control in the Presence of Multi-input Magnitude Saturation

This chapter investigates the design of an adaptive controller in the presence of multiple actuator saturation as well as uncertainties. An augmented control architecture is proposed where the adaptive controller is designed in the outer-loop of a fixed PI controller which serves as a baseline control. In order to avoid the adaptive controller parameters to be misleadingly adjusted by the saturation error, we utilize the augmented error method in the adaptive control design that Karason and Annaswamy developed in [19] for SISO systems and provide the stability analysis rigorously. The overall controller is proved to result in semi-global boundedness with respect to the size of saturation limits in the sense that the region of attraction extends to the entire space as the the saturation level decreases. To perform more realistic simulation studies, we reconstruct a nonlinear model of the NASA X-15 hypersonic aircraft based upon aerodynamic data in [13]. Theoretical findings are validated with simulation studies through this model with realistic actuator constraints and failures. Simulation results show that adaptive control stabilizes the closed-loop system and tracks the reference model properly while the nominal controller is unable to overcome instability. Compensation for magnitude saturation is proven to be useful to avoid high

oscillation in the adaptive control inputs due to saturation errors.

3.1 Problem Statement

3.1.1 Plant with Uncertainties

The problem is under consideration is the control of a linear plant of the form

$$\begin{aligned} \dot{x} &= Ax + Bu \\ y &= Cx \end{aligned} \tag{3.1}$$

where $x \in \mathbb{R}^n$ is the state, $u \in \mathbb{R}^m$ is the control input, and $y \in \mathbb{R}^l$ is the output of the plant with $l \leq m$. $A \in \mathbb{R}^{n \times n}$, $B \in \mathbb{R}^{n \times m}$, and $C \in \mathbb{R}^{l \times n}$ are a known system, input, and output matrix respectively. When there exist uncertainties and disturbances in the plant in (3.1), we consider a plant in the form of

$$\begin{aligned} \dot{x} &= A_\lambda x + B\Lambda(u + d) \\ y &= Cx \end{aligned} \tag{3.2}$$

where $A_\lambda \in \mathbb{R}^{n \times n}$ is an unknown system matrix. $\Lambda \in \mathbb{R}^{m \times m}$ is an unknown diagonal matrix which represents actuator anomalies such as uncertainties, loss of control effectiveness, and reversal in the control input. λ_i denotes the ith element of Λ. For the purpose of control design, we assume that the followings hold:

Assumption 3.1. *$(A_\lambda, B\Lambda)$ is controllable.*

Assumption 3.2. *The sign of λ_i, denoted by $sgn(\lambda_i)$, for $i = 1, \cdots, m$ is known.*

3.1.2 Augmentation with Integral Action

The goal of the control design is that the output tracks a given command signal despite the the presence of uncertainties and disturbances. Toward this goal, we

design an inner-loop controller that integrates the output tracking error as

$$\dot{x}_c = B_c(y - r) \tag{3.3}$$

where $x_c \in \mathbb{R}^{n_c}$ is the controller state and $r \in \mathbb{R}^l$ is the command signal such that $\|r\| \leq r_{\max}$ without loss of generality. The plant combined with the inner-loop controller is wriiten as

$$\underbrace{\begin{bmatrix} \dot{x} \\ \dot{x}_c \end{bmatrix}}_{\dot{x}_p} = \underbrace{\begin{bmatrix} A_\lambda & \mathbf{0}_{n\times n_c} \\ B_cC & \mathbf{0}_{n_c\times n_c} \end{bmatrix}}_{A_{p\lambda}} \underbrace{\begin{bmatrix} x \\ x_c \end{bmatrix}}_{x_p} + \underbrace{\begin{bmatrix} B \\ \mathbf{0}_{n_c\times m} \end{bmatrix}}_{B_{p_1}} \Lambda(u+d) + \underbrace{\begin{bmatrix} \mathbf{0}_{n\times l} \\ -B_c \end{bmatrix}}_{B_{p_2}} r \tag{3.4}$$

or equivalently as

$$\dot{x}_p = A_{p\lambda}x_p + B_{p_1}\Lambda(u+d) + B_{p_2}r \tag{3.5}$$

where $x_p \in \mathbb{R}^{n_p}$, $A_{p\lambda} \in \mathbb{R}^{n_p\times n_p}$, $B_{p_1} \in \mathbb{R}^{n_p\times m}$, and $B_{p_2} \in \mathbb{R}^{n_p\times l}$. $\mathbf{0}_{i\times j}$ denotes the $i \times j$ zero matrix. The controllability of the pair (A_λ, B) is not sufficient for that of the pair $(A_{p\lambda}, B_{p_1})$ so that the following assumption is required [7]:

Assumption 3.3.

$$\begin{bmatrix} A & B \\ B_cC & \mathbf{0}_{n_c\times m} \end{bmatrix} \tag{3.6}$$

has full rank n.

3.1.3 Multi-input Saturation

The inputs from actuators to the plant in (3.2) are constrained in magnitude. We, therefore, introduce two multi-dimensional saturation functions: elliptical and rectangular saturation functions.

Definition 3.1. *The function, $E_s(\cdot)$, is an elliptical multi-dimensional saturation function defined by*

$$E_s(u) = \begin{cases} u, & \text{if } \|u\| \leq g_e(u) \\ \bar{u}, & \text{if } \|u\| > g_e(u) \end{cases} \tag{3.7}$$

where $g_e(u)$ *is given by*

$$g_e(u) = \left[\sum_{i=1}^{m} \left(\frac{\hat{e}_i}{u_{i,\max}} \right)^2 \right]^{-1/2},$$

$\hat{e}_i = u/\|u\|$ *denotes the unit vector in the direction of* u, $u_{i,\max}$ *is the saturation limit of the* i*th actuator, and* $\bar{u}$ *is given by*

$$\bar{u} = \hat{e} g(u).$$

Definition 3.2. *The function,* $R_s(\cdot)$*, is an rectangular multi-dimensional saturation function defined by*

$$R_s(u) = \begin{bmatrix} u_{1,\max} sat\left(\dfrac{u_1}{u_{1,\max}} \right) \\ \vdots \\ u_{m,\max} sat\left(\dfrac{u_m}{u_{m,\max}} \right) \end{bmatrix} \tag{3.8}$$

where $sat(\cdot)$ *is given by*

$$sat(x) = \begin{cases} x, & if \quad |x| \leq 1 \\ sgn(x), & if \quad |x| > 1. \end{cases}$$

for $x \in \mathbb{R}$.

Aspects of two saturation functions should be discussed for comparison. In $E_s(u)$, the function $g_e(u)$ returns the magnitude of the projection of u onto the boundary surface of the m-dimensional ellipsoid defined by $\|u\| = g_e(u)$. Hence, it is obvious from (3.1) that $E_s(u)$ preserves the direction of u as shown in Figure 3-1(a). However, $E_s(u)$ brings unnecessary dependency between control inputs which leads to conservative saturation limits and increases computational workload. On the contrary, $R_s(u)$ is simpler, more intuitive and realistic than $E_s(u)$ as it is able to replicate the independent saturation of each control input (Figure 3-1(b)). Despite the advantages in $R_s(u)$, the direction of $R_s(u)$ is not necessarily consistent with that of u, which causes additional complexities in the stability analysis.

As the first step, we study the case where $E_s(u)$ is present in the adaptive control input. We extend the previous results in [34] to the closed-loop stability of a multi-input system with the baseline PI controller. This step, in turn, naturally provides a clue to the stability analysis in the case where $R_s(u)$ is present. As $E_s(u)$ is combined with the plant in (3.5), the overall plant to be controlled is obtained as

$$\dot{x}_p = A_{p\lambda}x_p + B_{p_1}\Lambda\left(E_s(u) + d\right) + B_{p_2}r \tag{3.9}$$

and the main goal is to design the adaptive control which ensures the best possible tracking performance in the presence of uncertainties, disturbances, and actuator anomalies such as multi-input saturation.

3.2 Adaptive Controller

3.2.1 Nominal Controller and Reference Model Design

In order to utilize all prior information for the best possible performance, the proposed adaptive controller is designed in augmentation with a nominal controller. The nominal controller input, u_{nom}, is chosen as

$$u_{nom} = K^\top x_p \tag{3.10}$$

where $K \in \mathbb{R}^{n_p \times m}$ is the nominal feedback gain matrix. This is designed so as to ensure that the controller optimizes the performance when uncertainties and actuator constraints are absent. Thus, the reference model that is desired for the plant to track is generated as

$$\dot{x}_m = A_m x_m + B_m r \tag{3.11}$$

where

$$A_m = A_p + B_{p_1}K^\top, \quad B_m = B_{p_2}, \quad A_p = \begin{bmatrix} A & 0 \\ B_c C & 0 \end{bmatrix}.$$

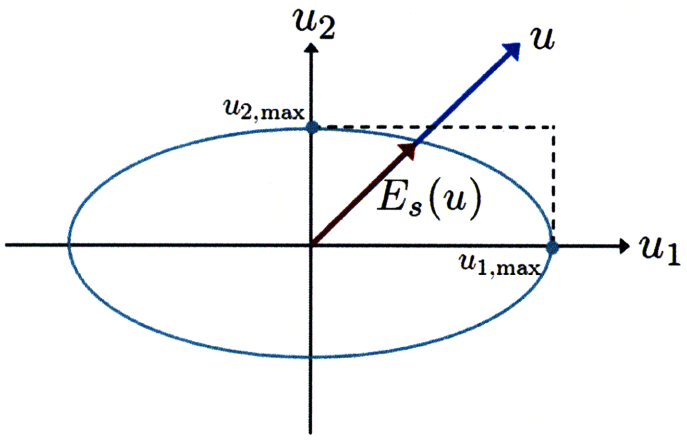

(a) Elliptical Saturation

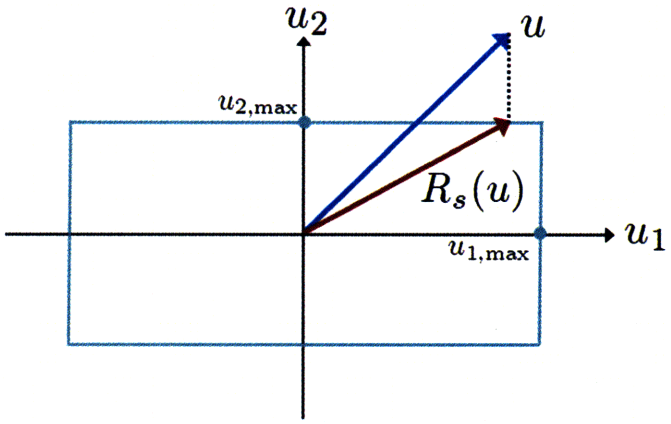

(b) Rectangular Saturation

Figure 3-1: Elliptical and rectangular multi-input saturation functions when inputs are two dimensional.

From the controllability of the pair (A_p, B_{p_1}) and Assumption 3.3, K can be chosen such that A_m is Hurwitz.

3.2.2 Adaptive Controller design

Before we design the adaptive controller for the plant in (3.9), we introduce an additional saturation block for the command signal, r, so that the plant in (3.9) can be written as

$$\dot{x}_p = A_{\lambda p} x_p + B_p \Xi(E_s(\nu) + d_p) \tag{3.12}$$

where

$$B_p = [B_{p_1} \quad B_{p_2}], \quad \Xi = \begin{bmatrix} \Lambda & \mathbf{0}_{m\times l} \\ \mathbf{0}_{l\times m} & I_{l\times l} \end{bmatrix}, \quad \nu = \begin{bmatrix} u \\ r \end{bmatrix}, \quad d_p = \begin{bmatrix} d \\ \mathbf{0}_{l\times 1} \end{bmatrix}.$$

where $I_{l\times l}$ is the l-dimensional identity matrix. Then, $g_e(\nu)$ in (3.1) needs to be written as

$$g_e(\nu) = \left[\sum_{i=1}^{m}\left(\frac{\hat{e}_i}{u_{i,\max}}\right)^2 + \sum_{j=1}^{l}\left(\frac{\hat{e}_{m+j}}{r_{j,\max}}\right)^2\right]^{-1/2}. \tag{3.13}$$

where $\hat{e} = \nu/\|\nu\|$ is the unit vector in the direction of ν and $r_{j,\max}$ is the saturation limit of the jth command signal.

The overall control input in (3.9) consists of the nominal controller in (3.10) and the adaptive controller as

$$u = u_{nom} + u_{ad} \tag{3.14}$$

and u_{ad} is designed as

$$u_{ad} = \theta^\top \omega = \begin{bmatrix} \theta_x^\top & \theta_d^\top \end{bmatrix} \begin{bmatrix} x_p \\ \mathbf{1}_{m\times 1} \end{bmatrix} \tag{3.15}$$

where $\mathbf{1}_{m\times 1}$ is the m-dimensional column vector whose each element is one. The ultimate goal is to achieve that the adaptive parameters, $\theta_x \in \mathbb{R}^{n_p\times m}$ and $\theta_d \in \mathbb{R}^{1\times m}$ are determined such that all signals in the plant in (3.9) is guaranteed to be bounded, and that y tracks r. The deficiency of ν is defined as

$$\Delta\nu = \begin{bmatrix} \Delta u \\ \Delta r \end{bmatrix} = \nu - E_s(\nu) \tag{3.16}$$

or $\Delta\nu = \nu - R_s(\nu)$ when the rectangular saturation is considered. The plant in (3.12) can be rewritten as

$$\dot{x}_p = A_{p\lambda}x_p + B_{p_1}\Lambda(u+d) + B_{p_2}r - B_{p_1}\Lambda\Delta u - B_{p_2}\Delta r. \tag{3.17}$$

The following assumption represents the matched uncertainty conditions which is required only for the stability analysis, not for the design:

Assumption 3.4. *There exists an ideal gain θ^* that results in perfect matching between the reference model in* (3.11) *and the plant in* (3.9) *in the absence of input constraints such that*

$$\begin{aligned} A_{p\lambda} + B_{p_1}\Lambda(\theta_x^* + K)^\top &= A_m \\ \theta_d^{*\top} &= -d. \end{aligned} \tag{3.18}$$

The parameter error is defined to be $\tilde{\theta} = \theta - \theta^*$. Subtracting the reference model from the plant in (3.17), a closed-loop error dynamics equation is obtained as

$$\dot{e} = A_m e + B_{p_1}\Lambda\tilde{\theta}^\top\omega - B_{p_1}\Lambda\Delta u - B_{p_2}\Delta r \tag{3.19}$$

where $e = x_p - x_m$. The error occurs due to two reasons: the uncertainty, Λ, and the input deficiency, $\Delta\nu$, as shown in (3.19). To eliminate the adverse effect of the disturbance $\Delta\nu$, we generate a signal e_Δ as

$$\dot{e}_\Delta = A_m e_\Delta - B_{p_1} diag(\hat{\lambda})\Delta u - B_{p_2}\Delta r \tag{3.20}$$

where $\hat{\lambda} \in \mathbb{R}^m$ is an estimation of diagonal terms of the unknown matrix Λ. The undesirable effects due to control input saturation can be removed from the error dynamics in (3.19) by defining an augmented error, $e_\Delta = e - e_u$. Its dynamics can be determined as

$$\dot{e}_u = A_m e_u + B_{p_1}\Lambda\tilde{\theta}^\top\omega - B_{p_1} diag(\Delta u)\tilde{\lambda} \tag{3.21}$$

where $diag(\tilde{\lambda}) = \Lambda - diag(\hat{\lambda})$. Derivation of (3.21) is based on the fact that $diag(\tilde{\lambda})\Delta u = diag(\Delta u)\tilde{\lambda}$. We now choose the adaptive laws for adjusting parameters, θ and $\hat{\lambda}$, as

$$\dot{\theta} = -\Gamma\omega e_u^\top P B_{p_1} sgn(\Lambda), \quad \dot{\hat{\lambda}} = -\Gamma_\lambda diag(\Delta u) B_{p_1}^\top P e_u \tag{3.22}$$

where $P = P^\top > 0$ is the unique solution of $A_m^\top P + P A_m^\top = -Q$ for a given positive

$Q = Q^\top > 0$. The adaptation rates, $\Gamma > 0$ and $\Gamma_\lambda > 0$, are designed to be diagonal matrices. $sgn(\Lambda)$ is defined to be

$$sgn(\Lambda) = diag(sgn(\lambda_1),\ sgn(\lambda_2), \cdots,\ sgn(\lambda_m)). \tag{3.23}$$

In order to prove boundedness of the closed-loop system with the proposed controller, a Lyapunov candidate function $V(e_u, \tilde{\theta}, \tilde{\lambda})$ is considered as

$$V = e_u^\top P e_u + Trace(\tilde{\theta}^\top \Gamma^{-1} \tilde{\theta} |\Lambda|) + \tilde{\lambda}^\top \Gamma_\lambda^{-1} \tilde{\lambda} \tag{3.24}$$

where $|\Lambda| = sgn(\Lambda)\Lambda$. The time-derivative of the Lyapunov function candidate along the error dynamics in (3.21) and the adaptive laws in (3.22) leads to

$$\dot{V} = -e_u^\top Q e_u \leq 0, \qquad \forall t \geq t_0. \tag{3.25}$$

This implies that e_u, θ, and $\hat{\lambda}$ are uniformly bounded. This result, however, cannot guarantee the boundedness of the tracking error, e.

Remark 3.1. *In* (3.12), *we introduce the additional saturation block for the command signal, r. It is worth noting that the adverse effects due to the command deficiency Δr are completely removed from* (3.21) *by generating e_Δ.*

3.2.3 Proof of Bounded Tracking - Elliptical Saturation

This section and the next one describe the details of stability analysis in the presence of elliptical and rectangular saturation functions respectively. In the stability analysis, the same approach is taken for both cases but differences between two saturation functions arises mainly because the direction of $R_s(u)$ is not consistent with that of u. In this section, we start to analyze the stability of the closed-loop system in the presence of the elliptical saturation.

In order to prove the boundedness of all signals in the closed-loop system, we can

rewrite the plant in (3.12) in the form of

$$\dot{x}_p = A_{\lambda p} x_p + B_p \Xi \left((\Theta_x + \mathbf{K})^\top x_p + \Theta_d^\top + \begin{pmatrix} \mathbf{0}_{m \times l} \\ r \end{pmatrix} - \Delta\nu + d_p \right) \tag{3.26}$$

where

$$\Theta_x = [\theta_x \quad \mathbf{0}_{n \times l}], \qquad \Theta_d = [\theta_d \quad \mathbf{0}_{1 \times l}], \qquad \mathbf{K} = [K \quad \mathbf{0}_{l \times n}]$$

Correspondingly, ideal gains can be written as

$$\Theta_x^* = [\theta_x^* \quad \mathbf{0}_{n \times l}], \qquad \Theta_d^* = [\theta_d^* \quad \mathbf{0}_{1 \times l}]. \tag{3.27}$$

In a similar manner, the parameter error of Θ_x and Θ_d are redefined as

$$\tilde{\Theta}_x = \Theta_x - \Theta_x^*, \qquad \tilde{\Theta}_d = \Theta_d - \Theta_d^*. \tag{3.28}$$

We also define $\Theta_{\max}$ as

$$\Theta_{\max} = \max \left[\sup \left\| \tilde{\Theta}_x^\top \right\|, \quad \sup \left\| \tilde{\Theta}_d^\top \right\| \right]. \tag{3.29}$$

and $\Theta_{\max}$ is finite because θ is proved to be uniformly bounded in 3.25. For efficiency of notation, we define the followings:

$$\begin{aligned}
q_{\min} &= \min(eig(Q)) \\
p_{\min} &= \min(eig(P)), \quad p_{\max} = \max(eig(P)) \\
\rho &= \sqrt{\frac{p_{\max}}{p_{\min}}} \\
\nu_{\min} &= \min_i(\nu_{i,\max}), \quad \nu_{\max} = \max_i(\nu_{i,\max}) \\
\gamma_{\max} &= \max\left[\max(eig(\Gamma)), \quad \max(eig(\Gamma_\lambda))\right] \\
\lambda_{\min} &= \min(eig(|\Lambda|)), \quad d_{\max} = \max(\|d_p\|)
\end{aligned} \tag{3.30}$$

where $\nu_{i,\max}$ is the limit of the ith element of ν and $P_B \in \mathbb{R}$ is defined using the

induced norm by the vector 2-norm such that the property is described by

$$\|x_p^\top P B_p \Xi\| \leq P_B \|x_p\|. \tag{3.31}$$

We also defines following constatns for simplicity:

$$\begin{aligned}
a_0 &= P_B \left(\frac{\nu_{\min} \Theta_{\max}}{\left\| (\Theta_x^* + \mathbf{K})^\top \right\| + \Theta_{\max}} - 2d_{\max} \right) \\
b_0 &= \frac{P_B \Theta_{\max}}{\left\| (\Theta_x^* + \mathbf{K})^\top \right\| + \Theta_{\max}} \\
c_0 &= \left| q_{\min} - 2P_B \left\| (\Theta_x^* + \mathbf{K})^\top \right\| \right| \\
x_{\min} &= \frac{P_B \left(2\nu_{\max} + 3r_{\max} + 3\Theta_{\max} + d_{\max} \right)}{q_{\min} - 3P_B \Theta_{\max}} \\
x_{\max} &= \frac{a_0}{c_0} \\
\Omega_{\max} &= \frac{q_{\min} - P_B \rho \frac{c_0}{a_0} \left(2\nu_{\max} + 3r_{\max} + d_{\max} \right)}{3P_B \left(\rho \frac{c_0}{a_0} + 1 \right)}
\end{aligned} \tag{3.32}$$

Assumption 3.5. *$\nu_{\min}$ is such that $a_0 > 0$.*

Assumption 3.5 implies that there is a constraint imposed on the maximum magnitude of the unknow disturbance, d_p, with respect to the level of saturation. Particularly, Assumption 3.5 implies that

$$d_{\max} < \frac{\nu_{\min} \Theta_{\max}}{2 \left(\left\| (\Theta_x^* + \mathbf{K})^\top \right\| + \Theta_{\max} \right)}. \tag{3.33}$$

This, in turn, indicates that the amount of disturbance which can be tolerated by the proposed adaptive controller can be reduce when the degree of saturation heightens.

Theorem 3.1. *Under Assumptions 3.1, 3.2, 3.3, 3.4, and 3.5, for the system in* (3.12) *with the controller in* (3.14) *and the adaptive law in* (3.22), *$x_p(t)$ has a semi-globally bounded trajectory with respect to the level of saturation for all $t \geq t_0$ if*

(i) $\|x_p(t_0)\| < \dfrac{x_{\max}}{\rho}$

(ii) $\sqrt{V(t_0)} < \Omega_{\max}\sqrt{\dfrac{\lambda_{\min}}{\gamma_{\max}}}$.

Further,

$$\|x_p(t)\| < x_{\max}, \quad \forall t \geq t_0$$

and the error, $e(t)$*, is in the order of*

$$\|e(t)\| = O\left[\sup_{\tau \leq t} \|\Delta\nu(\tau)\|\right].$$

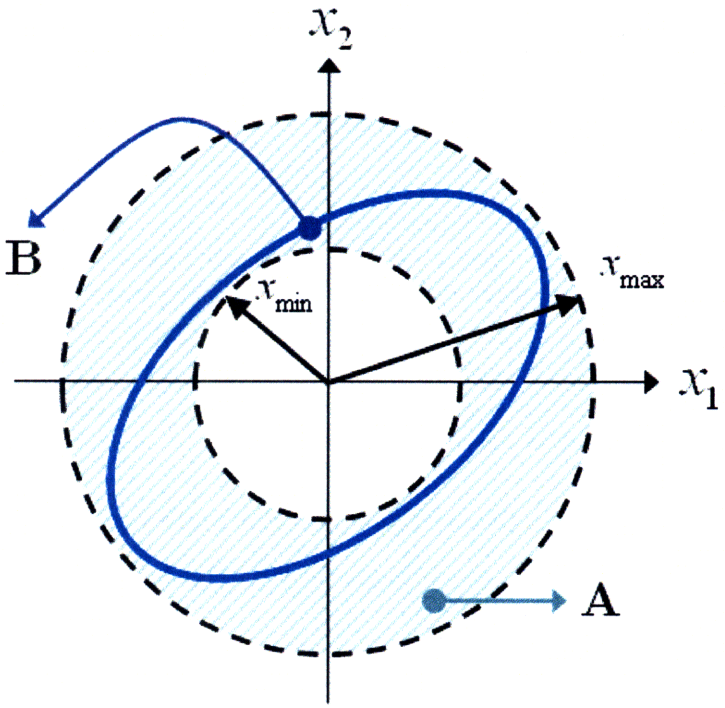

Figure 3-2: A schematic of the level set B and the region of attraction A.

Proof. We choose a positive definite function, $W(x_p)$, as

$$W(x_p) = x_p^\top P x_p \tag{3.34}$$

and define a level set, $\mathbf{B}$, of $W(x_p)$ as

$$\mathbf{B} = \{\ x_p \mid W(x_p) = p_{\min} x_{\max}^2\ \} \tag{3.35}$$

where $x_{\max}$ and $p_{\min}$ are defined in (3.29). We now define an annulus region $\mathbf{A}$ as

$$\mathbf{A} = \{ \, x_p \mid x_{\min} < \|x_p\| < x_{\max} \, \}. \tag{3.36}$$

The proof proceeds in two steps. In the first step, we show that Condition (ii) in Theorem 3.1 implies that $\mathbf{B} \subset \mathbf{A}$. In the second step, we show that $\dot{W}(x_p) < 0, \ \forall x_p \in \mathbf{A}$. Condition (i) in Theorem 3.1 implies that

$$W(x_p(t_0)) < W(\mathbf{B}). \tag{3.37}$$

Therefore, the results of these two steps show that

$$W(x_p(t)) < W(x_p(t_0)), \quad \forall t \geq t_0 \tag{3.38}$$

and Theorem 3.1 follows directly. Figure 3-2 shows a schematic of the level set $\mathbf{B}$ and the region of attraction $\mathbf{A}$ in the two-dimensional space.

Step 1: In this step, we show that $\mathbf{B} \subset \mathbf{A}$. From Condition (ii) in Theorem 3.1, it follows that $\Theta_{\max} < \Omega_{\max}$. Substituting the expression for $\Omega_{\max}$ yields

$$\rho \frac{P_B \left(2\nu_{\max} + 3r_{\max} + 3\Theta_{\max} + d_{\max}\right)}{q_{\min} - 3P_B\Theta_{\max}} < \frac{a_0}{c_0}. \tag{3.39}$$

The inequality in (3.39) with (3.30) directly implies

$$\rho x_{\min} < x_{\max}. \tag{3.40}$$

In (3.34), $W(x_p)$ can be lower-bounded by $p_{\min}\|x_p\|^2 \leq W(x_p)$, which implies from (3.35) that

$$\|x_p\| \leq x_{\max}, \quad \forall x_p \in \mathbf{B}. \tag{3.41}$$

In a similar way, from (3.36), $W(x_p)$ can be upper-bounded by $W(x_p) \leq p_{\max}\|x_p\|^2$. This, in turn, implies from (3.35) and (3.40) that

$$x_{\min} < \frac{1}{\rho}x_{\max} < \|x_p\|, \quad \forall t \geq t_0. \tag{3.42}$$

From the definition of $\mathbf{A}$, we conclude that $\mathbf{B} \subset \mathbf{A}$.

Step 2: We now show that $\dot{W} < 0$, $\forall x_p \in \mathbf{A}$. Two cases are considered which are $\Delta\nu = 0$ and $\Delta\nu \neq 0$.

Case A: $\Delta\nu = 0$

From (3.26)$\sim$(3.28), we obtain

$$\dot{x_p} = A_m x_p + B_p \Xi \left(\tilde{\Theta}_x^\top x_p + \tilde{\Theta}_d^\top + \begin{pmatrix} \mathbf{0}_{m\times 1} \\ r \end{pmatrix} \right) \tag{3.43}$$

which leads to

$$\dot{W} = x_p^\top \left(-Q + 2PB_p \Xi \tilde{\Theta}_x^\top \right) x_p + 2x_p^\top P B_p \Xi \left(\tilde{\Theta}_d^\top + \begin{pmatrix} \mathbf{0}_{m\times 1} \\ r \end{pmatrix} \right). \tag{3.44}$$

By taking bounds on the right-hand side of (3.44), we have

$$\dot{W} < \left(2P_B\Theta_{\max} - q_{\min}\right)\|x_p\|^2 + 2\|x_p\|P_B\left(r_{\max} + \Theta_{\max}\right). \tag{3.45}$$

From Condition (ii) in Theorem 3.1 and the definition of $\Theta_{\max}$, it leads to that

$$\Theta_{\max} < \Omega_{\max} < \frac{q_{\min}}{3P_B}. \tag{3.46}$$

Therefore,

$$\dot{W} < 0, \quad \|x_p\| > \frac{2P_B\left(r_{\max} + \Theta_{\max}\right)}{q_{\min} - 2P_B\Theta_{\max}}. \tag{3.47}$$

The choice of $x_{\min}$ in (3.32) implies that

$$x_{\min} > \frac{2P_B\left(r_{\max} + \Theta_{\max}\right)}{q_{\min} - 2P_B\Theta_{\max}}. \tag{3.48}$$

Hence, it is shown that

$$\dot{W} < 0, \quad \forall x_p \in \mathbf{A} \tag{3.49}$$

in *Case A*.

Case B: $\Delta\nu \neq 0$

Using the matching condition in Assumption 3.4, the plant in (3.12) can be written as

$$\dot{x_p} = A_m x_p - B_p\Xi\left(\Theta_x^* + \mathbf{K}\right)^\top x_p + B_p\Xi\left(\bar{\nu} + d_p\right) \tag{3.50}$$

where $\bar{\nu} = g(\nu)\hat{e}$. The time derivative of $W(x_p)$ along the trajectory of (3.50) is obtained as

$$\dot{W} = -x_p^\top\left(Q - 2PB_p\Xi\left(\Theta_x^* + \mathbf{K}\right)^\top\right)x_p + 2x_p^\top PB_p\Xi\left(\bar{\nu} + d_p\right). \tag{3.51}$$

Two sub-cases are considered.

Sub-case (i): $2x_p^\top PB_p\Xi\bar{\nu} < -\nu_{\min}b_0\|x_p\|$

Using the condition for this sub-case and previously defined bounds, we can bound $\dot{W}$ as

$$\dot{W} < \left|2P_B\right|\left\|\left(\Theta_x^* + \mathbf{K}\right)^\top\right\| - q_{\min}\left|\|x_p\|^2 + \left(2P_B d_{\max} - \nu_{\min}b_0\right)\|x_p\|. \tag{3.52}$$

This implies that

$$\dot{W} < 0, \quad \|x_p\| \leq \frac{a_0}{c_0}. \tag{3.53}$$

From the definition of $x_{\max}$, we can conclude that

$$\dot{W} < 0, \quad \forall x_p \in \mathbf{A} \tag{3.54}$$

in *Sub-case (i)* of *Case B.*

Sub-case (ii): $2x_p^\top PB_p\Xi\bar{\nu} \geq -\nu_{\min}b_0\|x_p\|$

The condition to this sub-case implies that

$$2x_p^\top PB_p\Xi\frac{\nu}{\|\nu\|}\|\bar{\nu}\| + \nu_{\min}b_0\|x_p\| \geq 0. \tag{3.55}$$

Substituting ν with u and r, (3.55) can be represented as

$$2x_p^\top PB_p\Xi\left((\Theta_x + \mathbf{K})^\top x_p + \Theta_d^\top + \begin{pmatrix} \mathbf{0}_{m\times 1} \\ r \end{pmatrix}\right) + \nu_{\min}b_0\|x_p\|\frac{\|\nu\|}{\|\bar{\nu}\|} \geq 0. \tag{3.56}$$

Using $\Theta_x = \tilde{\Theta}_x + \Theta_x^*$, (3.56) becomes as

$$\begin{aligned} &2x_p^\top PB_p\Xi\left(\tilde{\Theta}_x^\top x_p + \Theta_d^\top + \begin{pmatrix} \mathbf{0}_{m\times 1} \\ r \end{pmatrix}\right) \\ &+ \nu_{\min}b_0\|x_p\|\frac{\|\nu\|}{\|\bar{\nu}\|} \geq -2x_p^\top PB_p\Xi(\Theta_x^* + \mathbf{K})^\top x_p. \end{aligned} \tag{3.57}$$

Then, we add terms in order to construct $\dot{W}$ on the right side of (3.57) and obtain an inequality as

$$\begin{aligned} &- x_p^\top Qx_p + 2x_p^\top PB_p\Xi\left(\tilde{\Theta}_x^\top x_p + \tilde{\Theta}_d^\top + \begin{pmatrix} \mathbf{0}_{m\times 1} \\ r \end{pmatrix}\right) \\ &+ \nu_{\min}b_0\|x_p\|\frac{\|\nu\|}{\|\bar{\nu}\|} + 2x_p^\top PB_p\Xi\bar{\nu} \geq \dot{W} \end{aligned} \tag{3.58}$$

since $\Theta_d^{*\top} = -d_p$. Using definitions in (3.30) and (3.32) and the fact that $\nu_{\min} \leq \|\bar{\nu}\| \leq \nu_{\max}$, we can bound the left side of (3.58) as

$$\begin{aligned} &- q_{\min}\|x_p\|^2 + b_0\|\nu\|\|x_p\| + 2P_B\nu_{\max}\|x_p\| \\ &+ 2P_B\left(\Theta_{\max}\|x_p\| + r_{\max} + \Theta_{\max}\right)\|x_p\| \geq \dot{W}. \end{aligned} \tag{3.59}$$

We note that

$$\|\nu\| \leq \left(\left\| \left(\Theta_x^* + \mathbf{K}\right)^\top \right\| + \Theta_{\max} \right) \|x_p\| + \left\|\Theta_d^{*\top}\right\| + \Theta_{\max} + r_{\max} \tag{3.60}$$

and that from the definition of b_0,

$$0 < b_0 < P_B. \tag{3.61}$$

From (3.59)$\sim$(3.61), we derive the following inequality as

$$\left(3P_B\Theta_{\max} - q_{\min}\right) \|x_p\|^2 + P_B \left(2\nu_{\max} + 3r_{\max} + 3\Theta_{\max} + d_{\max}\right) \|x_p\| \geq \dot{W} \tag{3.62}$$

since $\left\|\Theta_d^{*\top}\right\| = \|d_p\| < d_{\max}$. From (3.46), $3P_B\Theta_{\max} - q_{\min} < 0$ and (3.62) implies that

$$\dot{W} < 0, \quad \|x_p\| > \frac{P_B \left(2\nu_{\max} + 3r_{\max} + 3\Theta_{\max} + d_{\max}\right)}{q_{\min} - 3P_B\Theta_{\max}}. \tag{3.63}$$

From the choice of $x_{\min}$, we conclude that

$$\dot{W} < 0, \quad \forall x_p \in \mathbf{A} \tag{3.64}$$

in *Sub-case (ii)* of *Case B*. As a consequence from (3.49), (3.54), and, (3.64), it follows that

$$\dot{W} < 0, \quad \forall x_p \in \mathbf{A}. \tag{3.65}$$

As $\nu_{\min}$, which is the minimum among saturation limits, tends to ∞, $x_{\max}$ approaches to ∞ and hence, the condition, $\|x(t_0)\| < x_{\max}/\rho$, can be relaxed. In addition to that, the constraint on $d_{\max}$ in (3.33) is relieved. In this sense, semi-global boundedness is achieved with respect to the level of saturation. □

Remark 3.2. *In the case of magnitude saturation, global boundedness of $x_p(t)$ is impossible with the integral action in* (3.3) *since poles at the origin prevent BIBO stability of the open-loop plant. Initial conditions can be always found to cause $x_p(t)$ to become unbounded regardless of the controller design. Therefore, any stability result,*

in nature, must be semi-global as presented in Theorem 3.1.

Remark 3.3. *When there is no integral action, the stability result in the presence of magnitude saturation depends on the stability of the open-loop plant. In the case of the open-loop stable plant, the bounded trajectory of $x(t)$ is guaranteed for all initial conditions. If A_λ is stable, (3.2) is BIBO stable and (3.7) implies $E_s(u)$ is bounded. Therefore, $x(t)$ is bounded in the closed-loop plant. However, when the open-loop plant is unstable, boundedness of $x(t)$ is not globally guaranteed as presented in [34].*

3.2.4 Proof of Bounded Tracking - Rectangular Saturation

In this section, the boundedness of x_p is deal with when actuators are constrained under the rectangular saturation. To avoid redundancy, similar procedures in the stability analysis introduced in Section 3.2.3 are not discussed in details. We begin with the plant in the form of

$$\dot{x}_p = A_{\lambda p}x_p + B_p\Xi\left(\left(\Theta_x + \mathbf{K}\right)^\top x_p + \Theta_d^\top + \begin{pmatrix} \mathbf{0}_{m\times l} \\ r \end{pmatrix} - \Delta\nu + d_p\right) \tag{3.66}$$

where $\Delta\nu = \nu - R_s(\nu)$. Definitions in (3.27)$\sim$(3.31) are used as well as a_0, b_0, c_0 and $x_{\max}$ in (3.32). Since $\left\|\left(\Theta_x^* + \mathbf{K}\right)^\top\right\|$ are $\Theta_{\max}$ are positive and finite, there exists the smallest $N \in \mathbb{N}$ such that

$$\left\|\left(\Theta_x^* + \mathbf{K}\right)^\top\right\| \leq N\Theta_{\max}. \tag{3.67}$$

We newly defines following constants:

$$\begin{aligned}
\nu_0 &= \sqrt{\sum_{i=1}^{m+l} \nu_{i,\max}^2} \\
\bar{x}_{\min} &= \frac{P_B\left(2\nu_0 + 5r_{\max} + 5\Theta_{\max} + 3d_{\max}\right)}{q_{\min} - (2N+5)P_B\Theta_{\max}} \\
\bar{\Omega}_{\max} &= \frac{q_{\min} - P_B\rho\dfrac{c_0}{a_0}(2\nu_0 + 5r_{\max} + 3d_{\max})}{P_B\left(5\rho\dfrac{c_0}{a_0} + 2N + 5\right)}.
\end{aligned} \tag{3.68}$$

Theorem 3.2. *Under Assumptions 3.1, 3.2, 3.3, 3.4, and 3.5, for the system in* (3.12) *with the controller in* (3.14) *and the adaptive law in* (3.22), $x_p(t)$ *has a semi-globally bounded trajectory with respect to the level of saturation for all* $t \geq t_0$ *if*

(i) $\|x_p(t_0)\| < \dfrac{x_{\max}}{\rho}$

(ii) $\sqrt{V(t_0)} < \bar{\Omega}_{\max}\sqrt{\dfrac{\lambda_{\min}}{\gamma_{\max}}}$.

Further,

$$\|x_p(t)\| < x_{\max}, \quad \forall t \geq t_0$$

and the error, $e(t)$, *is in the order of*

$$\|e(t)\| = O\left[\sup_{\tau \leq t} \|\Delta\nu(\tau)\|\right].$$

Proof. We define $\bar{\mathbf{A}}$ as

$$\bar{\mathbf{A}} = \{\ x_p \mid \bar{x}_{\min} < \|x_p\| < x_{\max}\ \} \tag{3.69}$$

The stability is proved in two steps. From Conditions (ii), we prove that $\mathbf{B} \subset \bar{\mathbf{A}}$. In the second step, we prove that $\dot{W} < 0,\ \forall x_p \in \bar{\mathbf{A}}$.

Step 1: Approached in this step is identical to that in Theorem 3.1. Replacing $x_{\min}$ and $\Omega_{\max}$ with $\bar{x}_{\min}$ and $\bar{\Omega}_{\max}$ respectively, we can take the same steps from (3.39) to (3.42). Then, we obtain that $\mathbf{B} \subset \bar{\mathbf{A}}$ from the definition of $\bar{\mathbf{A}}$.

Step 2: We prove that $\dot{W} < 0,\ \forall x_p \in \bar{\mathbf{A}}$ in this step. The first case is that there is no saturation in the control inputs and the second one is that the control inputs are limited by the magnitude saturation.

Case A: $\Delta\nu = 0$

Procedures in (3.43), (3.44), and (3.45) are established as in Theorem 3.1 and the Condition (ii) in Theorem 3.2 results in

$$\Theta_{\max} < \bar{\Omega}_{\max} < \frac{q_{\min}}{(2N+5)P_B}. \tag{3.70}$$

Therefore, we can have the same result in (3.47). From the choice of $\bar{x}_{\min}$ in (3.68), the following holds:

$$\bar{x}_{\min} > \frac{2P_B\left(r_{\max} + \Theta_{\max}\right)}{q_{\min} - 2P_B\Theta_{\max}}. \tag{3.71}$$

Hence, it is shown that

$$\dot{W} < 0, \quad \forall x_p \in \bar{\mathbf{A}} \tag{3.72}$$

in *Case A*.

Case B: $\Delta\nu \neq 0$

In this case, two sub-cases are considered as in Theorem 3.1.

Sub-case (i): $2x_p^\top P B_p \Xi \bar{\nu} < -\nu_{\min} b_0 \|x_p\|$

Since there is no difference in the first sub-case between Theorem 3.1 and 3.2, we now discuss the second sub-case.

Sub-case (ii): $2x_p^\top P B_p \Xi \bar{\nu} \geq -\nu_{\min} b_0 \|x_p\|$

Complexities arise in the stability analysis due to that the rectangular saturation does not necessary preserve the direction of the control input as the control inputs

hit their limits. Therefore, $\bar{\nu}$ is decomposed into ν_d and $\tilde{\nu}$ as

$$\bar{\nu} = \nu_d + \tilde{\nu} = \frac{\nu}{\|\nu\|}\|\nu_d\| + \tilde{\nu} \tag{3.73}$$

and ν_d is chosen such that

$$\|\nu_d\| > \max[\|\tilde{\nu}\|, \quad \nu_{\min}]. \tag{3.74}$$

as shown in Figure 3-3. This decomposition can be constructed without loss of generality. The condition to this sub-case implies that

$$2x_p^\top PB_p\Xi\frac{\nu}{\|\nu\|}\|\nu_d\| + \nu_{\min}b_0\|x_p\| + 2x_p^\top PB_p\Xi\tilde{\nu} \geq 0. \tag{3.75}$$

Multiplying $\|\nu\|/\|\nu_d\|$ in (3.76), we have

$$2x_p^\top PB_p\Xi\nu + \nu_{\min}b_0\|x_p\|\frac{\|\nu\|}{\|\nu_d\|} + 2x_p^\top PB_p\Xi\tilde{\nu}\frac{\|\nu\|}{\|\nu_d\|} \geq 0. \tag{3.76}$$

Since ν_d in (3.74) is chosen such that $\nu_{\min}/\|\nu_d\| < 1$ and $\|\tilde{\nu}\|/\|\nu_d\| < 1$ hold, we have

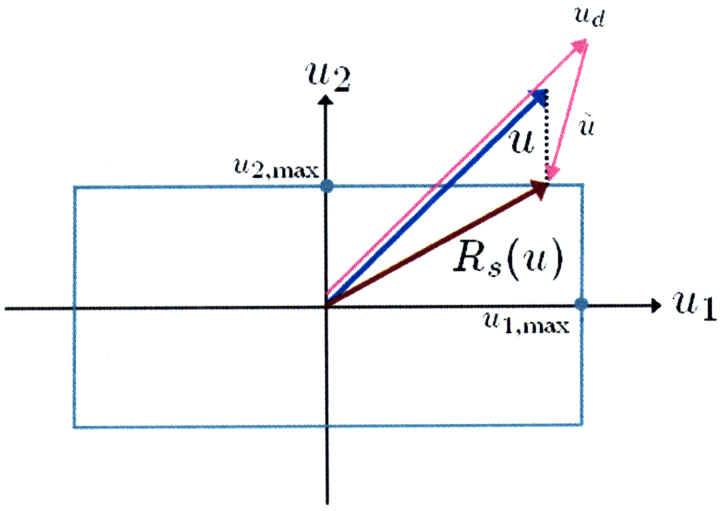

Figure 3-3: The control input, $\bar{u}$, saturated by the rectangular saturation can be decomposed into u_d and $\tilde{u}$.

$$2x_p^\top PB_p\Xi\nu + b_0\|x_p\|\|\nu\| + 2P_B\|x_p\|\|\nu\| \geq 0. \tag{3.77}$$

We construct $\dot{W}$ in the right side of (3.77) and have an inequality as

$$\begin{aligned} &- x_p^\top Q x_p + 2x_p^\top P B_p \Xi \left(\tilde{\Theta}_x^\top x_p + \tilde{\Theta}_d^\top + \begin{pmatrix} \mathbf{0}_{m\times 1} \\ r \end{pmatrix} \right) \\ &+ b_0 \|x_p\| \|\nu\| + 2x_p^\top P B_p \Xi \bar{\nu} + 2P_B \|x_p\| \|\nu\| \geq \dot{W}. \end{aligned} \tag{3.78}$$

Using the upper bound on $\|\nu\|$ in (3.60) and the inequality in (3.67), we have

$$2P_B \|x_p\| \|\nu\| \leq 2(N+1) P_B \Theta_{\max} \|x_p\|^2 + 2P_B (d_{\max} + \Theta_{\max} + r_{\max}) \|x_p\|. \tag{3.79}$$

Incorporating (3.79) into (3.78), we have

$$\begin{aligned} &\left[(2N+5) P_B \Theta_{\max} - q_{\min} \right] \|x_p\|^2 \\ &+ P_B \left(2\nu_0 + 5r_{\max} + 5\Theta_{\max} + 3d_{\max} \right) \|x_p\| \geq \dot{W} \end{aligned} \tag{3.80}$$

since $\|\bar{\nu}\| \leq \nu_0$. From (3.70), we know that $(2N+5)P_B\Theta_{\max} - q_{\min} < 0$ and then we have

$$\dot{W} < 0, \quad \|x_p\| > \frac{P_B \left(2\nu_0 + 5r_{\max} + 5\Theta_{\max} + 3d_{\max} \right)}{q_{\min} - (2N+5) P_B \Theta_{\max}}. \tag{3.81}$$

From the choice of $\bar{x}_{\min}$, we conclude that

$$\dot{W} < 0, \quad \forall x_p \in \bar{\mathbf{A}} \tag{3.82}$$

in *Sub-case (ii)* of *Case B*. As a consequence from (3.72) and (3.82), it follows that

$$\dot{W} < 0, \quad \forall x_p \in \bar{\mathbf{A}}. \tag{3.83}$$

□

Remark 3.4. *As shown in* (3.75), *we have an additional term* $2x_p^\top P B_p \Xi \tilde{\bar{\nu}}$ *as the rectangular saturation changes the direction of the control inputs. This brings conservativeness in the analysis such that* $x_{\min} < \bar{x}_{\min}$. *This, in turn, is followed by* $\bar{\Omega}_{\max} < \Omega_{\max}$. *This implies that Condition (ii) in Theorem 3.2 is more restrictive*

than that in Theorem 3.1.

3.3 Simulation

This section validate the proposed adaptive controller which consists of a combination of a PI baseline controller with the adaptive controller. A nonlinear 6–DoF hypersonic aircraft model is employed to demonstrate the performance of the proposed adaptive controller in Section 3.2. Aerodynamic data of the NASA X–15 hypersonic aircraft discussed in [13] are combined with nonlinear flight dynamics as

$$\dot{X} = F(X,\ U) \tag{3.84}$$

whose states (X) and inputs (U) are defined as

$$\begin{aligned} X &= [V_T\ \ \alpha\ \ \beta\ \ P\ \ Q\ \ R\ \ \Phi\ \ \Theta\ \ \Psi\ \ N\ \ E\ \ D]^\top \\ U &= [U_{thrust}\ \ U_{left}\ \ U_{right}\ \ U_{rudder}]^\top. \end{aligned} \tag{3.85}$$

U_{left} and U_{right} represent the left and right control surface of the elevon system. Elevator and aileron inputs can be computed as

$$U_{elevator} = \frac{U_{left} + U_{right}}{2},\ U_{aileron} = \frac{U_{left} - U_{right}}{2}. \tag{3.86}$$

Actuator limits are imposed as

$$U_{left/right} \in [-15,\ 15], \quad U_{rudder} \in [-30,\ 30]. \tag{3.87}$$

Details regarding the NASA X-15 hypersonic aircraft are discussed in Appendix A.

3.3.1 Nominal Controller Design

For the purpose of control design, the nonlinear flight dynamics is linearized at the trim point ($X_0,\ U_0$) condition where straight and level flight is achieved with a con-

stant speed. Trim states and inputs are shown in Table 3.1. This leads to a LTI

States and Inputs	Symbols	Quantity
Airspeed	V_T	1929.7 ft/sec (Mach 3)
Altitude	$h(=-D)$	60000 ft
Angle of Attack	α	5.5 deg
Thrust	U_{thrust}	7062 lb
Left & Right Elevon	$U_{left/right}$	-7.3 deg
Rudder	U_{rudder}	0 deg

Table 3.1: Trim conditions and inputs.

system with full state vector $x = X - X_0$ and full input vector $u = U - U_0$. To efficiently design the controller, weakly coupled or decoupled states and inputs are neglected from the LTI system and this results in the linearized flight dynamics in the form of (3.1) with states and inputs given by

$$\begin{aligned} x &= [\Delta\alpha \;\; \Delta\beta \;\; p \;\; q \;\; r]^\top \\ u &= [u_{left} \;\; u_{right} \;\; u_{rudder}]^\top. \end{aligned} \tag{3.88}$$

The states of the integral controller and the command in (3.3) are given as

$$\begin{aligned} x_c &= [\Delta\alpha_I \;\; p_I \;\; r_I]^\top \\ r &= [\Delta\alpha_{cmd} \;\; \Delta\beta_{cmd} \;\; p_{cmd} \;\; r_{cmd}]^\top \end{aligned} \tag{3.89}$$

where $\Delta\alpha_I$, p_I and r_I are the output error integrations defined by

$$\begin{aligned} \Delta\alpha_I &= \int_0^t [\Delta\alpha_{cmd}(t) - \Delta\alpha(t)]\, dt \\ p_I &= \int_0^t [p_{cmd}(t) - p(t)]\, dt, \\ r_I &= \int_0^t [r_{cmd}(t) - r(t)]\, dt. \end{aligned} \tag{3.90}$$

This, in turn, determines the error combination matrix B_c as

$$B_c = \begin{bmatrix} -1 & 0 & 0 & 0 & 0 \\ 0 & 0 & -1 & 0 & 0 \\ 0 & 0 & 0 & 0 & -1 \end{bmatrix}. \tag{3.91}$$

As the linearized plant with integral actions is constructed, we design a LQR PI controller by minimizing the the cost function given by

$$J = \int_0^\infty x_p^\top \left(\bar{Q} + K\bar{R}K^\top\right) x_p dt \tag{3.92}$$

where K is the controller gain.

3.3.2 Adaptive Controller Design

The adaptive controller is designed as in (5.17). First, we choose $Q = 100I_{8\times 8}$ and then compute P from $A_m^\top P + PA_m^\top = -Q$. The adaptive rate denoted by Γ is designed using an empirical rule in [8] described by

$$\Gamma = \left| \frac{diag(\vartheta)}{\tau_{\min} p r_{\max}^2} \right| + \Gamma_0 \tag{3.93}$$

where

i. $\vartheta \in \mathbb{R}^{n_p+l}$ is a vector given by the sum of the columns of $\bar{\theta}^*$ where $\bar{\theta}^*$ corresponds to the uncertainty $\bar{\Lambda}$ for which the plant has the most unstable eigenvalues.

ii. $\tau_{\min}$ is the smallest time constant in the reference model.

iii. p is the norm of $B_{p_1}^\top P$.

iv. $r_{\max}$ is the maximum among the norm of the command signal r.

v. Γ_0 is a small positive definite diagonal matrix which ensures that Γ is positive definite.

Combining the adaptive controller with the nominal one, the full control input becomes as in (3.14). The reference model and the overall control architecture can be seen in Figure 3-4.

3.3.3 Simulation Results

Simulation 1 – $\Lambda_1 = diag([1 \quad 1 \quad 0.2 \quad 1])$

The uncertainty, Λ_1, implies that the right control surface in the elevon system has lost 80% of effectiveness but the others have no loss. For example, the right elevon is deflected only by 2° when 10° is given as a control input. At $t = 10sec$, the uncertainty was applied to the nonlinear flight dynamics. A pulse of 4° angle of attack was given as the command signal and the simulation was executed for $60sec$. In order to ensure that the aircraft has endurable accelerations, the verical acceleration, A_z, was also considered. Figure 3-5 shows that the plant with the augmented adaptive controller (subscripted by "ad") is able to track the reference model (subscripted by "ref") while the nominal controller (subscripted by "nom") fails to stabilize the plant. Oscillation between 0 and $10sec$ is due to non-zero initial conditions. As shown in Figure 3-5, the adaptive controller can regulate the non-zero initial conditions compared to the nominal controller. This also indicates that the vertical acceleration remains $\pm 2g$.

Simulation 2 – $\Lambda_2 = diag([1 \quad 1 \quad -0.2 \quad 1])$

The uncertainty, Λ_2, has control reversal in addition to the same loss of effectiveness in Λ_1. Control reversal represents the case when the sign of the control input becomes opposite. This phenomenon was demonstrated in this simulation study. The right control surface has both 80% loss of control surface effectiveness and control reversal. The same command signal as in Simulation 1 was used. In order to compare the performance of the nominal controller with that of the adaptive counterpart fairly, information regarding the sign of Λ_2 was also provided when the nominal controller is designed. Similar to the previous simulation results, Figure 3-6 shows that the proposed adaptive controller guarantees close tracking of reference model while the

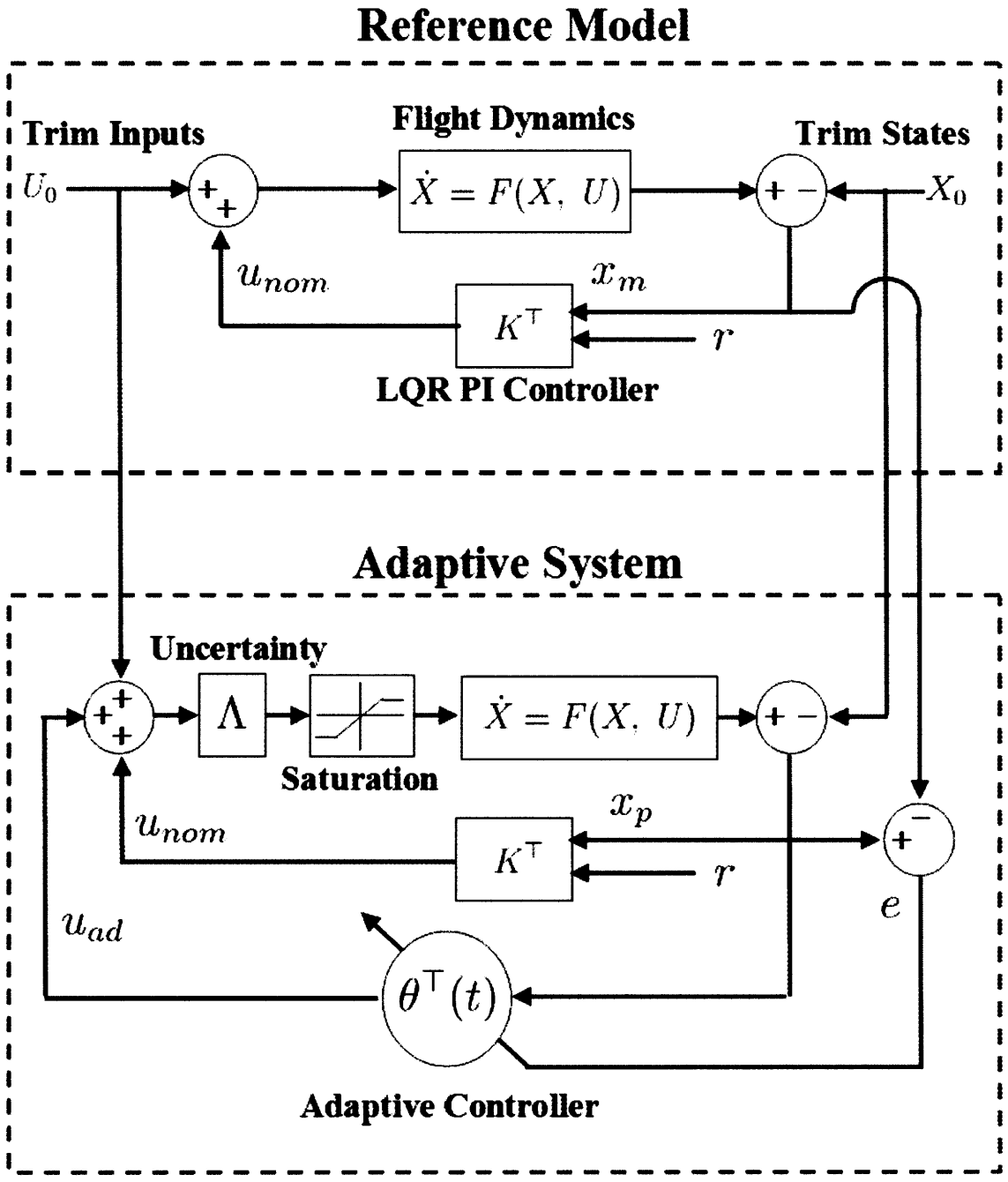

Figure 3-4: The block diagram of the reference model and the overall control architecture in nonlinear simulation.

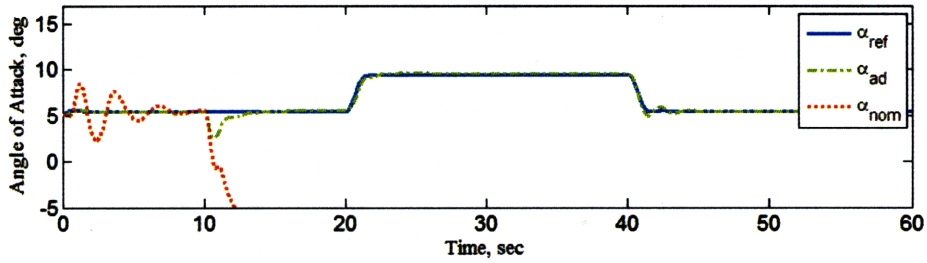

(a) Angle of Attack

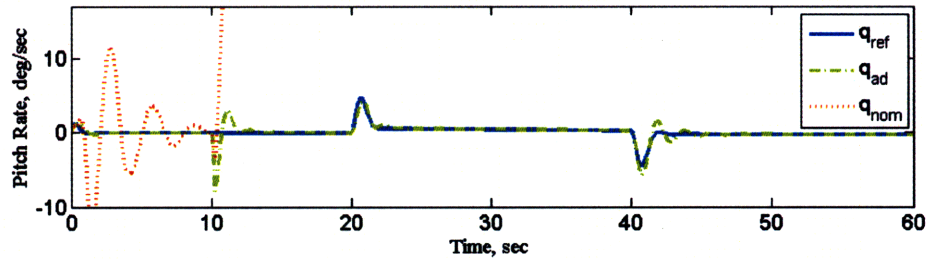

(b) Pitch Rate

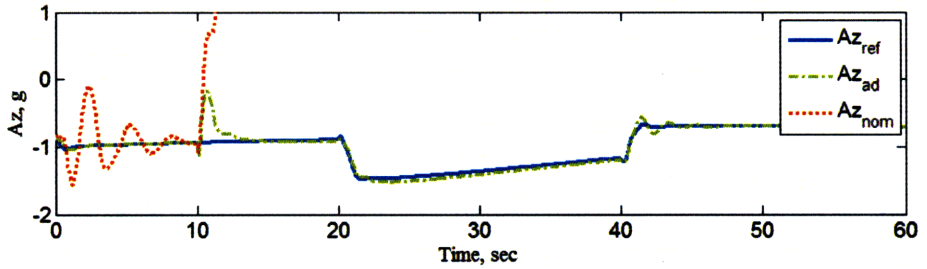

(c) Vertical Acceleration

Figure 3-5: Response of angle of attack, pitch rate, and vertical acceleration of reference (ref), adaptive (ad), and nominal (nom) systems under Λ_1.

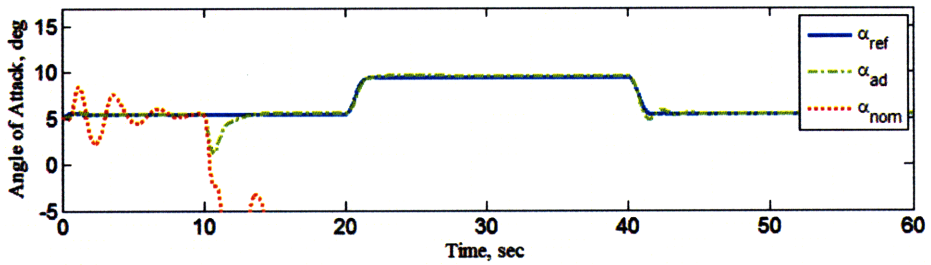

(a) Angle of Attack

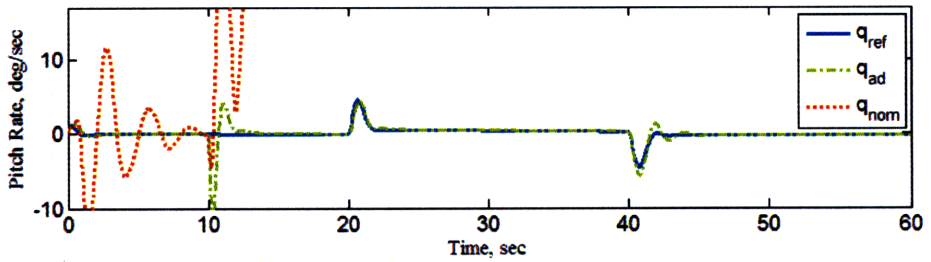

(b) Pitch Rate

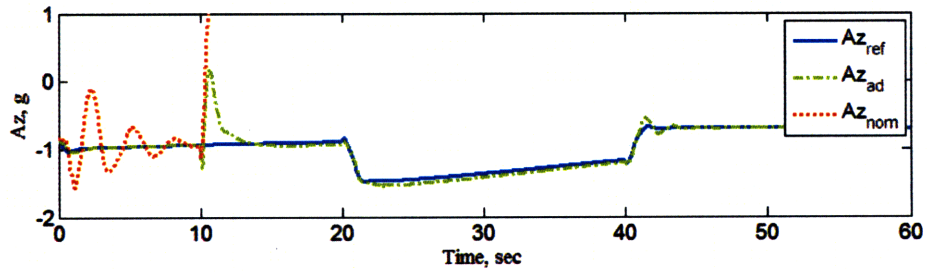

(c) Vertical Acceleration

Figure 3-6: Response of angle of attack, pitch rate and vertical acceleration of reference, adaptive, and nominal systems under Λ_2.

nominal controller fails to track even though the sign of Λ_2 is incorporated.

Simulation 3 – $\Lambda_3 = diag([1 \quad 1 \quad -0.5 \quad 1])$

In this simulation, we introduce 50% loss of effectiveness as well as control reversal in the right elevon. A more aggressive command which is 6° of α_{cmd} was given to the plant in this simulation. This causes magnitude saturation in both elevons while the aircraft is still subject to the uncertainty in Λ_3. The uncertainty implies that the right elevon is subject to 50% loss of control surface effectiveness and control reversal at the same time. The actuator uncertainty Λ_3 was introduced at $t = 30sec$. When the uncertainty occurs at $t = 30sec$, the nominal controller fails to stabilize the plant and the states and hence inputs diverges. In Figure 3-7, the responses, $\alpha_{ad(eu)}$, $q_{ad(eu)}$ and $Az_{ad(eu)}$, are obtained by using the adaptive controller proposed in this chapter. In the presence of magnitude saturation, this controller shows a satisfactory tracking. It is noted that the responses, $\alpha_{ad(e)}$, $q_{ad(e)}$ and $Az_{ad(e)}$, by the standard adaptive controller whose adaptive law is based on e instead of e_u performs poorly. These responses have high oscillation compared to $\alpha_{ad(eu)}$, $q_{ad(eu)}$ and $Az_{ad(eu)}$. This illustrates that the adaptive control designed by (5.17) improves the tracking performance when magnitude of inputs is constrained.

Figure 3-8 shows $\Lambda R_s(u)$ which is the control input transmitted to the aircraft with adaptive controller based on e_u and e respectively. In Figure 3-8(b), the adaptive controller based on e causes high oscillation in all three control inputs and both elevons continues to hit the lower limits. This shows control inputs are beyond the bandwidth and control surfaces are susceptible to structural failure. On the contrary, the proposed adaptive controller provides admissible oscillation in the presence of magnitude saturation. It is because the proposed controller activates adaptation based on e_u from which the error due to magnitude saturation is subtracted. Consequently, the proposed adaptive controller succeeds to remove the error due to uncertainties and hence smooth control inputs are possible.

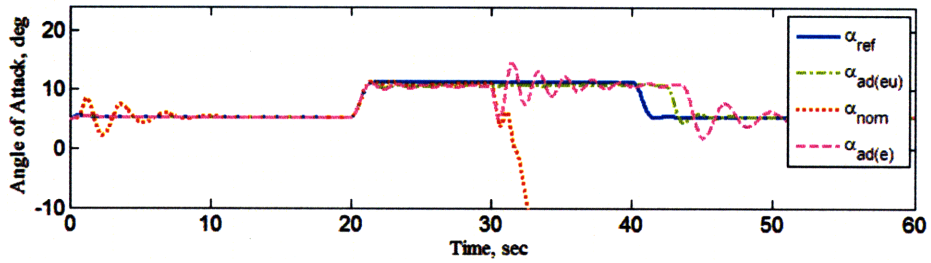

(a) Angle of Attack

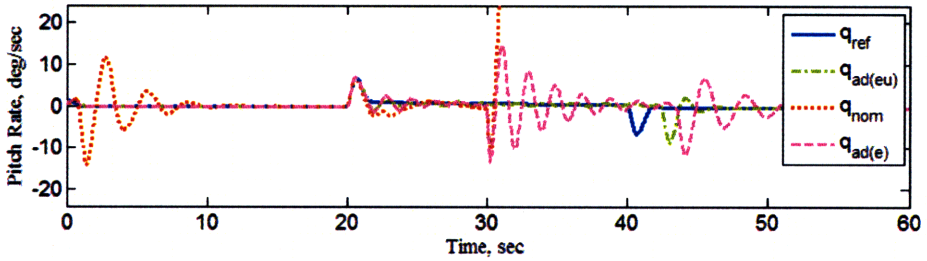

(b) Pitch Rate

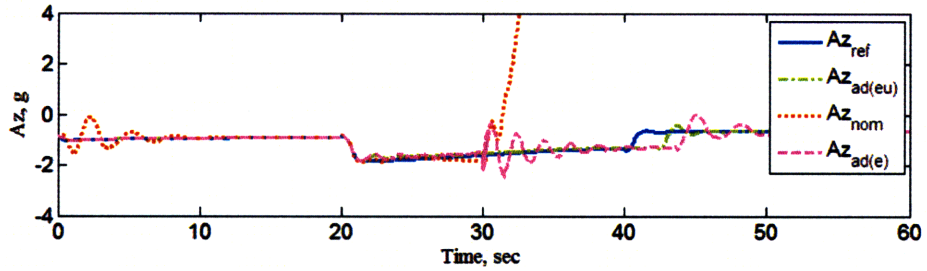

(c) Vertical Acceleration

Figure 3-7: Response of angle of attack, pitch rate, and vertical acceleration of reference, adaptive, and nominal systems under Λ_3.

3.4 Summary

In this chapter, we developed an extension of the approach used in [19] to multi-input systems with realistic magnitude-constrained inputs while a PI baseline controller is augmented with an adaptive controller. Sufficient conditions for uniform boundedness of the closed-loop system were derived. A semi-global stability result was proved with respect to the level of saturation for open-loop unstable plants while the stability result becomes global for open-loop stable plants. Through the simulation based on a nonlinear model of NASA X-15 hypersonic aircraft, it was demonstrated that the proposed adaptive controller tracks the reference model even in the presence of actu-

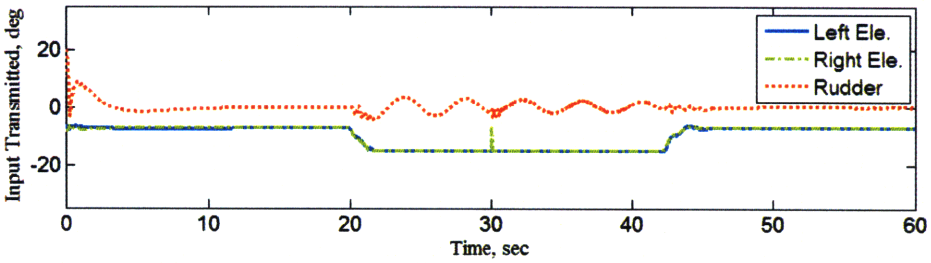

(a) Control inputs based on e_u

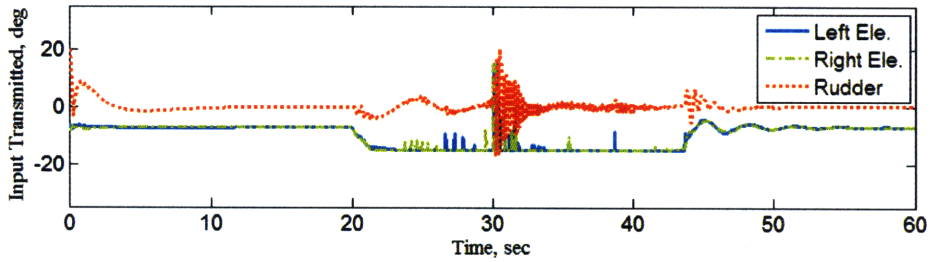

(b) Control inputs based on e

Figure 3-8: Control inputs transmitted to the aircraft: Left elevon, right elevon, and rudder based on e_u and e. Saturation starts at $t = 21sec$ and endns at $t = 42sec$.

ator anomalies such as loss of control effectiveness, control reversal, and magnitude saturation.

Chapter 4

Adaptive Gain-scheduled Controller

In this chapter, we address the problem of controlling a nonlinear multi-rate plant in the presence of parametric uncertainties. It is assumed that the plant consists of multi-rate state variables and that it has multiple trim points over which its dynamic characteristics vary significantly. A nominal controller based on gain-scheduling is designed to control fast-varying states in the inner-loop and the outer loop which consists of slowly-varying states is closed by fixed controllers. Slowly-varying states such as altitude and velocity are used as gain-scheduling variables. An adaptive controller that employs gain-scheduling as a nominal component and adjustable parameters for accommodating uncertainties as an adaptive component is proposed. The closed-loop system with the proposed controller is shown to be globally bounded under certain conditions. Commands that are sufficiently slow and the trim points that are sufficiently close to each other guarantee the stability of the overall closed-loop with the nominal gain-scheduling controller and the adaptive time-varying controller. The theoretical results are validated using nonlinear flight simulation models of a high performance aircraft. The performance of the augmented adaptive controller is compared with both the nominal and the adaptive controller without gain scheduling in the presence of actuator uncertainties when aggressive commands are given to those closed-loop systems.

4.1 Problem Statement

4.1.1 Linear Time-varying System

We consider a nonlinear multi-rate plant in the form of

$$\begin{aligned} \dot{X} &= f(X,\, X_g) + g(X,\, X_g)U_1 \\ \dot{X}_g &= h(X_g,\, U_2) \end{aligned} \tag{4.1}$$

where the system state is partitioned into two components, $X \in \mathbb{R}^n$ and $X_g \in \mathbb{R}^{n_g}$ so that the former represents the fast-varying controlled states relative to the slowly-varying states, X_g. The latter will become gain-scheduling variables. The input is also separated by the time-scale into $U_1 \in \mathbb{R}^m$ and $U_2 \in \mathbb{R}^{\bar{m}}$. The block diagram of a multi-rate plant is depicted in Figure 4-1.

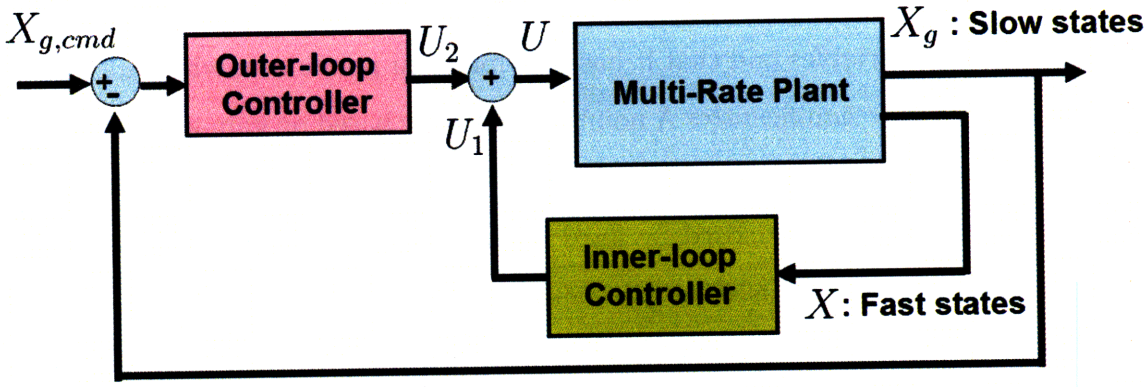

Figure 4-1: A block diagram of a multi-rate plant. Fast states and slow states are controlled separately.

It is assumed that sufficient information is available about the nonlinearity of h so that the outer-loop controller, $U_2 = h_c(X_g,\, X_{g,cmd})$, can be chosen so that $X_g(t)$ tracks $X_{g,cmd}(t)$, its desired command signal, and satisfies the following assumption:

Assumption 4.1. *$X_{g,cmd}(t)$ is continuously differentiable and slowly varying, i.e.*

$$\left\| \dot{X}_{g,cmd}(t) \right\| < \epsilon_1, \quad \forall t \geq t_0. \tag{4.2}$$

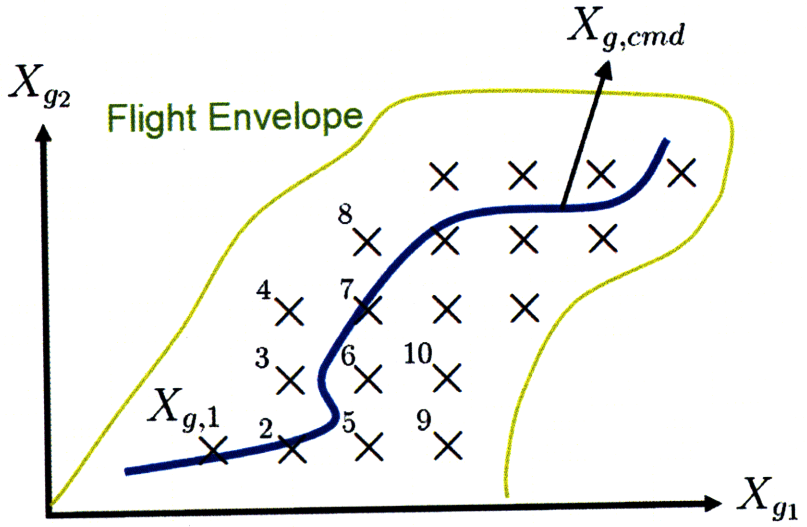

Figure 4-2: A schematic of trim points inside the operating envelope in the X_g space.

The goal is now to design U_2 in (4.1) such that the closed-loop system has bounded solutions in the presence of uncertainties in f and g. In order to control the nonlinear system in (4.1) for arbitrary initial conditions and command signals encompassing multiple trim points, we consider a family of k trim points near a given command $X_{g,cmd}(t)$ as

$$\sigma_g = \{X_{g,1},\ X_{g,2}, \cdots, X_{g,k}\}. \tag{4.3}$$

The dimension of $X_{g,i}$ is n_g and its rth component is defined as $X_{g_r,i}$.

Definition 4.1. *$X_{g,i}$ and $X_{g,j}$ are separated trim points if $X_{g_r,i} \neq X_{g_r,j}$ for all $1 \leq r \leq n_g$.*

In Figure 4-2, $X_{g,1}$ and $X_{g,5}$ are not separated trim points since $X_{g_2,1} = X_{g_2,5}$ but $X_{g,1}$ and $X_{g,6}$ are separated ones.

Assumption 4.2. *There exist k operating points to satisfy the following condition for all separated trim points $X_{g,i}$ and $X_{g,j}$*

$$\max_{1\leq i\leq k}\left[\min_{1\leq j\leq k}\|X_{g,i} - X_{g,j}\|\right] < \epsilon_2. \tag{4.4}$$

The assumption implies that over the operating envelope, a large number of trim

points are required so that adjacent trim points are close enough. For each frozen trim point $X_{g,i}$, we obtain a family of equilibrium states and inputs as

$$\sigma_p = \{X(X_{g,1}),\ X(X_{g,2}),\ \cdots,\ X(X_{g,k})\} \tag{4.5}$$

$$\sigma_u = \{U_1(X_{g,1}),\ U_1(X_{g,2}),\ \cdots,\ U_1(X_{g,k})\} \tag{4.6}$$

such that

$$f(X(X_{g,i}),\ X_{g,i}) + g(X(X_{g,i}),\ X_{g,i})U_1(X_{g,i}) = 0. \tag{4.7}$$

σ_g, σ_p, and σ_u are tabulated off-line and are utilized to construct the desired state and input $(X^*(t),\ U_1^*(t))$ by linear interpolation as

$$\begin{aligned} X^*(t) &= X(X_{g,i}) + M_i(X_g(t) - X_{g,i}) \\ U_1^*(t) &= U_1(X_{g,i}) + N_i(X_g(t) - X_{g,i}) \end{aligned} \tag{4.8}$$

where M_i and N_i are constant matrices which map X_g into X and U respectively. In Figure 4-3, construction of $X^*(t)$ is illustrated.

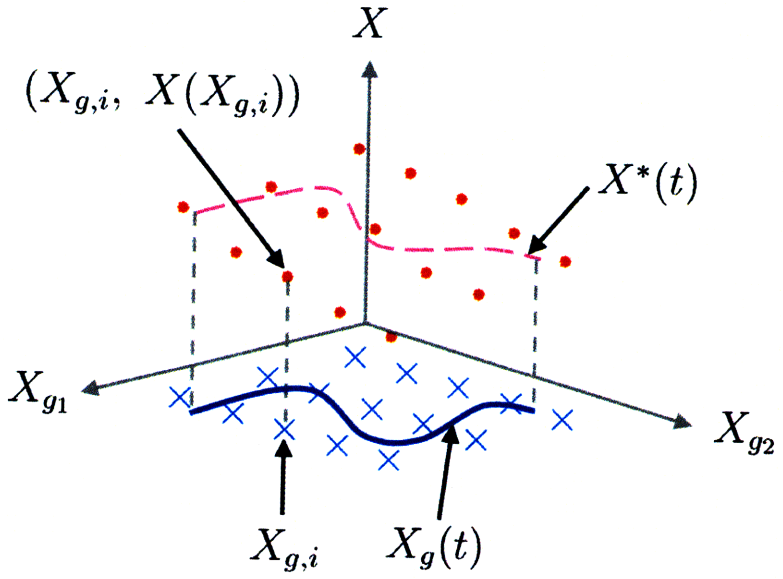

Figure 4-3: This figure illustrates the construction of desired states, $X^*(t)$.

Using these trajectories, we linearize the plant in (4.1) about $(X_g(t),\ X^*(t),\ U_1^*(t))$ as

$$\dot{x} = A(t)x_p + B(t)u + \epsilon_x(t) \tag{4.9}$$

where $x = X - X^*(t)$, $u = U_1 - U_1^*(t)$ and

$$\begin{aligned}
A(t) &= \left.\frac{\partial f}{\partial X}\right|_{(X^*(t),\, X_g(t))} + \left.\frac{\partial g}{\partial X}\right|_{(X^*(t),\, X_g(t))} U_1^*(t) \\
B(t) &= g(X^*(t),\ X_g(t)) \\
\epsilon_x(t) &= f(X^*(t), X_g(t)) + g(X^*(t), X_g(t))U_1^*(t) - \dot{X}^*(t) + O(x^2).
\end{aligned}$$

When the plant is linearized around a single trim point, we simply obtain $\epsilon_x(t) = O(x^2)$ because (4.7) holds. However, the nonliearity $\epsilon_x(t)$ is in more complicated form in linearization around the time-varying trajectory as in (4.9). The following proposition quantifies the slow variations in $X_g(t)$, which is the gain-scheduling variable.

Proposition 4.1. *If $O(x^2)$ is neglected, it can be shown under Assumptions 4.1 and 4.2 that*

$$\|\epsilon_x(t)\| \leq a\epsilon_1 + b\epsilon_2 \tag{4.10}$$

where a and b are arbitrary positive constants.

Proof. See Appendix B. □

Remark 4.1. *By making ϵ_1 and ϵ_2 suitably small, ϵ_x can be made arbitrarily small. In other words, if the gain-scheduling variable is varying sufficiently slowly, and trim points around which the gains are scheduled are sufficiently close to each other, ϵ_x can be made arbitrarily small.*

The problem that we consider in this chapter is the control of the system in (4.9) under Assumptions 4.1 and 4.2 in the presence of uncertainties introduced due to control anomalies. In particular, we consider the case where the nonlinear dynamics in (4.1) is of the form

$$\dot{X} = f(X,\ X_g) + g(X,\ X_g)\Lambda U_1 \tag{4.11}$$

where Λ is an unknown diagonal matrix with nonzero diagonal entries, and represents loss of effectiveness in control input. If the nonlinear dynamics in (4.11) is linearized about the same trajectory in (4.8), using the same procedure as described above, we can obtain the linear time-varying system to be controlled as

$$\dot{x} = A_\lambda(t)x + B(t)\Lambda(u + d(t)) + \epsilon_x(t) \tag{4.12}$$

where

$$A_\lambda(t) = \left.\frac{\partial f}{\partial X}\right|_{(X^*(t),\, X_g(t))} + \left.\frac{\partial g}{\partial X}\right|_{(X^*(t),\, X_g(t))} \Lambda U_1^*(t)$$
$$d(t) = (I - \Lambda^{-1})U_1^*(t)$$

and $d(t)$ is the input disturbance due to Λ. Therefore, when there is no uncertainty in the control input, i.e. $\Lambda = I$, $d(t)$ becomes zero.

4.1.2 Augmentation with Integral Actions

The overall goal of the controller design is that the state, $X(t)$, follows a desired trajectory, $X^*(t)$, in spite of disturbances and uncertainties. Toward this goal, we design an inner-loop controller that integrates the tracking error as

$$\dot{x}_c = B_c(X - X^*) = B_c x \tag{4.13}$$

where $x_c \in \mathbb{R}^{n_c}$ is the controller state. The plant in (4.12) combined with the controller state is written as

$$\underbrace{\begin{bmatrix} \dot{x} \\ \dot{x}_c \end{bmatrix}}_{\dot{x}_p} = \underbrace{\begin{bmatrix} A_\lambda(t) & \mathbf{0}_{n\times n_c} \\ B_c & \mathbf{0}_{n_c\times n_c} \end{bmatrix}}_{A_{p\lambda}(t)} \underbrace{\begin{bmatrix} x \\ x_c \end{bmatrix}}_{x_p} + \underbrace{\begin{bmatrix} B(t) \\ \mathbf{0}_{n_c\times m} \end{bmatrix}}_{B_p(t)} \Lambda(u + d(t)) + \epsilon_x(t) \tag{4.14}$$

or equivalently as

$$\dot{x}_p = A_{p\lambda}(t)x_p + B_p(t)\Lambda(u + d(t)) + \epsilon_x(t) \tag{4.15}$$

where $x_p \in \mathbb{R}^{n_p}$, $A_{p\lambda} \in \mathbb{R}^{n_p \times n_p}$, and $B_p \in \mathbb{R}^{n_p \times m}$. $\mathbf{0}_{i\times j}$ denotes the $i \times j$ zero matrix. The plant in (4.15) is the overall plant to be controlled.

4.2 Adaptive Controller

4.2.1 Reference Model and Baseline Controller Design

In order to ensure that a priori knowledge about the plant and controller design is utilized to achieve best possible performance, the adaptive controller is augmented with a nominal controller which guarantees satisfactory performance in the absence of uncertainties. For the purpose of the nominal controller design, we utilize the principles of gain-scheduling, similar to those in [32] and [26], and develop a time-varying controller, under the premise that no uncertainties are present. The details of the gain-scheduled controller are given below.

We linearize the nonlinear plant in (4.1), where no uncertainties are present, at every frozen equilibrium point and combine the integral action in (4.13). Then, we obtain LTI plants at every trim points as

$$\underbrace{\begin{bmatrix} \dot{x} \\ \dot{x}_c \end{bmatrix}}_{\dot{x}_p} = \underbrace{\begin{bmatrix} A_i & \mathbf{0}_{n\times n_c} \\ B_c & \mathbf{0}_{n_c\times n_c} \end{bmatrix}}_{A_{p,i}} \underbrace{\begin{bmatrix} x \\ x_c \end{bmatrix}}_{x_p} + \underbrace{\begin{bmatrix} B_i \\ \mathbf{0}_{n_c\times m} \end{bmatrix}}_{B_{p,i}} u \tag{4.16}$$

or equivalently as

$$\dot{x}_p = A_{p,i}x_p + B_{p,i}u \tag{4.17}$$

where

$$A_i = \left.\frac{\partial f}{\partial X}\right|_{(X(X_{g,i}),\, X_{g,i})} + \left.\frac{\partial g}{\partial X}\right|_{(X(X_{g,i}),\, X_{g,i})} U_1(X_{g,i})$$

$$B_i = g(X(X_{g,i}),\ X_{g,i}).$$

At the ith trim point, the nominal controller is designed as

$$u_{nom} = K_i^\top x_p \tag{4.18}$$

where the feedback control gain, K_i, is found by the LQR method [10] which guarantees proper closed-loop performance of (4.17). Therefore, the reference model at each trim point is designed as

$$\dot{x}_m = A_{m,i} x_m \tag{4.19}$$

where $A_{m,i} = A_{p,i} + B_{p,i} K_i^\top$ and $A_{m,i}$ is Hurwitz. The nominal controller is designed at several fixed points, the controller gain is scheduled based on the gain-scheduling variables X_g as

$$u_{nom} = K^\top(t) x_p \tag{4.20}$$

where $K(t) = K_i + L_i(X_g(t) - X_{g,i})$ and L_i is a constant matrix which represents a linear mapping from X_g to the controller gain K. The strategy of gain-scheduling is shown in Figure 4-4. While measuring the gain-scheduling variable, $X_g(t)$, online, it updates the corresponding gain, $K(t)$, by linearly interpolating gains in the off-line gain table based on current values of $X_g(t)$ in the gain-scheduling variable domain. As a consequence of the design of the gain-scheduling of the nominal controller, we choose a time-varying reference model that the plant in (4.15) needs to track as

$$\dot{x}_m = A_m(t) x_m + \epsilon_x(t) \tag{4.21}$$

where $A_m(t) = A_p(t) + B_p(t) K^\top(t)$. In order to design stable adaptive control, stability of the reference model in (4.21) should be guaranteed in the first place. Stability analysis of the time-varying reference model will be provided in Section 4.3.

4.2.2 Adaptive Controller Design

In order to improve the tracking performance in the presence of uncertainties, we augment the nominal controller with an adaptive counterpart. The overall control

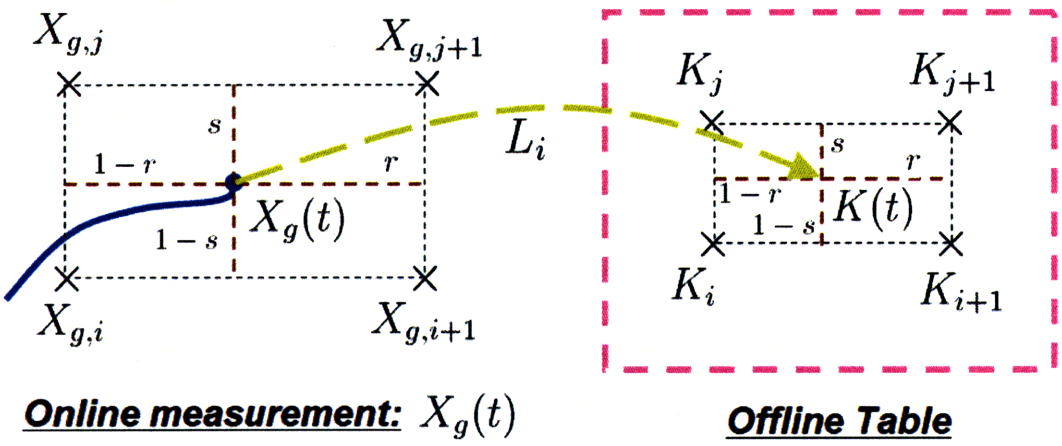

Figure 4-4: Gain-scheduling strategy: linear mapping from online mearsurement of $X_g(t)$ to the offine gain table.

input is designed as

$$u = u_{nom} + u_{ad}. \tag{4.22}$$

The adaptive control input, u_{ad}, is given by

$$u_{ad} = \theta^\top \omega \tag{4.23}$$

where

$$\theta = \begin{bmatrix} \theta_x \\ \theta_d \end{bmatrix}, \quad \omega = \begin{bmatrix} x_p \\ \mathbf{1}_{m\times 1} \end{bmatrix}.$$

For the model-matching condition, it is assumed that there exists an ideal control parameter, $\theta^*(t)$, such that

$$\begin{aligned} &A_{p\lambda}(t) + B_p(t)\Lambda\left(K(t) + \theta_x^*(t)\right)^\top = A_m(t) \\ &\theta_d^*(t)^\top + d(t) = 0. \end{aligned} \tag{4.24}$$

We define the tracking error to be $e = x - x_m$ and the adaptive parameter error to be $\tilde{\theta} = \theta - \theta^*$. Subtracting (4.21) from (4.12), the error model is obtained as The

adaptive law is designed as in [21]

$$\dot{\theta} = -\Gamma \omega e^\top P B_p(t) sign(\Lambda) - \theta \left(1 - \frac{\|\theta\|}{\theta^*_{\max}}\right)^2 f(\theta) \tag{4.25}$$

where

$$f(\theta) = \begin{cases} 1 & \text{if } \|\theta\| > \theta^*_{\max} \\ 0 & \text{otherwise.} \end{cases}$$

$P = P^\top > 0$ is the solution of $A_m^\top P + P A_m = -Q$ for a given $Q = Q^\top > 0$, $\Gamma = \Gamma^\top > 0$ is a diagonal matrix which represents adaptation rate, $sign(\Lambda) = diag\,(sign(\lambda_1),\ sign(\lambda_2),\ \cdots, sign(\lambda_{m_1}))$, $\|\theta^*\| \leq \theta^*_{\max}$, $\theta^*_{\max}$ is a known constant. The second term in (4.25) is added to ensure the boundedness of $\theta(t)$ in the presence of the bounded disturbance $\epsilon_x(t)$.

4.3 Stability Analysis

Since the adaptive control basically enforces to the unknown plant to follow a given reference model, stability of the reference model should be guaranteed first of all.

Assumption 4.3. *Given $Q = Q^\top > 0$, there exist $P(t) = P(t)^\top > 0$ and ϵ_3 such that*

$$A_m^\top(t) P(t) + P(t) A_m^\top = -Q, \quad \|\dot{P}\| \leq \epsilon_3 < q_{\min} \tag{4.26}$$

where $q_{\min}$ is the minimum eigenvalue of Q.

The above assumption implies that $P(t)$, and hence $A_m(t)$, vary slowly. This is indeed true because the time-vary characteristic of $A_m(t)$ originates from the slowly-varying $X_g(t)$. This assumption, in turn, implies that the time-derivative of the positive function

$$W = x_m^\top P x_m \tag{4.27}$$

along with (4.21) is given by

$$\dot{W} = x_m^\top(-Q + \dot{P}) x_m + 2 P \epsilon_x x_m \leq -(q_{\min} - \epsilon_3)\|x_m\|^2 + 2\|P\|\|\epsilon_x\|\|x_m\|. \tag{4.28}$$

Defining a compact set $\mathbf{M}$ such as

$$\mathbf{M} = \left\{ x_m \;\middle|\; \|x_m\| \leq \frac{2\|P\|\|\epsilon_x\|}{(q_{\min} - \epsilon_3)} \right\}. \tag{4.29}$$

Outside $\mathbf{M}$, we have $\dot{W} < 0$ so that the reference model in (4.21) is globally bounded.

Remark 4.2. *Assumption 4.3 is introduced primarily for the purpose of accommodating the reference model as in* (4.21). *Such a reference model may often be desired in an application in order to accommodate different transient characteristics at different trim points in the operating envelope.*

We now prove the main result of the chapter.

Theorem 4.1. *Under Assumptions 4.1, 4.2, and 4.3, the plant in* (4.15) *with the controller in* (4.22) *and the adaptive law in* (4.25), *has globally bounded solutions for all* $t \geq t_0$.

Proof. A Lyapunov candidate function is chosen as

$$V = e^\top P e + trace\left(\tilde{\theta}^\top \Gamma^{-1} \tilde{\theta} |\Lambda|\right) \tag{4.30}$$

where a time-derivative is given by

$$\begin{aligned} \dot{V} = &- e^\top \left(Q - \dot{P}\right) e + 2e^\top P \epsilon_x - 2trace\left(\tilde{\theta}^\top \Gamma^{-1} \dot{\theta}^*\right) \\ &- 2trace\left[\tilde{\theta}^\top \Gamma^{-1} \theta |\Lambda| \left(1 - \frac{\|\theta\|}{\theta^*_{max}}\right)^2 f(\theta)\right] \end{aligned} \tag{4.31}$$

where $|\Lambda| = sign(\Lambda)\Lambda$.

Two cases are considered, (i) $\|\theta\| \leq \theta^*_{\max}$ and (ii) $\|\theta\| \geq \theta^*_{\max}$.

Case (i): $\|\theta\| \leq \theta^*_{\max}$

$\|\theta\| \leq \theta^*_{\max}$ implies that $\|\tilde{\theta}\| \leq 2\theta^*_{\max}$ and $f(\theta) = 0$ from which we obtain

$$\dot{V} = -e^\top \left(Q - \dot{P}\right) e + 2e^\top P \epsilon_x - 2trace\left(\tilde{\theta}^\top \Gamma^{-1} \dot{\theta}^*\right). \tag{4.32}$$

By taking bounds on right-hand side of (4.32), we have

$$\dot{V} \leq -\left(q_{\min} - \epsilon_3\right)\|e\|^2 + 2\|P\|\|\epsilon_x\|\|e\| + 2\frac{\|\dot{\theta}^*\|}{\gamma_{\min}}\|\tilde{\theta}\| \tag{4.33}$$

where $\gamma_{\max(\min)}$ is the maximum(minimum) of the diagonal elements of Γ. Hence, we define a compact set D_1 as

$$D_1 = \left\{ \left(e, \tilde{\theta}\right) \middle| \left(\|e\| - \frac{\|P\|\|\epsilon_x\|}{q_{\min} - \epsilon_3}\right)^2 \leq k_1, \|\tilde{\theta}\| \leq 2\theta^*_{\max} \right\} \tag{4.34}$$

where

$$k_1 = \frac{4\|\dot{\theta}^*\|\theta^*_{\max}}{\gamma_{\min}(q_{\min} - \epsilon_1)} + \frac{\|P\|^2\|\epsilon_x\|^2}{(q_{\min} - \epsilon_1)^2}.$$

Case (ii): $\|\theta\| \geq \theta^*_{\max}$

Time derivative of V in (4.30) becomes

$$\begin{aligned} \dot{V} = &- e^\top \left(Q - \dot{P}\right) e + 2e^\top P\epsilon_x - 2trace\left(\tilde{\theta}^\top \Gamma^{-1}\dot{\theta}^*\right) \\ &- 2trace\left(\tilde{\theta}^\top \Gamma^{-1}\theta|\Lambda|\right)\left(1 - \frac{\|\theta\|}{\theta^*_{\max}}\right)^2 \end{aligned} \tag{4.35}$$

From (4.35), we have the following inequality as

$$\begin{aligned} \dot{V} \leq &-\left(q_{\min} - \epsilon_3\right)\|e\|^2 + 2\|P\|\|\epsilon_x\|\|e\| + 2\frac{\|\dot{\theta}^*\|}{\gamma_{\min}}\|\tilde{\theta}\| \\ &- 2\frac{\lambda_{\min}}{\gamma_{\max}}\|\tilde{\theta}\|\left(\|\tilde{\theta}\| - \frac{\lambda_{\max}\gamma_{\max}}{\lambda_{\min}\gamma_{\min}}\|\theta^*\|\right)\left(1 - \frac{\|\theta\|}{\theta^*_{\max}}\right)^2 \end{aligned} \tag{4.36}$$

where $\lambda_{\max(\min)}$ is the maximum(minimum) of the diagonal elements of $|\Lambda|$. We define a constant a_0 and K by

$$a_0 = \frac{\lambda_{\max}\gamma_{\max}}{\lambda_{\min}\gamma_{\min}}, \quad K = 1 + a_0 + \epsilon_4 \quad \epsilon_4 > 0. \tag{4.37}$$

We consider two sub-cases, (a) $\theta^*_{\max} < \|\theta\| \leq K\theta^*_{\max}$ and (b) $\|\theta\| > K\theta^*_{\max}$.

Sub-case (a): $\theta^*_{\max} < \|\theta\| \leq K\theta^*_{\max}$

For a given condition on $\|\theta\|$, we have following inequalities by using $K - 1 = a_0 + \epsilon_4$

$$\begin{aligned} \|\tilde{\theta}\| &\leq (K+1)\theta^*_{\max} \\ \|\tilde{\theta}\| - \frac{\lambda_{\max}\gamma_{\max}}{\lambda_{\min}\gamma_{\min}}\|\theta^*\| &\leq (K+1+a_0)\theta^*_{\max} \\ \left(1 - \frac{\|\theta\|}{\theta^*_{max}}\right)^2 &\leq (a_0+\epsilon_4)^2 \end{aligned} \tag{4.38}$$

Using these inequalities, we have

$$\begin{aligned} \dot{V} \leq &-(q_{\min} - \epsilon_3)\|e\|^2 + 2\|P\|\|\epsilon_x\|\|e\| + 2\frac{\|\dot{\theta}^*\|}{\gamma_{\min}}\|\tilde{\theta}\| \\ &+ 2\frac{\lambda_{\min}}{\gamma_{\max}}(K+1)(K+1+a_0)(a_0+\epsilon_4)^2\theta^{*2}_{\max} \end{aligned} \tag{4.39}$$

Therefore, we obtian a compact set D_2 as

$$D_2 = \left\{ (e,\tilde{\theta}) \middle| \left(\|e\| - \frac{\|P\|\|\epsilon_x\|}{q_{\min} - \epsilon_3}\right)^2 \leq k_2, \|\tilde{\theta}\| \leq (K+1)\theta^*_{\max} \right\} \tag{4.40}$$

where

$$k_2 = \frac{2(K+1)\|\dot{\theta}^*\|\theta^*_{\max}}{\gamma_{\min}(q_{\min} - \epsilon_3)} + \frac{\|P\|^2\|\epsilon_x\|^2}{(q_{\min} - \epsilon_3)^2} + \frac{2\lambda_{\min}(K+1)(K+1+a_0)(a_0+\epsilon_4)^2\theta^{*2}_{\max}}{\gamma_{\max}(q_{\min} - \epsilon_3)}.$$

Since $k_2 > k_1$, we note that $D_2 \supset D_1$.

Sub-case (b): $\|\theta\| > K\theta^*_{\max}$

In this case, we obtain following inequalities as

$$\begin{aligned} \|\tilde{\theta}\| = \|\theta - \theta^*\| &\geq (a_0+\epsilon_4)\theta^*_{\max}, \\ \left(1 - \frac{\|\theta\|}{\theta^*_{\max}}\right)^2 &\geq (a_0+\epsilon_4)^2, \\ \|\tilde{\theta}\| - \frac{\lambda_{\max}\gamma_{\max}}{\lambda_{\min}\gamma_{\min}}\|\theta^*\| \geq \|\tilde{\theta}\| - a_0\theta^*_{\max} &\geq \frac{\epsilon_4}{a_0+\epsilon_4}\|\tilde{\theta}\|. \end{aligned} \tag{4.41}$$

Correspondingly, we have from (4.36)

$$\dot{V} \leq -(q_{\min} - \epsilon_3)\|e\|^2 + 2\|P\|\|\epsilon_x\|\|e\| - 2\frac{\lambda_{\min}}{\gamma_{\max}}\epsilon_4(a_0 + \epsilon_4)\|\tilde{\theta}\|^2 + 2\frac{\|\dot{\theta}^*\|}{\gamma_{\min}}\|\tilde{\theta}\|. \quad (4.42)$$

Hence, we have a compact set D_3 as

$$D_3 = \left\{ (e,\ \tilde{\theta}) \;\middle|\; \left(\|e\| - \frac{\|P\|\|\epsilon_x\|}{q_{\min} - \epsilon_3}\right)^2 + \frac{k_3}{q_{\min} - \epsilon_3}\left(\|\tilde{\theta}\| - \frac{\|\dot{\theta}^*\|}{\gamma_{\min} k_3}\right)^2 \leq k_4 \right\} \quad (4.43)$$

where

$$k_3 = 2\frac{\lambda_{\min}}{\gamma_{\max}}\epsilon_4(a_0 + \epsilon_4), \quad k_4 = \frac{\|P\|^2\|\epsilon_x\|^2}{(q_{\min} - \epsilon_3)^2} + \frac{\|\dot{\theta}^*\|^2}{\gamma_{\min}^2 k_3 (q_{\min} - \epsilon_3)}.$$

We define a compact set D to be $D = D_2 \cup D_3$. Then, outside D, $\dot{V} \leq 0$ and this guarantees global boundedness of $(e,\ \tilde{\theta})$, which results in bounded x_p and θ. This, in turn, proves control input u is globally bounded. □

Remark 4.3. *The above proof established that outside the compact set, D, we have $\dot{V} < 0$ which in turn implies that all trajectories converge to the compact set. As a result, the tracking error is of the order of the variations in the gain-scheduling variables.*

4.4 Simulation

A nonlinear 6-DoF hypersonic aircraft model is employed to demonstrate the performance of the proposed adaptive controller in Section 4.2. To accommodate the nonlinear simulation studies, BANTAM architecture is utilized where the dynamics of a given aircraft model are loaded with aerodynamics data of the corresponding aircraft [9]. The aerodynamics data of NASA X-15 hypersonic aircraft discussed in [13] are combined with nonlinear flight controller which consists of a PI baseline controller and the adaptive controller. Details regarding NASA X-15 hypersonic aircraft

are discussed in Appendix A. The nonlinear flight dynamics is written in the form of

$$\dot{\mathbb{X}} = F(\mathbb{X}, \mathbb{U}) \tag{4.44}$$

whose states and inputs are represented as

$$\begin{aligned} \mathbb{X} &= [V_T \ \alpha \ \beta \ \bar{P} \ \bar{Q} \ \bar{R} \ \Phi \ \Theta \ \Psi \ N \ E \ D]^\top \\ \mathbb{U} &= [U_{Thrust} \ U_{Left} \ U_{Right} \ U_{Rudder}]^\top. \end{aligned} \tag{4.45}$$

where U_{Left} and U_{Right} are the left and right control surface of the elevon system. The elevator and aileron inputs can be computed as

$$U_{Elevator} = \frac{U_{Left} + U_{Right}}{2}, \qquad U_{Aileron} = \frac{U_{Left} - U_{Right}}{2}. \tag{4.46}$$

Neglecting decoupled or weakly coupled states and inputs in (4.44), the nonlinear plant in (4.44) is cast into the form of (4.1) with states and inputs as

$$\begin{aligned} X &= [\alpha \ \beta \ P \ Q \ R]^\top, \qquad U_1 = [U_{Aileron} \ U_{Elevator_1} \ U_{Rudder}]\top \\ X_g &= [V \ h]^\top, \qquad U_2 = [U_{Thrust} \ U_{Elevator_2}]^\top. \end{aligned} \tag{4.47}$$

Since the elevator input controls both the pitching moment and the altitude, it is decomposed into two parts: $U_{Elevator_1}$ and $U_{Elevator_2}$. Considering the difference in the dynamic characteristics of the pitching moment and the altitude, this decomposition is plausible based on the time-scale.

4.4.1 Nominal Controller Design

To begin with, the outer loop controller, $h_c(X_g, X_{g,cmd})$, is designed to adjust the gain scheduling variables h, V so that they track the designed command signals h_{cmd}, V_{cmd} respectively. This controller closes the loop using the error between the actual and commanded signals. A fixed PID controller (with an approximated derivative) is

chosen, with a transfer function given by

$$G_c(s) = K_p + \frac{K_i}{s} + \frac{K_d s}{Ns+1}. \tag{4.48}$$

The PID gains for both velocity and altitude controllers are tuned based on Ziegler-Nichols tuning rule [10].

As the second step, we find the flight envelope of NASA X-15 [13] in which we selected 44 trim points for the purpose of nominal (inner-loop) controller design as shown in Figure 4-5. The intervals in Figure 4-5 between trim points are determined

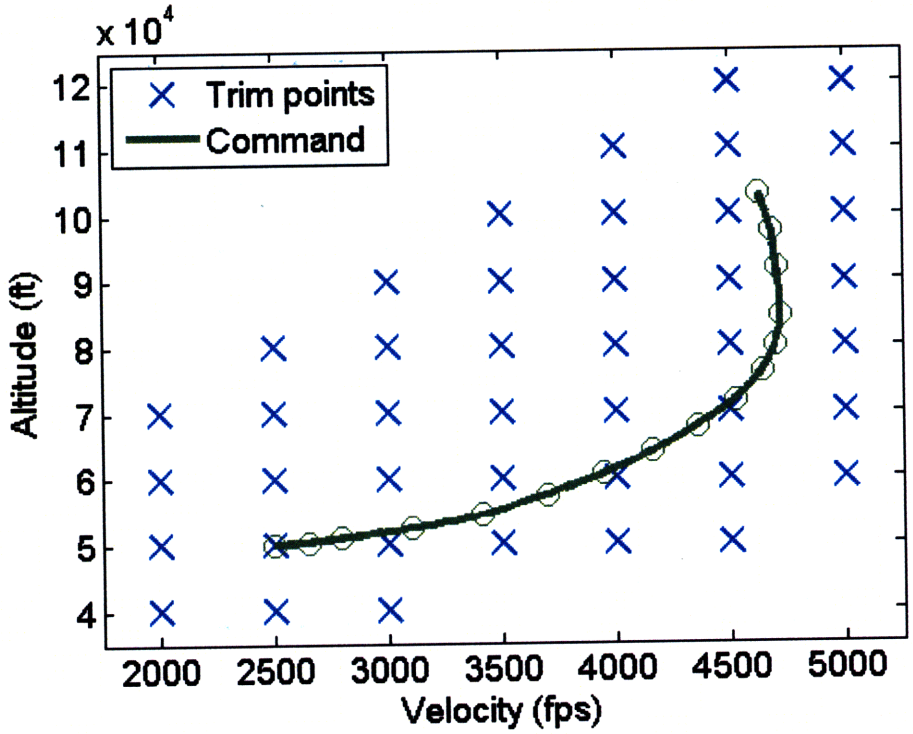

Figure 4-5: Trim points and commands (h_{cmd}, V_{cmd}) on the $V - h$ space.

such that that the linearization error, $\epsilon_x(t)$, in (3.5) is sufficiently small. The simulation is executed for 150s while the command, $X_{g,cmd}$ is given as shown in Figure 4-5. The initial altitude is 50,000ft and it increases up to 100,000ft, and the velocity increases by more than 4,500fps (Mach 5). Green circles on the command line in Figure 4-5 indicate the way-points for every 10s. Figure 4-6 shows profiles of the velocity and alitutde commands.

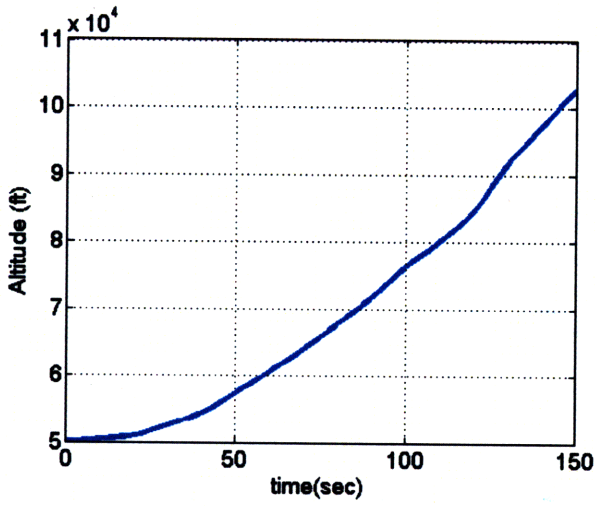

(a) Altitude command

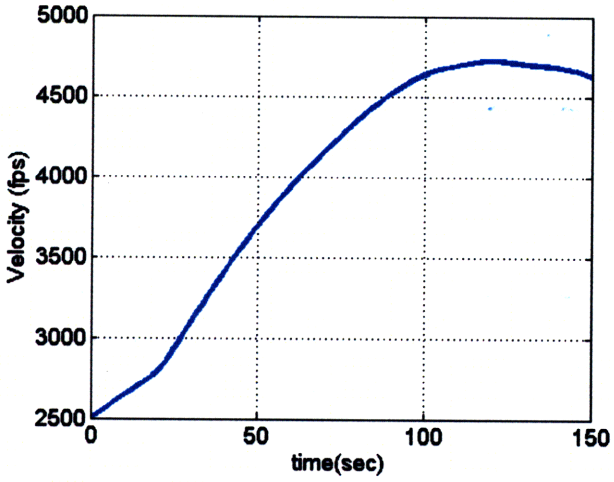

(b) Velocity command

Figure 4-6: Profiles of altitude and velocity commands

Linearizing the nonlinear flight dynamics in (4.1) at each trim point, we obtain the linearized plant and combine the integral actions with the linearized plant. The controller state vector, x_c, in (4.13) consists of e_p, e_α, and e_r given by

$$\begin{aligned} e_p &= \int_0^t [P^*(t) - P(t)]\, dt, \quad e_\alpha = \int_0^t [\alpha^*(t) - \alpha(t)]\, dt, \text{ and} \\ e_r &= \int_0^t [R^*(t) - R(t)]\, dt \end{aligned} \tag{4.49}$$

where $X^*(t) = [\alpha^*(t)\ \beta^*(t)\ P^*(t)\ Q^*(t)\ R^*(t)]^\top$ is the desired state defined in (4.8).

This, in turn, determines the error combination matrix B_c as

$$B_c = \begin{bmatrix} 0 & 0 & -1 & 0 & 0 \\ -1 & 0 & 0 & 0 & 0 \\ 0 & 0 & 0 & 0 & -1 \end{bmatrix}. \tag{4.50}$$

As the linearized plant in (4.17) is constructed, we design LQR PI controller by minimizing the the cost function given by

$$J_i = \int_0^\infty x_p^\top \left(Q_i + K_i R_i K_i^\top\right) x_p dt \tag{4.51}$$

where K_i is the controller gain. Figure 4-7(a) shows the pole location of the open-

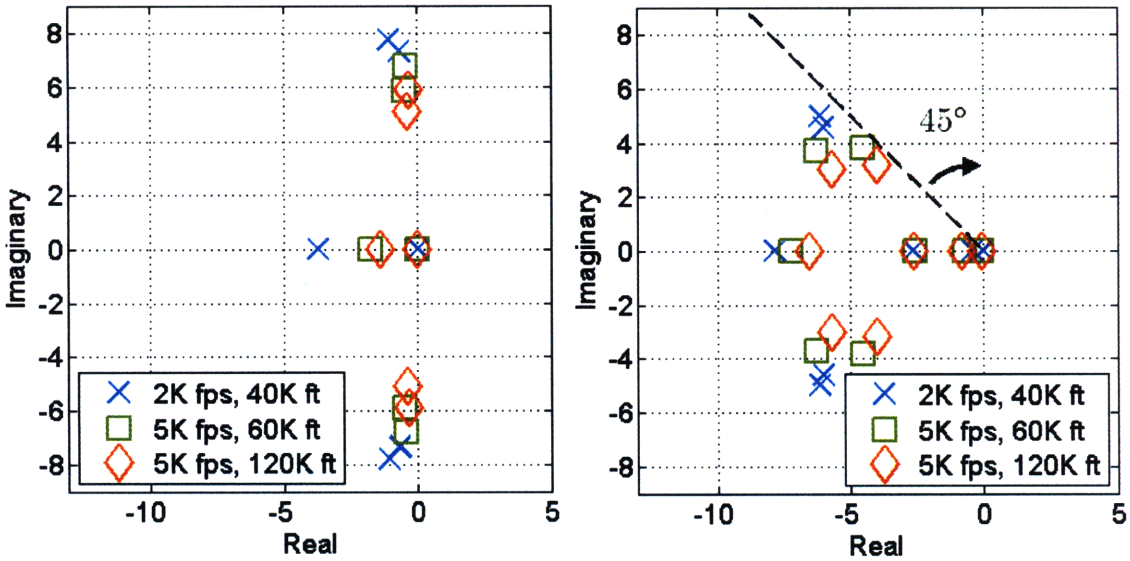

(a) Pole location of open-loop plants, $A_{p,i}$ (b) Pole location of reference models, $A_{m,i}$

Figure 4-7: Poles of the open-loop plants and the reference models

loop system at three different trim points: (2,000fps, 40,000ft), (5,000fps, 60,000ft), and (5,000fps, 120,000ft). This plot implies dynamic characteristics of the plant vary significantly as trim points differ, which necessitates a gain-scheduling controller. We also note that as altitude and velocity become higher, open-loop poles are closer to imaginary axis, and damping characteristic becomes worse. In Figure 4-7(b), poles of the reference model are described for the same three trim points. The poles of the

reference model at each frozen trim point is located such that the dominant damping ratio is less than 0.7. To meet this specification as well as well-behaved steady state performance, we choose Q_i and R_i in (4.51).

4.4.2 Adaptive Controller Design

First of all, we note that $h_c(X_g, X_{g,cmd})$ in the outermost-loop is a fixed controller. Since $h_c(X_g, X_{g,cmd})$ only controls slow state variables, it enables those variables to track given commands in the presence of uncertainties. However, as uncertainties heighten, the performance of $h_c(X_g, X_{g,cmd})$ will worsen which later requires the design of adaptive parts in $h_c(X_g, X_{g,cmd})$ for improved performance. This will be developed in future studies.

The adaptive controller is augmented with the nominal gain-scheduling controller. The adaptive parameter, $\theta(t)$, is governed by the adaptive law specified in (4.25). Q is chosen as $10I_{8\times 8}$ and $P(t)$ is followed by solving $A_m^\top(t)P(t) + P(t)A_m(t) = -Q$ at each time step. The adaptive rate, Γ, is determined based on the heuristic rule [8].

4.4.3 Simulation Results

The controllers, $h_c(X_g, X_{g,cmd})$, u_{nom}, and u_{ad}, are employed to the 6-DoF nonlinear plant in (4.44). To represent the uncertainties in the plant, the control failure, $\Lambda = diag([1 \quad 0.4 \quad 1])$, is introduced at 30s and this failure implies a 60% loss of congrol surface effectiveness on the right elevon and no losses in the other control surfaces. In practice, the NASA X-15 has the input saturation limits which are included in this simulation study. The limit for the left and right elevons is 30° and one for the rudder is set to 15°. Stability analysis guarantees the global boundedness of signals in the closed-loop system in a similar manner as derived in Section 4.3. Figure 4-8 shows the overall command-following performance of the proposed controller. When the uncertainty occurs at 30s, the adaptive controller combined with the gain-scheduling nominal one is able to stabilize and complete the commanded mauneuver. Even the non-augmented adaptive controller performs the tracking in a

stable manner. However, the plant only with the nominal controller starts to deviate from the command around 40s and results in instabilty.

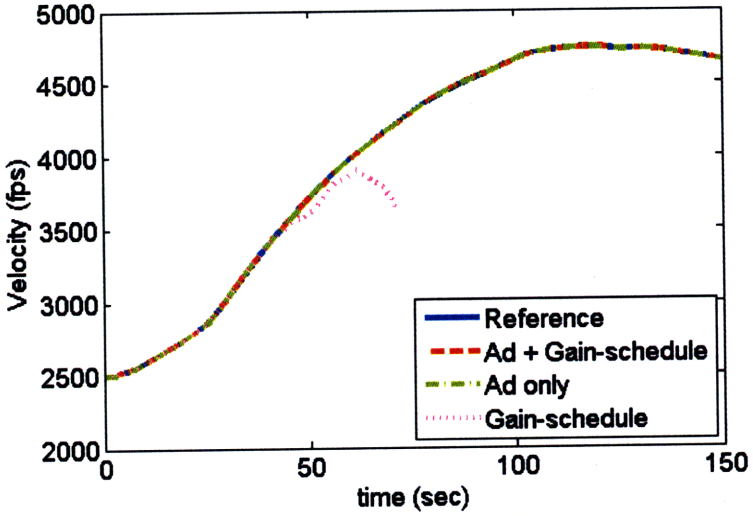

(a) Velocity command-following

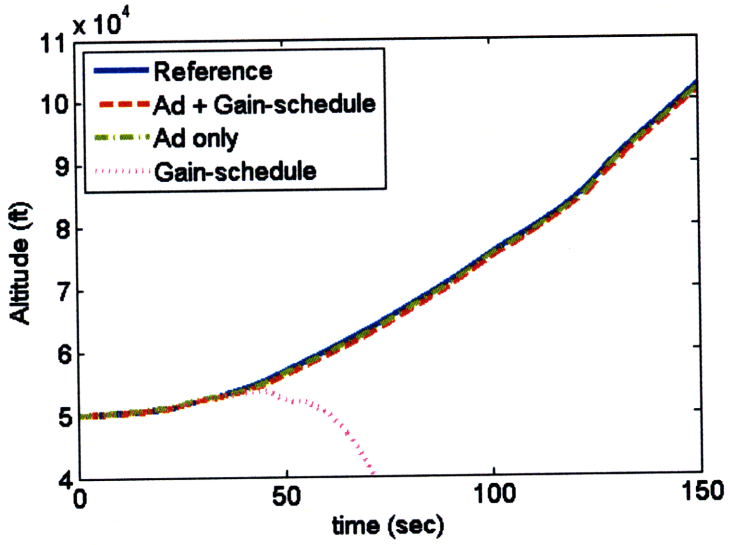

(b) Altitude command-following

Figure 4-8: Velocity and altitude command-following in the presence of the uncertainty, Λ.

Figure 4-9 shows the state variables of the closed loop systems and the reference model, where the performance of the augmented adaptive controller (denoted as "Ad + gain-schedule") is compared with the nominal controller (denoted as "Gain-Schedule").

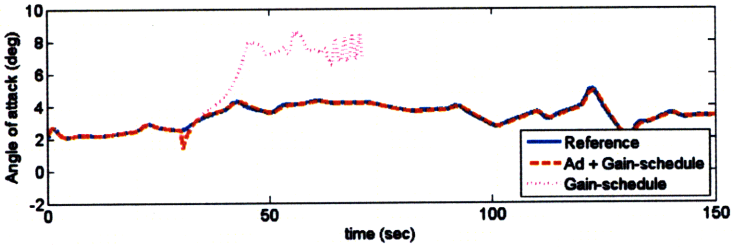

(a) Angle of attack (α)

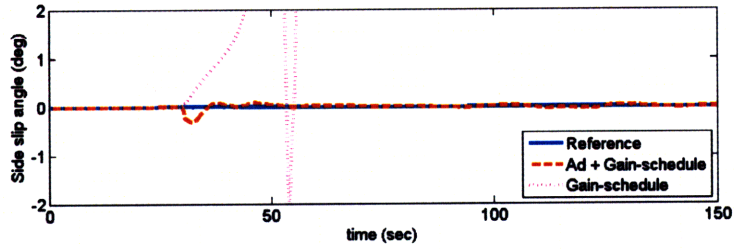

(b) Side slip angle (β)

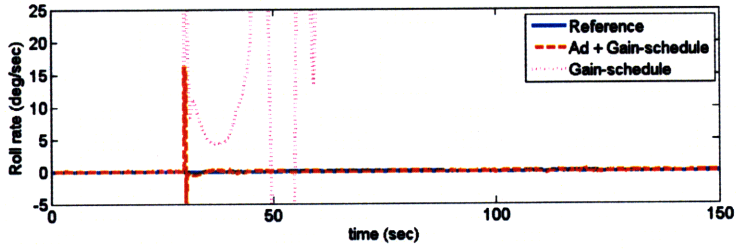

(c) Roll rate (P)

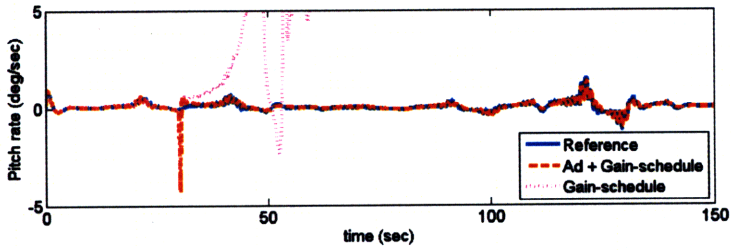

(d) Pitch rate (Q)

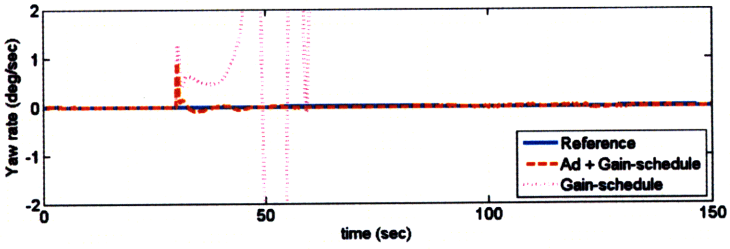

(e) Yaw rate (R)

Figure 4-9: State variables of the closed loop systems and the reference model

The state variables includes angle of attack (α), side-slip angle (β), roll rate (P), pitch rate (Q), and roll rate (R). When the control failure occurs at 30s, all state variables become unstable with the nominal gain-scheduling controller whereas instability is overcome when the adaptive controller is augmented with the nominal one. As the asymmetric uncertainty, Λ, generates the rolling and pitching moment instantly, the nominal controller is unable to regulate P and R which results in the sudden increase of β. The elevator and aileron inputs in the augmented adaptive control intelligently increase their magnitudes to cope with the uncertainties so that P and R are corrected back to those of the reference model.

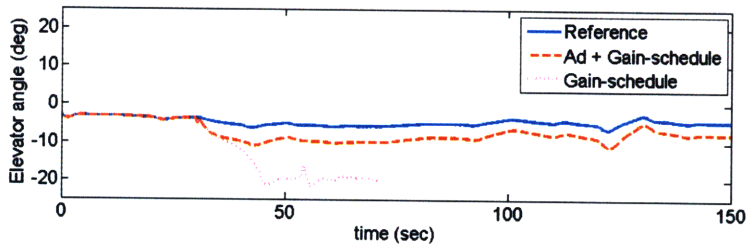

(a) Elevator

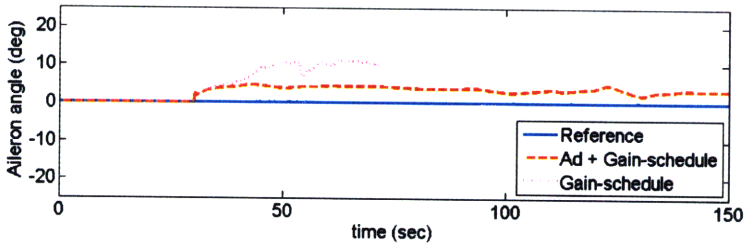

(b) Aileron

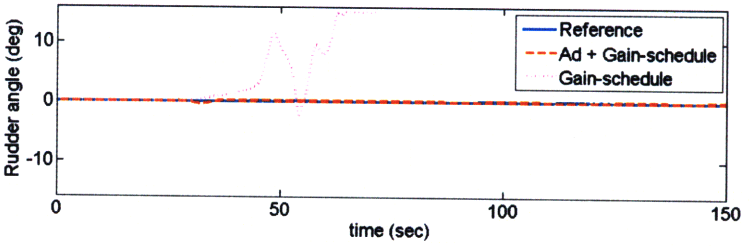

(c) Rudder

Figure 4-10: Control surfaces of the closed loop systems and the reference model

When the control failure occurs at 30s, the elevator and the aileron are deflected to mitigate the adverse effect of the control failure while satisfactory tracking perfor-

mance is carried out simultaneously. As shown in Figure 4-10, as instability worsens, the rudder is saturated at 60s which explains that the failure of the nominal controller is primarily due to the uncertainty not the saturation.

For comparison purposes, we consider the case (denoted as "Ad only") where only the adaptive controller is used without the gain-scheduling nominal controller, and is illustrated in Figure 4-11. Even though stability is guaranteed and the command-following of the velocity and altitude is obtained with both the augmented and non-augmented adaptive controllers, it has undesirable oscillations in P, Q, and R with the non-augmented adaptive controller particularly when the uncertainty occurs.

In Figure 4-12, control inputs are shown when the adaptive control is designed without the nominal gain-scheduling controller. Since P, Q, and R with the non-augmented adaptive controller have high oscillations, the control inputs also show high frequency signals which is not desirable to aircraft control surfaces. This demonstrates that the augmented adaptive controller shows better performance because a-priori knowledge about the plant is utilized in the controller design appropriately. Overall, it could be argued that the gain-scheduling controller deals with the variation in the plant dynamics between trim points while the adaptive component copes with the variation due to the uncertainty.

4.5 Summary

In this chapter, we have introduced design, stability analysis, and validation of an adaptive control in augmentation with gain-scheduling for the control of nonlinear plants with multi-rate state variables. The adaptive control architecture includes an outer-loop and an inner-loop controller. The former controls the slow state variables whereas the later is designed to regulate fast ones. The adaptive controller augmented with the nominal gain-scheduling controller is proposed for the inner-loop controller and a fixed controller is designed in the outer-loop. The adaptive law is derived based on Lyapunov stability theory and global boundedness of states and control inputs is proved.

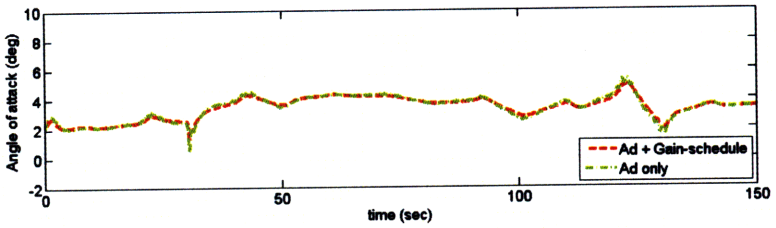

(a) Angle of attack (α)

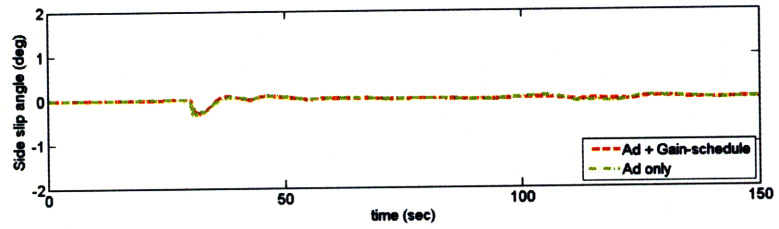

(b) Side slip angle (β)

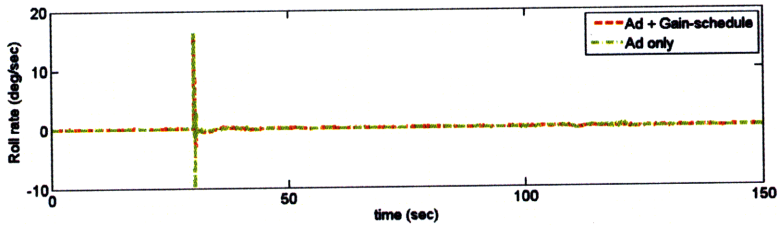

(c) Roll rate (P)

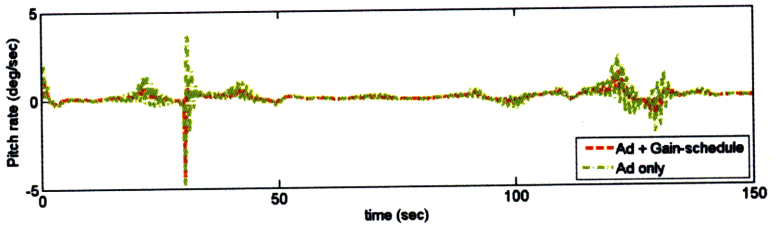

(d) Pitch rate (Q)

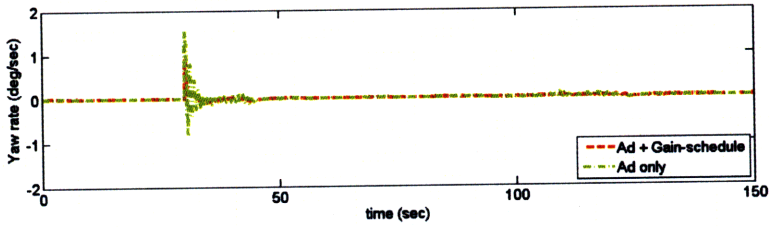

(e) Yaw rate (R)

Figure 4-11: State variables of augmented and non-augmented adaptive control

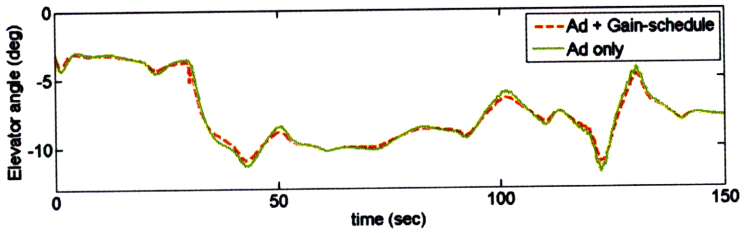

(a) Elevator

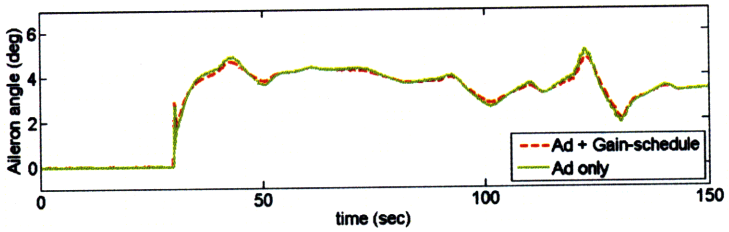

(b) Aileron

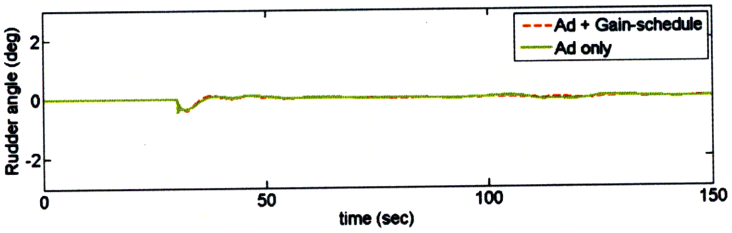

(c) Rudder

Figure 4-12: Control surfaces of augmented and non-augmented adaptive control

Nonlinear 6-DOF flight dynamics of a hypersonic aircraft is employed to validate the control architecture through simulations. The adaptive controller proposed has the benefit of safe performance compared to the nominal controller. It is also shown that the augmented adaptive controller performs better than non-augmented one.

Chapter 5

Stability Margins for Adaptive Control in the Presence of Time-delay

In this chapter, we derive stability margins for adaptive control. The starting point of the derivation is well known stability properties of adaptive control. In the absence of perturbations due to unmodeled dynamics, delays, or disturbances, the underlying closed-loop system obtained with the adaptive controller can be shown to be stable under certain conditions [28]. In such cases, the closed-loop system transitions to a linear time-invariant system asymptotically when constant command signals are given. Therefore, one can argue that the stability margins of the adaptive system tend toward this "asymptotic" linear system. However, the response of the adaptive system, understandably, is more vulnerable to perturbations during the initial transient stage where the overall system is markedly nonlinear. As such, the degrees of robustness that the adaptive system has with respect to the perturbations during the transient stage are the margins that become relevant. Therefore, in this chapter, we focus on the margins of the AFCS during the adaptive phase. Standard stability and robustness tools used for adaptive systems in [28, 15] are utilized in order to derive these margins. The stability margins are validated with the NASA X-15 and then they are compared with margins from simulation studies. To reduce the conservatism

in the stability margins, we introduce numerical methods which are demonstrated with a generic transport model aircraft.

5.1 Problem Statement

The motivation for adaptive control stems from several causes including aerodynamic uncertainties, modeling inaccuracies, environmental disturbances and the fact that often actuators used in flight control can exhibit various anomalies such as loss of effectiveness, saturation, or failure, the last of which is our focus in this chapter. The problem is under consideration is the control of a linear plant of the form

$$\begin{aligned} \dot{x} &= Ax + bu \\ y &= c^\top x \end{aligned} \tag{5.1}$$

where $x \in \mathbb{R}^n$ is the state, $y \in \mathbb{R}$ is the output, and $u \in \mathbb{R}$ is the control input of the plant. $A \in \mathbb{R}^{n\times n}$, $b \in \mathbb{R}^n$, and $c \in \mathbb{R}^n$ are a known system, input, and output matrices respectively. Suppose that there exists uncertainties and disturbances in the plant in (5.1), leading to a description

$$\begin{aligned} \dot{x} &= A_\lambda x + b\lambda(u + d) \\ y &= c^\top x \end{aligned} \tag{5.2}$$

where $A_\lambda \in \mathbb{R}^{n\times n}$ is an unknown system matrix, and $\lambda \in \mathbb{R}$ represents parametric uncertainties in the plant. It is assumed that the sign of λ is known. The main goal of the controller design is that the output tracks a given command signal in spite of uncertainties and disturbances. For this purpose, we integrate the output tracking error as

$$\dot{x}_c = y - r \tag{5.3}$$

where $x_c \in \mathbb{R}$ is the controller state vector and $r \in \mathbb{R}$ is a command signal such that $|r| \leq r_0$ without loss of generality. The overall plant to be controlled is outlined by

combining (5.2) with (5.3) as

$$\underbrace{\begin{bmatrix} \dot{x} \\ \dot{x}_c \end{bmatrix}}_{\dot{x}_p} = \underbrace{\begin{bmatrix} A_\lambda & \mathbf{0}_{n\times 1} \\ c^\top & 0 \end{bmatrix}}_{A_{p\lambda}} \underbrace{\begin{bmatrix} x \\ x_c \end{bmatrix}}_{x_p} + \underbrace{\begin{bmatrix} b \\ 0 \end{bmatrix}}_{b_{p_1}} \lambda(u+d) + \underbrace{\begin{bmatrix} \mathbf{0}_{n\times 1} \\ -1 \end{bmatrix}}_{b_{p_2}} r \tag{5.4}$$

or equivalently

$$\dot{x}_p = A_{p\lambda} x_p + b_{p_1}\lambda(u+d) + b_{p_2} r \tag{5.5}$$

where $x_p \in \mathbb{R}^{n_p}$, $A_{p\lambda} \in \mathbb{R}^{n_p \times n_p}$, $b_{p_1} \in \mathbb{R}^{n_p}$, and $b_{p_2} \in \mathbb{R}^{n_p}$.

Into the plant in (5.5), we now introduce nonparametric uncertainties that may occur due to time-delays in communication and processing or other unmodeled dynamics. While the rest of this chapter focuses only on time-delays, the same analysis holds for unmodeled dynamics as well. With an unknown input delay τ, the plant can be written as

$$\dot{x}_p = A_{p\lambda} x_p + b_{p_1}\lambda(e^{-\tau s}u + d) + b_{p_2} r. \tag{5.6}$$

For the purpose of analysis, $e^{-\tau s}$ can be approximated as the (n, n) Pade approximation in the form of

$$e^{-\tau s} \cong 1 + \frac{q_\Delta(s)}{p_\Delta(s)} \tag{5.7}$$

and $p_\Delta(s)$ is Hurwitz. Since the approximation is only valid on a certain range of frequencies, its usage needs to be justified. This issue will be discussed in Section 5.4.2. Then, the input delay is considered as an unmodeled dynamics in the control input as shown in figure 5-1. Therefore, the plant in (5.6) is approximated to

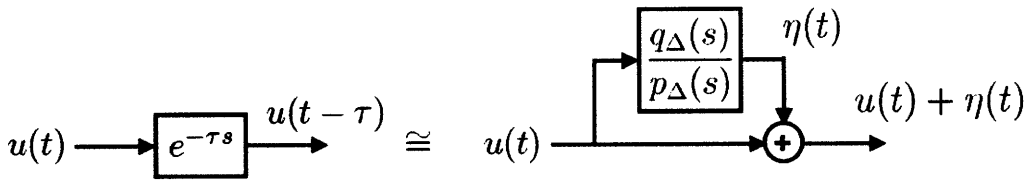

Figure 5-1: Time-delay approximation

$$\dot{x}_p = A_{p\lambda} x_p + b_{p_1}\lambda(u + \eta + d) + b_{p_2} r, \quad \eta = \frac{q_\Delta(s)}{p_\Delta(s)} u. \tag{5.8}$$

This assumption implies that the effect of time-delays can be approximated with the state-dependent disturbance η. Defining $\xi = [\eta \quad \tau\dot{\eta} \quad \tau^2\ddot{\eta} \cdots \tau^n\eta^{(n)}]^\top$, the state-space representation of $q_\Delta(s)/p_\Delta(s)$ can be derived as

$$\begin{aligned} \dot{\xi} &= \frac{1}{\tau}A_\tau\xi + b_\tau\dot{u} \\ \eta &= c_\tau\xi \end{aligned} \tag{5.9}$$

We note that the boundedness of ξ is not guaranteed even though A_τ is a stable matrix, since $\dot{u}$ has not been shown to be bounded. Hence ξ should be viewed as a state-dependent disturbance. The overall goal of this chapter is to design an adaptive controller in the presence of both parametric and non-parametric uncertainties such as delay, and to derive the guaranteed margins of the closed-loop system with proposed adaptive controller. We will also investigate the effect of adaptive parameters on the margins.

5.2 Adaptive controller

5.2.1 Nominal controller and reference model design

In order to ensure that all available information about the plant is utilized to obtain the best performance, the adaptive controller is designed in augmentation with a nominal controller. The nominal controller input, u_{nom}, is chosen as

$$u_{nom} = k^\top x_p \tag{5.10}$$

where $k \in \mathbb{R}^{n_p}$ is the nominal feedback gain. The nominal control input is designed so as to optimize the performance in the absence of uncertainties, disturbances, and unmodeled dynamics. Combining the nominal controller with the plant that does not have uncertainties and time-delays, the reference model is generated as

$$\dot{x}_m = A_m x_m + b_m r \tag{5.11}$$

where

$$A_m = A_p + b_{p_1} k^\top, \quad b_m = b_{p_2}, \quad A_p = \begin{bmatrix} A & 0 \\ c^\top & 0 \end{bmatrix}. \tag{5.12}$$

Since (A_p, b_{p_1}) is controllable, k can be chosen to ensure that A_m is Hurwitz. The reference model is the desired dynamics which need to be tracked by the adaptive controller. As the size of the delay is not known, the reference model is designed without the delayed input.

5.2.2 Adaptive controller design

An adaptive controller is designed based on the modeled part of the plant in (5.2) and the reference model. The overall control input, u, consists of the nominal and adaptive controller as

$$u = u_{nom} + u_{ad} \tag{5.13}$$

and we design the adaptive part as

$$u_{ad} = \theta^\top \omega = \begin{bmatrix} \theta_x^\top & \theta_d \end{bmatrix} \begin{bmatrix} x_p \\ 1 \end{bmatrix} \tag{5.14}$$

where $\theta \in \mathbb{R}^{n+1}$ is the adaptive parameter.

Assumption 5.1. *There exists an ideal gain $\theta^* = [\theta_x^{*\top} \quad \theta_d^*]^\top$ such that the plant can be matched with the reference model in the absence of delay, i.e.*

$$A_m = A_{p\lambda} + b_{p_1}\lambda(k + \theta_x^*)^\top, \quad \theta_d^* + d = 0. \tag{5.15}$$

We define the tracking error to be $e = x_p - x_m$ and the adaptive parameter error to be $\tilde{\theta} = \theta - \theta^*$. Subtracting the reference model in (5.11) and the plant in (5.2), we have an error dynamics as

$$\dot{e} = A_m e + b_{p_1}\lambda\tilde{\theta}^\top\omega + b_{p_1}\lambda\eta. \tag{5.16}$$

The adaptive parameter is governed by the following law as

$$\dot{\theta} = -\gamma\omega e^{\top} P b_{p_1} sign(\lambda) - \sigma\theta \tag{5.17}$$

where $P = P^{\top} > 0$ is the solution of $A_m^{\top} P + P A_m = -Q$ for a given $Q = Q^{\top} > 0$ and $\gamma > 0$ determines the adaptive rate. It should be noted that while (17) is an adaptive law based on sigma-modification, other standard methods that have been proposed in the literature for robust adaptive control can also be used with equivalent results. In the absence of the unmodeled dynamics, i.e. $q_{\Delta}(s)/p_{\Delta}(s) = 0$, it is straightforward to establish the global boundedness and asymptotic tracking of the closed-loop system with the proposed adaptive controller using standard Lyapunov stability analysis and robustness arguments in [28].

5.3 Delay Margins

We now derive the stability properties of the adaptive system in the presence of perturbations due to $q_{\Delta}(s)/p_{\Delta}(s) \neq 0$. First of all, we introduce the concept of semi-global boundedness.

Definition 5.1. *A system*

$$\dot{x} = G(x,\ u) \tag{5.18}$$

is said to be semi-globally bounded if, for each compact subset $E \subset \Re^n$ where $E^* \subset E$ for a compact subset $E^* \subset \Re^n$, there exists a feedback control input $u = u(x)$ such that the solutions $x(t)$ of the corresponding closed loop system , $\dot{x} = G(x,\ u(x))$, remain bounded inside E.

We note that when there is no disturbance, equilibrium points exist, and E^* shrinks to those equilibrium points; in such a case, semi-global boundedness can be conversed to semi-global stability as in [16]. In what follows, we first derive the guaranteed delay margins for the case of $(1, 1)$ Pade approximation.

5.3.1 (1,1) Pade approximation

The (1,1) Pade approximation of $e^{-\tau s}$ is described as

$$e^{-\tau s} \cong \frac{-s + 2/\tau}{s + 2/\tau} \tag{5.19}$$

and then we have the unmodeled dynamics $q_\Delta(s)/p_\Delta(s)$ as

$$\frac{q_\Delta(s)}{p_\Delta(s)} = \frac{-2s}{s + 2/\tau}. \tag{5.20}$$

To analyze the stability of the closed-loop system in the presence of $q_\Delta(s)/p_\Delta(s) \neq 0$, we express the unmodeled dynamics as the state form of

$$\dot{\eta} = -\frac{2}{\tau}\eta - 2\dot{u}. \tag{5.21}$$

For the purpose of simplicity in stability analysis, $y \in \mathbb{R}^{2n+2}$ is defined as $y = [e^\top \ \tilde{\theta}^\top \ \eta]^\top$.

Theorem 5.1. *The system in* (5.2) *in the presence of* $(1,1)$ *Pade approximation with the controller in* (5.13) *based on the adaptive law in* (5.17), *there exist* $\tau_m > 0$ *and* $y_{\max} > 0$ *such that* $x(t)$, $\theta(t)$, *and* $\eta(t)$ *have bounded trajectories for all* $t > t_0$ *if*

i. $0 < \tau < \tau_m$,

ii. $\|y(t_0)\| < y_{\max}$.

Furthermore, τ_m *is defined as a delay margin.*

Proof. We propose a Lyapunov candidate function as

$$V = e^\top P e + \frac{|\lambda|}{\gamma}\tilde{\theta}^\top\tilde{\theta} + \frac{\tau}{2}(e + b_{p_1}\lambda\eta)^\top P(e + b_{p_1}\lambda\eta). \tag{5.22}$$

The time-derivative of V can be obtained along the trajectories of (5.9), (5.16), and (5.17) as

$$\dot{V} = -e^\top Q e - \frac{2\sigma|\lambda|}{\gamma}\tilde{\theta}^\top\tilde{\theta} - 2\lambda^2 b_{p_1}^\top P b_{p_1}\eta^2 + \tau H(e,\tilde{\theta},\eta) - \frac{2\sigma|\lambda|}{\gamma}\tilde{\theta}^\top\theta^* \tag{5.23}$$

where

$$
\begin{aligned}
H(e,\tilde{\theta},\eta) = &-\frac{1}{2}e^\top Qe + \lambda b_{p_1}^\top Pe\tilde{\theta}^\top\omega + \lambda b_{p_1}^\top Pe\eta - 2\lambda b_{p_1}^\top Pe\dot{u} + \lambda b_{p_1}^\top PA_m e\eta \\
&+ \lambda^2 b_{p_1}^\top Pb_{p_1}\tilde{\theta}^\top\omega\eta + \lambda^2 b_{p_1}^\top Pb_{p_1}\eta^2 - 2\lambda^2 b_{p_1}^\top Pb_{p_1}\eta\dot{u}.
\end{aligned} \tag{5.24}
$$

From (5.13), we have $\dot{u} = k^\top\dot{x}_p + \dot{\theta}^\top\omega + \theta^\top\dot{\omega}$. In order to find a upper bound of $H(e,\tilde{\theta},\eta)$ in terms of $\|e\|$, $\|\tilde{\theta}\|$, and $|\eta|$, we need to find the upper bound of $-2\lambda b_{p_1}^\top Pe\dot{u}$ and $-2\lambda^2 b_{p_1}^\top Pb_{p_1}\dot{u}\eta$ first of all. Based on the adaptive law in (5.17), $-2\lambda b_{p_1}^\top Pe\dot{u}$ can be rewritten as

$$
\begin{aligned}
-2\lambda b_{p_1}^\top Pe\dot{u} &= -2\lambda b_{p_1}^\top Pe\left(k^\top\dot{x}_p + \dot{\theta}^\top\omega + \theta^\top\dot{\omega}\right) \\
&= -2\lambda b_{p_1}^\top Pe(k^\top\dot{x}_p + \theta^\top\dot{\omega}) + 2|\lambda|\gamma e^\top Pb_{p_1}b_{p_1}^\top Pe\omega^\top\omega \\
&\quad + 2\lambda\sigma b_{p_1}^\top Pe\theta^\top\omega
\end{aligned} \tag{5.25}
$$

We note that $\|\cdot\|$ denotes the vector 2-norm for a vector and it also denotes the matrix norm induced by the vector 2-norm for a matrix. From the bound on r, we have

$$
\|x_m\| \le c_0 r_0, \quad \|\dot{x}_m\| \le (\|A_m\|c_0 + \|b_m\|)\, r_0 \tag{5.26}
$$

for a constant $c_0 > 0$. Following inequalities can be useful to find the upper bound of (5.25):

$$
\begin{aligned}
\omega^\top\omega &= x_p^\top x_p + 1 = \|e\|^2 + 2x_m^\top e + \|x_m\|^2 + 1 \\
&\le \|e\|^2 + 2c_0 r_0\|e\| + c_0^2 r_0^2 + 1, \\
\theta^\top\omega &\le \|\tilde{\theta} + \theta^*\|\|\omega\| \\
&\le \|\tilde{\theta} + \theta^*\|(\|x_p\| + 1) \\
&\le (\|\tilde{\theta}\| + \|\theta^*\|)(\|e\| + \|x_m\| + 1) \\
&\le \|e\|\|\tilde{\theta}\| + \|\theta^*\|\|e\| + (c_0 r_0 + 1)\|\tilde{\theta}\| + (c_0 r_0 + 1)\|\theta^*\|.
\end{aligned} \tag{5.27}
$$

From (5.27), we obtain inequalities as

$$
\begin{aligned}
2|\lambda|\gamma e^\top P b_{p_1} b_{p_1}^\top P e \omega^\top \omega \leq & 2|\lambda|\gamma \|b_{p_1}^\top P\|^2 \Big[\|e\|^4 + 2c_0 r_0 \|e\|^3 + (c_0^2 r_0^2 + 1)\|e\|^2\Big] \\
2\lambda\sigma b_{p_1}^\top P e \theta^\top \omega \leq & 2|\lambda|\sigma \|b_{p_1}^\top P\| \Big[\|e\|^2 \|\tilde{\theta}\| + \|\theta^*\| \|e\|^2 \\
& + (c_0 r_0 + 1)\|e\| \|\tilde{\theta}\| + (c_0 r_0 + 1)\|\theta^*\| \|e\|\Big].
\end{aligned} \tag{5.28}
$$

We also have

$$
\begin{aligned}
& - 2\lambda b_{p_1}^\top P e (k^\top \dot{x}_p + \theta^\top \dot{\omega}) \\
& = -2\lambda b_{p_1}^\top P e (k + \theta_x)^\top (A_m e + b_{p_1} \lambda \tilde{\theta}^\top \omega + b_{p_1} \lambda \eta + \dot{x}_m) \\
& \leq 2|\lambda| \|b_{p_1}^\top P\| \left(\|\tilde{\theta}\| + \|k + \theta_x^*\|\right) \|A_m\| \|e\|^2 \\
& + 2\lambda^2 b_{p_1}^\top P b_{p_1} \|e\| \left(\|\tilde{\theta}\| + \|k + \theta_x^*\|\right) \Big[\|e\| \|\tilde{\theta}\| + (c_0 r_0 + 1)\|\tilde{\theta}\| + |\eta|\Big] \\
& + 2|\lambda| \|b_{p_1}^\top P\| \|e\| \left(\|\tilde{\theta}\| + \|k + \theta_x^*\|\right) (\|A_m\| c_0 + \|b_m\|) r_0.
\end{aligned} \tag{5.29}
$$

Combining (5.27) and (5.29), we have the upper bound of $-2\lambda b_{p_1}^\top P e \dot{u}$ in descending powers of $\|e\|$, $\|\tilde{\theta}\|$, and $|\eta|$ as

$$
\begin{aligned}
& - 2\lambda b_{p_1}^\top P e \dot{u} \\
& \leq 2\gamma |\lambda| \|b_{p_1}^\top P\|^2 \|e\|^4 + 2\lambda^2 b_{p_1}^\top P b_{p_1} \|e\|^2 \|\tilde{\theta}\|^2 \\
& + 4\gamma |\lambda| c_0 r_0 \|b_{p_1}^\top P\|^2 \|e\|^3 + 2\Big[|\lambda| \|b_{p_1}^\top P\| (\sigma + \|A_m\|) + \lambda^2 b_{p_1}^\top P b_{p_1} \|k + \theta_x^*\|\Big] \|e\|^2 \|\tilde{\theta}\| \\
& + 2\lambda^2 b_{p_1}^\top P b_{p_1} (c_0 r_0 + 1)\|e\| \|\tilde{\theta}\|^2 + 2\lambda^2 b_{p_1}^\top P b_{p_1} \|e\| \|\tilde{\theta}\| |\eta| \\
& + 2|\lambda| \|b_{p_1}^\top P\| \Big[\gamma \|b_{p_1}^\top P\| (c_0^2 r_0^2 + 1) + \sigma \|\theta^*\| + \|k + \theta_x^*\| \|A_m\|\Big] \|e\|^2 \\
& + \Big\{ 2|\lambda| \|b_{p_1}^\top P\| \Big[\sigma (c_0 r_0 + 1) + (\|A_m\| c_0 + \|b_m\|) r_0\Big] \\
& + 2\lambda^2 b_{p_1}^\top P b_{p_1} (c_0 r_0 + 1)\|k + \theta_x^*\| \Big\} \|e\| \|\tilde{\theta}\| + 2\lambda^2 b_{p_1}^\top P b_{p_1} \|k + \theta_x^*\| \|e\| |\eta| \\
& + 2|\lambda| \|b_{p_1}^\top P\| \Big[\sigma (c_0 r_0 + 1)\|\theta^*\| + \|k + \theta_x^*\| (\|A_m\| c_0 + \|b_m\|) r_0\Big] \|e\|.
\end{aligned} \tag{5.30}
$$

In a similar manner, we can find the upper bound on $-2\lambda^2 b_{p_1}^\top P b_{p_1} \dot{u}\eta$ in descending powers of $\|e\|$, $\|\tilde{\theta}\|$, and $|\eta|$. Using $\dot{u} = k^\top \dot{x}_p + \dot{\theta}^\top \omega + \theta^\top \dot{\omega}$ and the adaptive law in

(5.17), we obtain

$$
\begin{aligned}
-2\lambda^2 b_{p_1}^\top P b_{p_1} \dot{u}\eta &= -2\lambda^2 b_{p_1}^\top P b_{p_1} \left(k^\top \dot{x}_p + \dot{\theta}^\top \omega + \theta^\top \dot{\omega}\right) \eta \\
&= 2\gamma\lambda|\lambda| b_{p_1}^\top P b_{p_1} b_{p_1}^\top P e \omega^\top \omega \eta + 2\sigma\lambda^2 b_{p_1}^\top P b_{p_1} \theta^\top \omega \eta \\
&\quad - 2\lambda^2 b_{p_1}^\top P b_{p_1} (k^\top \dot{x}_p + \theta^\top \dot{\omega})\eta.
\end{aligned} \tag{5.31}
$$

From (5.28), we have following inequalities as

$$
\begin{aligned}
&2\gamma\lambda|\lambda| b_{p_1}^\top P b_{p_1} b_{p_1}^\top P e \omega^\top \omega \eta \\
&\leq 2\lambda^2 \gamma b_{p_1}^\top P b_{p_1} \|b_{p_1}^\top P\| \left[\|e\|^3 + 2c_0 r_0 \|e\|^2 + (c_0^2 r_0^2 + 1)\|e\|\right] |\eta| \\
&2\sigma\lambda^2 b_{p_1}^\top P b_{p_1} \theta^\top \omega \eta \\
&\leq 2\lambda^2 \sigma b_{p_1}^\top P b_{p_1} \left[\|e\|\|\tilde{\theta}\| + \|\theta^*\|\|e\| + (c_0 r_0 + 1)\|\tilde{\theta}\| + (c_0 r_0 + 1)\|\theta^*\|\right] |\eta|.
\end{aligned} \tag{5.32}
$$

We also have

$$
\begin{aligned}
&- 2\lambda^2 b_{p_1}^\top P b_{p_1} (k^\top \dot{x}_p + \theta^\top \dot{\omega})\eta \\
&= -2\lambda^2 b_{p_1}^\top P b_{p_1} (k + \theta_x)^\top (A_m e + \lambda b_{p_1} \tilde{\theta}^\top \omega + \lambda b_{p_1} \eta + \dot{x}_m)\eta \\
&\leq 2\lambda^2 b_{p_1}^\top P b_{p_1} \left(\|\tilde{\theta}\| + \|k + \theta_x^*\|\right) \|A_m\|\|e\||\eta| \\
&+ 2|\lambda|^3 b_{p_1}^\top P b_{p_1} \|b_{p_1}\| \left(\|\tilde{\theta}\| + \|k + \theta_x^*\|\right) \left[\|e\|\|\tilde{\theta}\| + (c_0 r_0 + 1)\|\tilde{\theta}\| \right. \\
&\left. + |\eta|\right] |\eta| + 2\lambda^2 b_{p_1}^\top P b_{p_1} \left(\|\tilde{\theta}\| + \|k + \theta_x^*\|\right) \left[\left(\|A_m\| c_0 + \|b_m\|\right) r_0\right] |\eta|.
\end{aligned} \tag{5.33}
$$

Combining (5.32) with (5.33), we find an upper bound on $-2\lambda^2 b_{p_1}^\top P b_{p_1} \dot{u}\eta$ as

$$
\begin{aligned}
&-2\lambda^2 b_{p_1}^\top P b_{p_1} \dot{u}\eta \\
&\le 2\gamma\lambda^2 b_{p_1}^\top P b_{p_1} \|b_{p_1}^\top P\| \|e\|^3 |\eta| + 2|\lambda|^3 b_p^\top P b_p \|b_p\| \|e\| \|\tilde{\theta}\|^2 |\eta| \\
&+ 4\gamma\lambda^2 c_0 r_0 b_{p_1}^\top P b_{p_1} \|b_{p_1}^\top P\| \|e\|^2 |\eta| \\
&+ 2\lambda^2 b_{p_1}^\top P b_{p_1} \big(\sigma + \|A_m\| + |\lambda| \|b_p\| \|k + \theta_x^*\|\big) \|e\| \|\tilde{\theta}\| |\eta| \\
&+ 2|\lambda|^3 b_{p_1}^\top P b_{p_1} \|b_{p_1}\| (c_0 r_0 + 1) \|\tilde{\theta}\|^2 |\eta| + 2|\lambda|^3 b_{p_1}^\top P b_{p_1} \|b_{p_1}\| \|\tilde{\theta}\| |\eta|^2 \\
&+ 2\lambda^2 b_{p_1}^\top P b_{p_1} \Big[\gamma \|b_{p_1}^\top P\| (c_0^2 r_0^2 + 1) + \sigma \|\theta^*\| + \|k + \theta_x^*\| \|A_m\|\Big] \|e\| |\eta| \\
&+ 2\lambda^2 b_{p_1}^\top P b_{p_1} \Big[(c_0 r_0 + 1)(\sigma + |\lambda| \|b_{p_1}\| \|k + \theta_x^*\|) + (\|A_m\| c_0 + \|b_m\|) r_0\Big] \|\tilde{\theta}\| |\eta| \\
&+ 2|\lambda|^3 b_{p_1}^\top P b_{p_1} \|b_{p_1}\| \|k + \theta_x^*\| |\eta|^2 \\
&+ 2\lambda^2 b_{p_1}^\top P b_{p_1} \Big[\sigma (c_0 r_0 + 1) \|\theta^*\| + \|k + \theta_x^*\| (\|A_m\| c_0 + \|b_m\|) r_0\Big] |\eta|.
\end{aligned} \tag{5.34}
$$

Other terms in $H(e, \tilde{\theta}, \eta)$ except $-2\lambda b_{p_1}^\top P e\dot{u}$ and $-2\lambda^2 b_{p_1}^\top P b_{p_1} \dot{u}\eta$ can be bounded as

$$
\begin{aligned}
-\frac{1}{2} e^\top Q e &\le -\frac{q_{\min}}{2} \|e\|^2 \\
\lambda b_{p_1}^\top P e \tilde{\theta}^\top \omega &\le |\lambda| \|b_{p_1}^\top P\| \|e\| \Big[\|e\| \|\tilde{\theta}\| + (c_0 r_0 + 1) \|\tilde{\theta}\|\Big] \\
&= |\lambda| \|b_{p_1}^\top P\| \|e\|^2 \|\tilde{\theta}\| + |\lambda| \|b_{p_1}^\top P\| (c_0 r_0 + 1) \|e\| \|\tilde{\theta}\| \\
\lambda b_{p_1}^\top P e \eta &\le |\lambda| \|b_{p_1}^\top P\| \|e\| |\eta| \\
\lambda b_{p_1}^\top P A_m e \eta &\le |\lambda| \|b_{p_1}^\top P\| \|A_m\| \|e\| |\eta| \\
\lambda^2 b_{p_1}^\top P b_{p_1} \tilde{\theta}^\top \omega \eta &\le \lambda^2 b_{p_1}^\top P b_{p_1} \Big[\|e\| \|\tilde{\theta}\| + (c_0 r_0 + 1) \|\tilde{\theta}\|\Big] |\eta| \\
&= \lambda^2 b_{p_1}^\top P b_{p_1} \|e\| \|\tilde{\theta}\| |\eta| + \lambda^2 b_{p_1}^\top P b_{p_1} (c_0 r_0 + 1) \|\tilde{\theta}\| |\eta| \\
\lambda^2 b_{p_1}^\top P b_{p_1} \eta^2 &\le \lambda^2 b_{p_1}^\top P b_{p_1} |\eta|^2
\end{aligned} \tag{5.35}
$$

where $q_{\min}$ is the minimum eigenvalue of Q. We now have an bound on $H(e, \tilde{\theta}, \eta)$ as

$$
H(e, \tilde{\theta}, \eta) \le H_4 + H_3 + H_2 + H_1. \tag{5.36}
$$

where H_i denotes the summation of i powers of $\|e\|, \|\tilde{\theta}\|$, and $|\eta|$ as

$$H_i = \sum_{\substack{p+q+s=i \\ p,q,s \in \mathbb{N} \cup \{0\}}} C_{p,q,s} \|e\|^p \|\tilde{\theta}\|^q |\eta|^s \tag{5.37}$$

and $C_{p,q,s}$ is the coefficient corresponding to $\|e\|^p \|\tilde{\theta}\|^q |\eta|^s$ from (5.30), (5.34), and (5.35). $C_{p,q,s}$'s are determined as follows:

$$\begin{aligned}
&C_{4,0,0} = 2\gamma|\lambda| \|b_{p_1}^\top P\|^2, \quad C_{3,0,1} = 2\gamma\lambda^2 b_{p_1}^\top P b_{p_1} \|b_{p_1}^\top P\|, \quad C_{2,2,0} = 2\lambda^2 b_{p_1}^\top P b_{p_1} \\
&C_{1,2,1} = 2|\lambda|^3 b_{p_1}^\top P b_{p_1} \|b_{p_1}\|, \quad C_{3,0,0} = 4\gamma|\lambda| c_0 r_0 \|b_{p_1}^\top P\|^2 \\
&C_{2,1,0} = 2|\lambda| \|b_{p_1}^\top P\| \left(\sigma + \|A_m\|\right) + 2\lambda^2 b_{p_1}^\top P b_{p_1} \|k + \theta_x^*\| + |\lambda| \|b_{p_1}^\top P\| \\
&C_{2,0,1} = 4\gamma\lambda^2 c_0 r_0 b_{p_1}^\top P b_{p_1} \|b_{p_1}^\top P\|, \quad C_{1,2,0} = 2\lambda^2 b_{p_1}^\top P b_{p_1} (c_0 r_0 + 1) \\
&C_{1,1,1} = \lambda^2 b_{p_1}^\top P b_{p_1} \Big[3 + 2(\sigma + \|A_m\| + |\lambda| \|b_{p_1}\| \|k + \theta_x^*\|)\Big] \\
&C_{0,2,1} = 2|\lambda|^3 b_{p_1}^\top P b_{p_1} \|b_{p_1}\| (c_0 r_0 + 1) \\
&C_{0,1,2} = 2|\lambda|^3 b_{p_1}^\top P b_{p_1} \|b_{p_1}\| \\
&C_{2,0,0} = 2|\lambda| \|b_{p_1}^\top P\| \Big[\gamma \|b_{p_1}^\top P\| (c_0^2 r_0^2 + 1) + \sigma \|\theta^*\| + \|k + \theta_x^*\| \|A_m\|\Big] - \frac{q_{\min}}{2} \\
&C_{1,1,0} = \Big\{ 2|\lambda| \|b_{p_1}^\top P\| \Big[\sigma(c_0 r_0 + 1) + (\|A_m\| c_0 + \|b_m\|) r_0\Big] \\
&\qquad + 2\lambda^2 b_{p_1}^\top P b_{p_1} (c_0 r_0 + 1) \|k + \theta_x^*\| \Big\} + |\lambda| \|b_{p_1}^\top P\| (c_0 r_0 + 1) \\
&C_{1,0,1} = 2\lambda^2 b_{p_1}^\top P b_{p_1} \Big[\gamma \|b_{p_1}^\top P\| (c_0^2 r_0^2 + 1) + \sigma \|\theta^*\| + \|k + \theta_x^*\| (\|A_m\| + 1)\Big] \\
&\qquad + |\lambda| \|b_{p_1}^\top P\| (\|A_m\| + 1) \\
&C_{0,1,1} = 2\lambda^2 b_{p_1}^\top P b_{p_1} \Big[(c_0 r_0 + 1)(\sigma + |\lambda| \|b_{p_1}\| \|k + \theta_x^*\|) + (\|A_m\| c_0 + \|b_m\|) r_0\Big] \\
&\qquad + \lambda^2 b_{p_1}^\top P b_{p_1} (c_0 r_0 + 1) \\
&C_{0,0,2} = \lambda^2 b_{p_1}^\top P b_{p_1} (2|\lambda| \|b_{p_1}\| k + \|\theta_x^*\| + 1) \\
&C_{1,0,0} = 2|\lambda| \|b_{p_1}^\top P\| \Big[\sigma(c_0 r_0 + 1) \|\theta^*\| + \|k + \theta_x^*\| (\|A_m\| c_0 + \|b_m\|) r_0\Big] \\
&C_{0,0,1} = 2\lambda^2 b_{p_1}^\top P b_{p_1} \Big[\sigma(c_0 r_0 + 1) \|\theta^*\| + \|k + \theta_x^*\| (\|A_m\| c_0 + \|b_m\|) r_0\Big].
\end{aligned} \tag{5.38}$$

In order to find the upper bound on H_i, we define constants c_i for $1 \leq i \leq 4$ such

that

$$
\begin{aligned}
c_4 &= \max\left\{C_{4,0,0},\ \frac{C_{3,0,1}}{4},\ \frac{C_{2,2,0}}{6},\ \frac{C_{1,2,1}}{12}\right\} \\
c_3 &= \max\left\{C_{3,0,0},\ \frac{C_{2,1,0}}{3},\ \frac{C_{2,0,1}}{3},\ \frac{C_{1,2,0}}{3},\ \frac{C_{0,2,1}}{3},\ \frac{C_{0,1,2}}{3},\ \frac{C_{1,1,1}}{6}\right\} \\
c_2 &= \max\left\{C_{2,0,0},\ C_{0,0,2},\ \frac{C_{1,1,0}}{2},\ \frac{C_{1,0,1}}{2},\frac{C_{0,1,1}}{2}\right\} \\
c_1 &= \max\left\{C_{1,0,0},\ C_{0,0,1}\right\}.
\end{aligned}
\tag{5.39}
$$

We define $y = [e^\top\ \tilde{\theta}^\top\ \eta]^\top$ and then obtain

$$
(\|e\| + \|\tilde{\theta}\| + |\eta|)^2 \leq 2\left(\|e\|^2 + \|\tilde{\theta}\|^2 + |\eta|^2\right) = 2\|y\|^2. \tag{5.40}
$$

Using the inequality in (5.40) and constants defined in (5.39), we have

$$
H_4 + H_3 + H_2 + H_1 \leq 4c_4\|y\|^4 + 2\sqrt{2}c_3\|y\|^3 + 2c_2\|y\|^2 + \sqrt{2}c_1\|y\|. \tag{5.41}
$$

We can rewrite (5.23) as

$$
\dot{V} \leq -d_2\|y\|^2 + \frac{\tau}{2}\left(4c_4\|y\|^4 + 2\sqrt{2}c_3\|y\|^3 + 2c_2\|y\|^2 + \sqrt{2}c_1\|y\|\right) + d_1\|y\| \tag{5.42}
$$

where

$$
d_2 = \min\left\{q_{\min},\ \frac{2\sigma|\lambda|}{\gamma},\ 2\lambda^2 b_{p_1}^\top P b_{p_1}\right\},\quad d_1 = \frac{2\sigma|\lambda|}{\gamma}\|\theta^*\|. \tag{5.43}
$$

We can rewrite the inequality in (5.42) as

$$
\dot{V} \leq 2c_4\tau\|y\|\left[\|y\|^3 + \frac{c_3}{\sqrt{2}c_4}\|y\|^2 + \frac{1}{2c_4}\left(c_2 - \frac{d_2}{\tau}\right)\|y\| + \frac{1}{2\sqrt{2}c_4}\left(c_1 + \frac{\sqrt{2}d_1}{\tau}\right)\right] \leq 0. \tag{5.44}
$$

For the purpose of analysis, we set $f(z)$ for $z > 0$ as

$$
f(z) = z^3 + \kappa_2 z^2 + \kappa_1 z + \kappa_0 \tag{5.45}
$$

where

$$\kappa_2 = \frac{c_3}{\sqrt{2}c_4}, \quad \kappa_1 = \frac{1}{2c_4}\left(c_2 - \frac{d_2}{\tau}\right), \quad \kappa_0 = \frac{1}{2\sqrt{2}c_4}\left(c_1 + \frac{\sqrt{2}d_1}{\tau}\right). \tag{5.46}$$

Since $f(z)$ is a third-order polynomial, $f(z)$ is continuous. From the facts that $\kappa_2 > 0$ and $\kappa_0 > 0$, $f(0) > 0$ and $\lim_{z\to+\infty} f(z) = +\infty$. From these facts, following two cases are possible which are mutually exclusive (Figure 5-2):

(a) $f(z)$ does not intersect with z-axis at $[0, \infty)$.

(b) $f(z)$ intersect with z-axis twice at $[0, \infty)$.

To show that the case (a) cannot occur for $\tau \in (0,\ \tau_m)$, it suffices to prove that (i) $z_1 = \arg\min_{z\in[0,\infty)} f(z)$ exists and (ii) $f(z_1) < 0$. If $\kappa_2 \geq 0$, i.e. $\tau \geq d_2/c_2$, then the case (a) occurs. Therefore, $\tau_m < d_2/c_2$ is necessary.

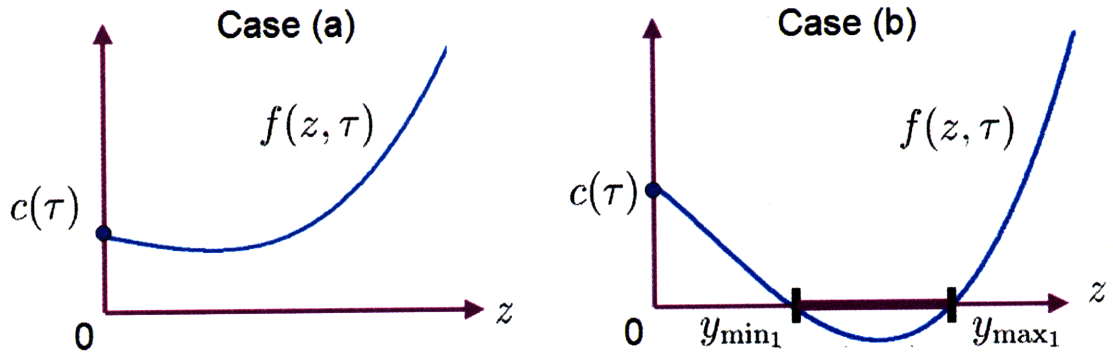

Figure 5-2: Two mutually exclusive cases in the cubic polynomial $f(z)$

Proof of (i) Roots of $f'(z) = 0$ are

$$z_1 = \frac{-\kappa_2 + \sqrt{\kappa_2^2 - 3\kappa_1}}{3}, \quad z_2 = \frac{-\kappa_2 - \sqrt{\kappa_2^2 - 3\kappa_1}}{3}. \tag{5.47}$$

In order for z_1 and z_2 to exist, $\kappa_2^2 - 3\kappa_1 > 0$. That is,

$$\tau < \frac{3d_2}{3c_2 - d_3^2}. \tag{5.48}$$

In order for $z_1 > 0$, we also requires

$$\tau < \frac{d_2}{c_2}. \tag{5.49}$$

Since $\tau_m < d_2/c_2$, this completes the proof. ∇

Proof of (ii) Using $3z_1^2 + 2\kappa_2 z_1 + \kappa_1 = 0$, the minimum of $f(z)$ can be simplified as

$$\begin{aligned}\min_{z\in[0,\infty)} f(z) = f(z_1) &= z_1^3 + \kappa_2 z_1^2 + \kappa_1 z_1 + \kappa_0 \\ &= \left(-\frac{2}{9}\kappa_2^2 + \frac{2}{3}\kappa_1\right) z_1 - \frac{\kappa_2\kappa_1}{9} + \kappa_0 \\ &= -\frac{2}{27}\left(\sqrt{\kappa_2^2 - 3\kappa_1}\right)^3 + \frac{2}{27}\kappa_2^3 - \frac{1}{3}\kappa_2\kappa_1 + \kappa_0.\end{aligned} \tag{5.50}$$

Since κ_1 and κ_0 are a function of τ, $f(z_1)$ is a function of τ which is denoted by $g(\tau)$ and given by

$$\begin{aligned}g(\tau) = &-\frac{2}{27}\left[\frac{c_3^2}{2c_4^2} - \frac{3}{2c_4}\left(c_2 - \frac{d_2}{\tau}\right)\right]^{\frac{3}{2}} + \frac{2c_3^3}{54\sqrt{2}c_4^3} - \frac{c_3}{6\sqrt{2}c_4^2}\left(c_2 - \frac{d_2}{\tau}\right) \\ &+ \frac{1}{2\sqrt{2}c_4}\left(c_1 + \frac{\sqrt{2}d_1}{\tau}\right).\end{aligned} \tag{5.51}$$

$g(\tau)$ is a continuous function of τ at $(0,\ \infty)$ and, $\lim_{\tau\to 0} g(\tau) = -\infty$ and $g(d_2/c_2) > 0$ so that by the intermediate value theorem, there exists $\tau_m \in (0,\ d_2/c_2)$ such that

$$g(\tau_m) = 0 \quad \text{and} \quad g(\tau) < 0, \quad \forall \tau \in (0,\ \tau_m). \tag{5.52}$$

This proves that $f(z_1) < 0$ for $\tau \in (0, \tau_m)$. ∇

Because $f(z_1) < 0$ for $\tau \in (0,\ \tau_m)$, there exist $y_{\min}$ and $y_{\max}$ such that $0 < y_{\min} < z_1 < y_{\max}$ and $f(y_{\min}) = f(y_{\max}) = 0$ by the intermediate value theorem. Defining a set $\mathbf{A}$ as

$$\mathbf{A} = \{y | y_{\min} < \|y\| < y_{\max}\}, \tag{5.53}$$

it leads that $\dot{V} < 0$ in $\mathbf{A}$. As τ tends to zero, z_1 and $y_{\max}$ approach to ∞. In this sense, the stability result obtained is semi-global as $\mathbf{A}$ expands to the whole space as $\tau \to 0$. □

Figure 5-3 illustrates the cubic polynomial $f(z)$ with $\tau > \tau_m$, $\tau = \tau_m$, and $\tau < \tau_m$. For $\tau < \tau_m$, we have the region where $f(z) < 0$ and hence $\dot{V} < 0$.

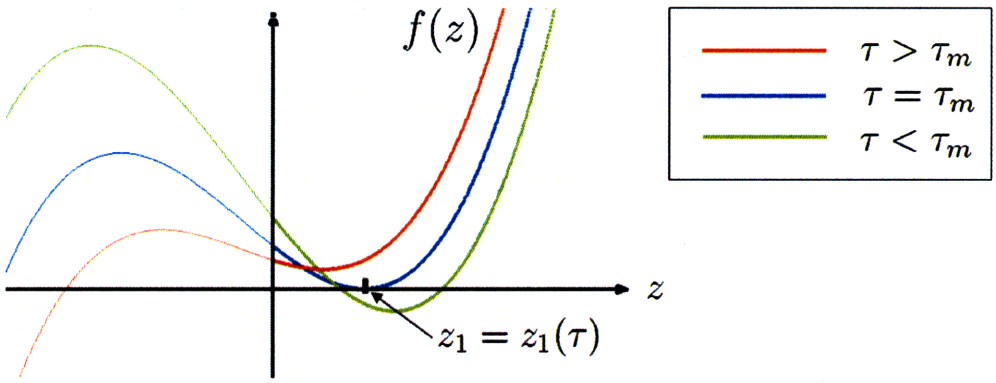

Figure 5-3: The cubic polynomial, $f(z)$, with $\tau > \tau_m$, $\tau = \tau_m$, and $\tau < \tau_m$.

5.3.2 (n,n) Pade approximation

We now extend Theorem 5.1 to the general (n, n) Pade approximation. As the unmodeled dynamics, $q_\Delta(s)/p_\Delta(s)$, have n states, $y \in \mathbb{R}^{3n+1}$ is redefined as $y = [e^\top \ \tilde{\theta}^\top \ \xi^\top]^\top$.

Theorem 5.2. *The system in* (5.8) *in the presence of* (n, n) *Pade approximation with the controller in* (3.9) *based on the adaptive law in* (5.17), *there exist* $\tau_m > 0$ *and* $y_{\max} > 0$ *such that* $x(t)$, $\theta(t)$, *and* $\xi(t)$ *have bounded trajectories for all* $t > t_0$ *if*

i. $0 < \tau < \tau_m$,

ii. $\|y(t_0)\| < y_{\max}$.

Furthermore, τ_m *is defined as a delay margin.*

Proof. We propose a Lyapunov candidate function as

$$V = e^\top P e + \frac{|\lambda|}{\gamma}\tilde{\theta}^\top\tilde{\theta} + \frac{\tau}{2}(e + b_{p_1}\lambda c_\eta^\top\xi)^\top P(e + b_{p_1}\lambda c_\eta^\top\xi) + a_0\tau\xi^\top R\xi. \tag{5.54}$$

where $a_0 = \lambda^2 b_{p_1}^\top P b_{p_1}$ and $c_\eta^\top$ is chosen such that

$$c_\eta^\top \dot{\xi} = -\frac{2}{\tau}\eta + c_\eta^\top b_\tau \dot{u}. \tag{5.55}$$

For a given $S = S^\top > 0$, $R = R^\top$ is chosen such that

$$A_r^\top \left(\frac{c_\eta c_\eta^\top}{2} + R \right) + \left(\frac{c_\eta c_\eta^\top}{2} + R \right) A_r = -S \tag{5.56}$$

and $\frac{c_\eta c_\eta^\top}{2} + R$ is positive-definite. The Lyapunov candidate function is similar to the one in Theorem 5.1 but it needs to have an extra term $a_0 \tau \xi^\top R \xi$ because the state vector ξ has n states. We obtain the time-derivative of V along the trajectories of (3.19), (5.17), and (5.9) as

$$\dot{V} = -e^\top Q e - \frac{2\sigma|\lambda|}{\gamma}\tilde{\theta}^\top \tilde{\theta} + -a_0 \xi^\top S \xi + \tau H(e, \tilde{\theta}, \xi) - \frac{2\sigma|\lambda|}{\gamma}\tilde{\theta}^\top \theta^* \tag{5.57}$$

and $H(e, \tilde{\theta}, \xi)$ is redefined as

$$\begin{aligned} H(e, \tilde{\theta}, \xi) =& \frac{1}{2}(\dot{e}^\top P e + e^\top P \dot{e}) + e^\top P \lambda b_{p_1} c_\eta^\top b_\tau \dot{u} + \xi^\top c_\eta b_{p_1}^\top \lambda P \dot{e} \\ &+ a_0 \xi^\top (c_\eta c_\eta^\top + 2R) b_\tau \dot{u}. \end{aligned} \tag{5.58}$$

By following a similar procedure as in the proof of Theorem 5.1, it can be shown that $\dot{V} < 0$ holds in an annulus which extends to the entire state space outside a compact set around the origin as τ tends to zero. □

$C_{p,q,s}$'s required to prove Theorem 5.2 are introduced in Appendix B.

5.4 Simulation

5.4.1 Delay Margins in the NASA X–15

In this section, we validate the proposed analytic margins based on the short period dynamics of the NASA X–15 hypersonic aircraft. Aerodynamic data of the NASA X–

15 hypersonic aircraft discussed in [13] are combined with nonlinear flight dynamics as

$$\dot{X} = F(X,\ U) \tag{5.59}$$

whose states (X) and inputs (U) are defined as

$$\begin{aligned} X &= [V_T\ \ \alpha\ \ \beta\ \ P\ \ Q\ \ R\ \ \Phi\ \ \Theta\ \ \Psi\ \ N\ \ E\ \ D]^\top \\ U &= [U_{thrust}\ \ U_{left}\ \ U_{right}\ \ U_{rudder}]^\top. \end{aligned} \tag{5.60}$$

U_{left} and U_{right} represent the left and right control surface of the elevon system. Elevator and aileron inputs can be computed as

$$U_{elevator} = \frac{U_{left} + U_{right}}{2},\ U_{aileron} = \frac{U_{left} - U_{right}}{2}. \tag{5.61}$$

Actuator limits are imposed as

$$U_{left/right} \in [-15,\ 15], \quad U_{rudder} \in [-30,\ 30]. \tag{5.62}$$

Details regarding the NASA X-15 hypersonic aircraft are discussed in Appendix A. The nonlinear flight dynamics are linearized at the trim point (X_0, U_0) shown in Table 3.1. The short period dynamics of $\alpha(deg)$ and $q(deg/sec)$ with the elevator input $u(deg)$ is in the form of (5.1) with

$$A = \begin{bmatrix} -0.2950 & 1.0000 \\ -13.0798 & -0.2084 \end{bmatrix}, \quad b = \begin{bmatrix} 0 \\ -9.4725 \end{bmatrix}, \quad c = \begin{bmatrix} 1 \\ 0 \end{bmatrix} \tag{5.63}$$

and the output is chosen to be $\alpha(deg)$. To build an unknown plant in (5.2), two unknown constants, λ_α and λ_q, are introduced as

$$A_\lambda = \begin{bmatrix} -0.2950 & 1.0000 \\ -13.0798\lambda_\alpha & -0.2084\lambda_q \end{bmatrix} \tag{5.64}$$

and an unknown parameter, λ, is used to model the control failure. In simulation studies, we compare the proposed margins with the delay margin found by simulations. To enhance the tracking performance, we integrate the output tracking error between the output and a given command signal (α_{cmd}) as

$$\dot{x}_c = \alpha - \alpha_{cmd} \tag{5.65}$$

such that the overall plant of interest is written in the form of (5.5).

Simulation 1 $\lambda = 0.5$, $\lambda_\alpha = 0.4$, and $\lambda_q = 1$

This uncertainty implies that the elevator input loses 50% of its control effectiveness and that 60% loss in one parameter occurs in the system matrix A. A step input to the angle of attack is given as a command (α_{cmd}). Then, we compute the guaranteed margins for various sets of adaptive parameters (γ, σ) with $(1,1)$ and $(2,2)$ Pade approximations. The $(2,2)$ Pade approximation can be written in the form of (5.9) with

$$A_\tau = \begin{bmatrix} 0 & -1 \\ -12 & -6 \end{bmatrix}, \quad b_\tau = \begin{bmatrix} 0 \\ -12 \end{bmatrix}, \quad c_\tau = \begin{bmatrix} 1 \\ 0 \end{bmatrix}. \tag{5.66}$$

The c_η and S for the Lyapunov candidate function in (5.54) are chosen as $c_\eta^\top = [1 \quad 1/6]$ and $S = 2I$. Figure 5-4 shows the plots of analytically guaranteed and simulation-based margins with the adaptive rate (γ) when σ is 0.5. 0.02, 0.1, and 0.01 respectively. As shown in Figure 5-4, for a given σ, the both analytical and simulation-based delay margins decrease as the adaptive rate increases. This explains that the increased adaptive rate enhances the performance but there is a trade-off between performance and robustness in the adaptive control. The maximum delay margin obtained analytically is 0.00134s which is conservative compared to 0.272s from simulation studies. It should be also noted that the margins are more conservative with $(2,2)$ Pade approximation than with $(1,1)$ Pade approximation. It is because stability analysis becomes more complex as the order of the time-delay approximation increases.

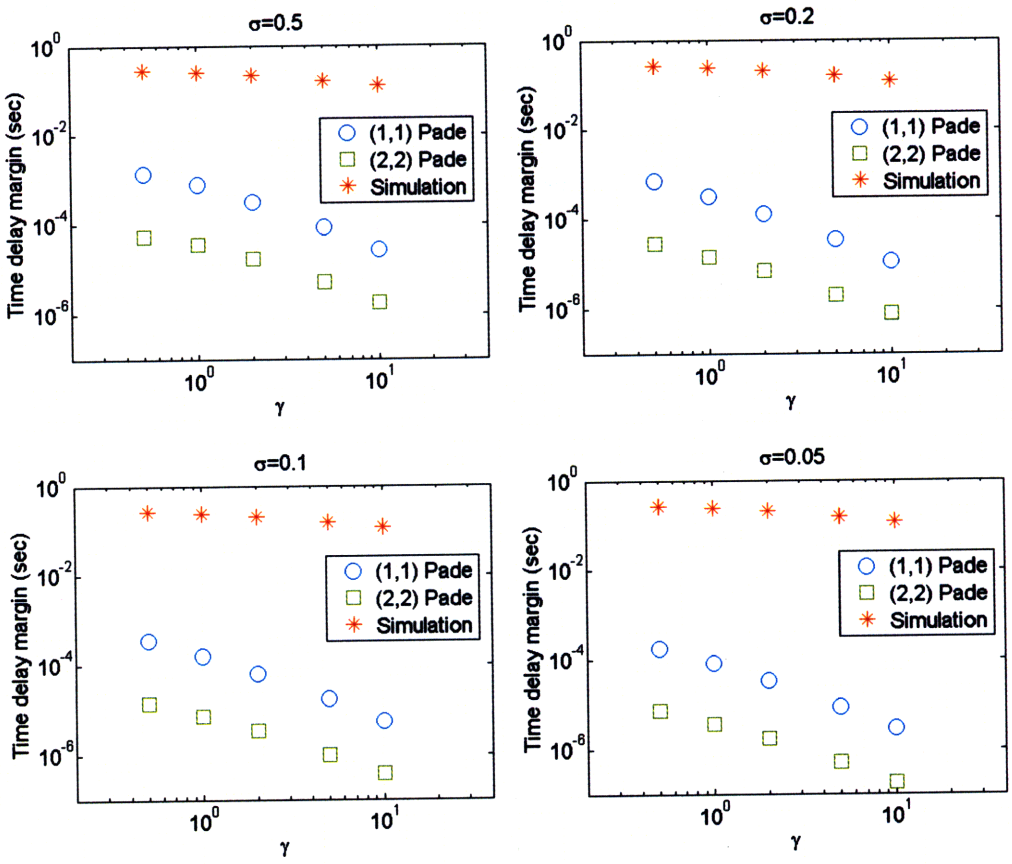

Figure 5-4: Analytically guaranteed and simulation-based margins with $\lambda = 0.5$, $\lambda_\alpha = 0.4$, and $\lambda_q = 1$.

Simulation 2 $\lambda = 0.5$, $\lambda_\alpha = -0.2$, and $\lambda_q = 1$

In this simulation, we employ a more aggressive uncertainty so that the closed-loop system with only the nominal controller is unstable. The same command input is utilized to compute the margins from $(1,1)$ and $(2,2)$ Pade approximation, and simulations. Figure 5-5 shows the plots of analytically guaranteed and simulation-based margins with the adaptive rate (γ) when σ is 0.5. 0.02, 0.1, and 0.01 respectively. We have similar results to Simulation 1 as the both analytical and simulation-based delay margins decrease as the adaptive rate increases. The maximum delay margin obtained analytically is 0.00083s which is conservative compared to 0.245s from simulation studies. Maximum delay margin from simulation is smaller than its counterpart in Simulation 1 because a more aggressive uncertainty is introduced in Simulation 2. This is also captured in the analytically guaranteed margins. In Simulation 1 and

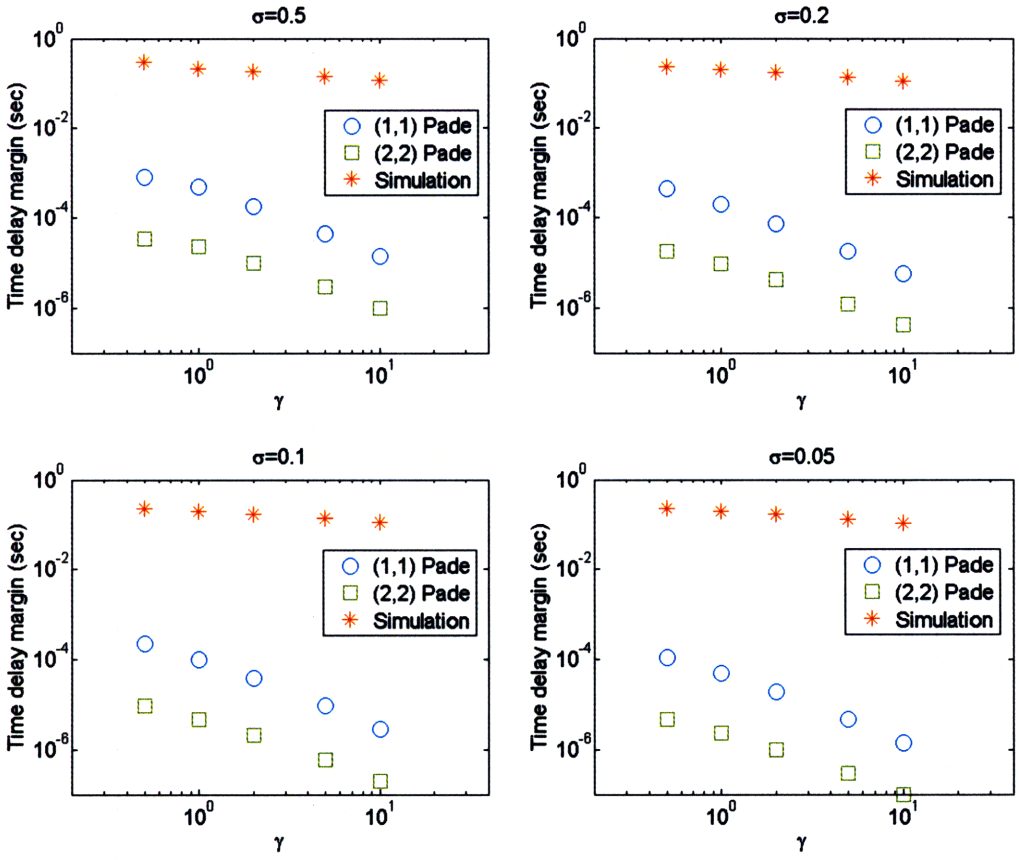

Figure 5-5: Analytically guaranteed and simulation-based margins with $\lambda = 0.5$, $\lambda_\alpha = -0.2$, and $\lambda_q = 1$.

2, it is found that robustness in both analytical margins and simulation-based margins decrease as the adaptive rate (γ) increases. We have heuristically known that increased σ contributes to gain more robustness which is captured in the analytic margins. In conclusion, physical significance of the adaptive controller parameters, γ and σ, is reflected in the proposed analytic margins though they are conservative. The conservatism in the analytic margins will be discussed in detail in the next two subsections.

5.4.2 Delay Margins in First Order Plants

As seen in the previous section, the analytically guaranteed margins are conservative compared to the ones from simulation studies. In order to bridge the gap between these margins, we thoroughly investigate Lyapunov analysis for the analytic margins.

To begin with, the first order plant is proposed with input time-delay as

$$\dot{x}_p = a_p x_p + e^{-\tau s} u \tag{5.67}$$

where a_p is an unknown parameter. When the delay is approximated with (1,1) Pade approximation, the plant of interest is written as

$$\begin{aligned} \dot{x}_p &= a_p x_p + u + \eta \\ \dot{\eta} &= -\frac{2}{\tau}\eta - 2\dot{u}. \end{aligned} \tag{5.68}$$

The reference model is designed as

$$\dot{x}_m = a_m x_m + r \tag{5.69}$$

and to track this reference model, the plant in (5.68) is combined with the adaptive controller described by

$$\begin{aligned} u &= \theta x_p + r \\ \dot{\theta} &= -\gamma x_p e - \sigma\theta. \end{aligned} \tag{5.70}$$

A Lyapunov candidate function is proposed as

$$V = \frac{1}{2}e^2 + \frac{1}{2}\tilde{\theta}^2 + \frac{\tau}{4}(e+\eta)^2. \tag{5.71}$$

The overall procedure to derive the analytic margins for the first order plant is the same in Section 5.3. Therefore, we will introduce the fundamental steps in this section. The time-derivative of V can be written as

$$\begin{aligned} \dot{V} = {} & a_m e^2 - \frac{\sigma}{\gamma}\tilde{\theta}^2 - \eta^2 - \frac{\sigma}{\gamma}\theta^*\tilde{\theta} \\ & + \frac{\tau}{2}(a_m e^2 + e\tilde{\theta}x_p + e\eta - 2e\dot{u} + a_m e\eta + \tilde{\theta}\eta x_p + \eta^2 - 2\eta\dot{u}) \end{aligned} \tag{5.72}$$

where $\theta^* = a_m - a_p$ is the ideal gain from the standard matching condition. Replacing $\dot{u}$ with $\dot{\theta}x_p + \theta\dot{x}_p + \dot{r}$ and taking bounds on the right-hand side of (5.72), we have the following inequality as

$$\dot{V} \leq a_m|e|^2 - \frac{\sigma}{\gamma}|\tilde{\theta}|^2 - |\eta|^2 + \frac{\sigma}{\gamma}|\theta^*||\tilde{\theta}| + \tau(H_4 + H_3 + H_2 + H_1) \tag{5.73}$$

where

$$H_i = \sum_{p+q+r=i} C_{p,q,r}|e|^p|\tilde{\theta}|^q|\eta|^r. \tag{5.74}$$

From the same steps as (5.40) and (5.41), we can obtain

$$\dot{V} < 4c_4\tau\|y\|f(\|y\|) \tag{5.75}$$

where $f(\|y\|)$ is the cubic polynomial as in (5.45) corresponding to the first order plant and the adaptive controller. y is defined to be $y = [e\ \tilde{\theta}\ \eta]^\top$. We now provides three methods to reduce the conservatism in the analytic margins. Each method is validated with the first order plant with the adaptive controller where the plant parameters are chosen as $a_p = 0.5$, $a_m = -1$, and the adaptive parameter are $\gamma = 0.5,\ 1,\ 2,\ 5$ and $\sigma = 0.5$.

Method 1 Mutipliers

One of the most conservative steps in deriving (5.75) occurs when H_i is bounded above, for example,

$$\begin{aligned} H_4 &= C_{4,0,0}|e|^4 + C_{3,0,1}|e|^3|\eta| + C_{2,2,0}|e|^2|\tilde{\theta}|^2 + C_{1,2,1}|e||\tilde{\theta}|^2|\eta| && (5.76)\\ &< c_4(|e| + |\tilde{\theta}| + |\eta|)^4 && (5.77)\\ &\leq 4c_4(|e|^2 + |\tilde{\theta}|^2 + |\eta|^2)^2 && (5.78)\\ &= 4c_4\|y\|^4. && (5.79) \end{aligned}$$

where

$$c_4 = \max\left\{C_{4,0,0},\ \frac{C_{3,0,1}}{4},\ \frac{C_{2,2,0}}{6},\ \frac{C_{1,2,1}}{12}\right\}. \tag{5.80}$$

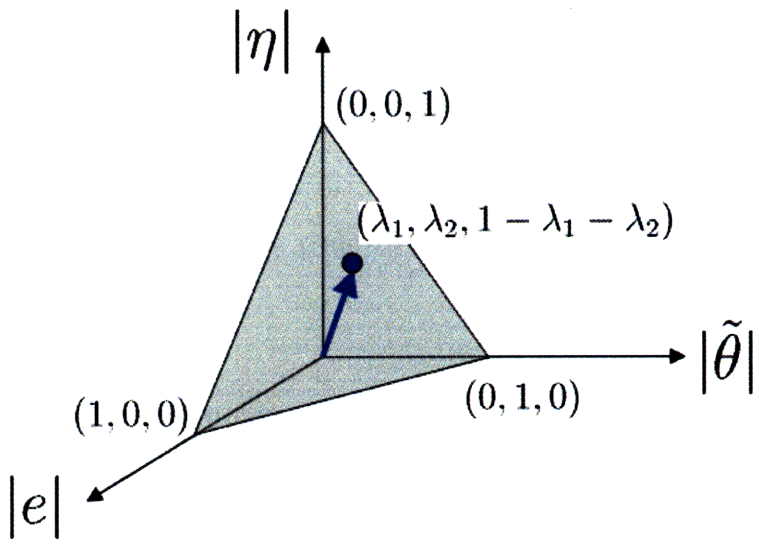

Figure 5-6: Multipliers

Inequalities above are the key steps to build a cubic polynomial $f(\|y\|)$ though the upper bound in (5.77) is the most conservative bound. Therefore, we utilize multiplies to provide less conservative bounds on H_i. For example, H_4 can be bounded above as

$$\begin{aligned} H_4 &= C_{4,0,0}|e|^4 + C_{3,0,1}|e|^3|\eta| + C_{2,2,0}|e|^2|\tilde{\theta}|^2 + C_{1,2,1}|e||\tilde{\theta}|^2|\eta| \\ &< c_4' \left(\lambda_1|e| + \lambda_2|\tilde{\theta}| + (1-\lambda_1-\lambda_2)|\eta|\right)^4 \\ &\leq 4c_4'\|y'\| \end{aligned} \tag{5.81}$$

where c_4' and y' are defined as

$$c_4' = \max\left\{\frac{C_{4,0,0}}{\lambda_1^4}, \frac{C_{3,0,1}}{4\lambda_1^3(1-\lambda_1-\lambda_2)}, \frac{C_{2,2,0}}{6\lambda_1^2\lambda_2^2}, \frac{C_{1,2,1}}{12\lambda_1\lambda_2^2(1-\lambda_1-\lambda_2)}\right\} \tag{5.82}$$

and $y' = [\lambda_1 e \ \lambda_2\tilde{\theta} \ (1-\lambda_1-\lambda_2)\eta]^\top$ with $\lambda_1 > 0$, $\lambda_2 > 0$, and $1-\lambda_1-\lambda_2 > 0$. A set of multipliers, $(\lambda_1,\ \lambda_2,\ 1-\lambda_1-\lambda_2)$, is shown in Figure 5-6. It should be also noted that the region of attraction in Theorem 5.1 is in the shape of an ellipsoid with multipliers whereas it has a spherical shape without multipliers. Then we optimize the analytic

margins over multipliers to obtain the lease conservative one as

$$\max_{\substack{\lambda_1>0,\lambda_2>0 \\ 1-\lambda_1-\lambda_2>0}} \tau_m. \tag{5.83}$$

Method 2 Search on $G(e,\ \tilde{\theta},\ \eta)$

In order to reduce the conservatism in the analytic margins, we directly search $G(e,\ \tilde{\theta},\ \eta)$ which is the right-hand side of (5.73) as

$$G(e,\ \tilde{\theta},\ \eta) = a_m|e|^2 - \frac{\sigma}{\gamma}|\tilde{\theta}|^2 - |\eta|^2 + \frac{\sigma}{\gamma}|\theta^*||\tilde{\theta}| + \tau(H_4 + H_3 + H_2 + H_1). \tag{5.84}$$

We evaluate $G(e,\ \tilde{\theta},\ \eta)$ in $(e,\ \tilde{\theta},\ \eta)$-space and find the minimum τ_m that provides a bounded set of attraction. Schematics of bounded and unbounded sets are shown in Figure 5-7. As described in Figure 5-7, stability of the overall system is not guaranteed

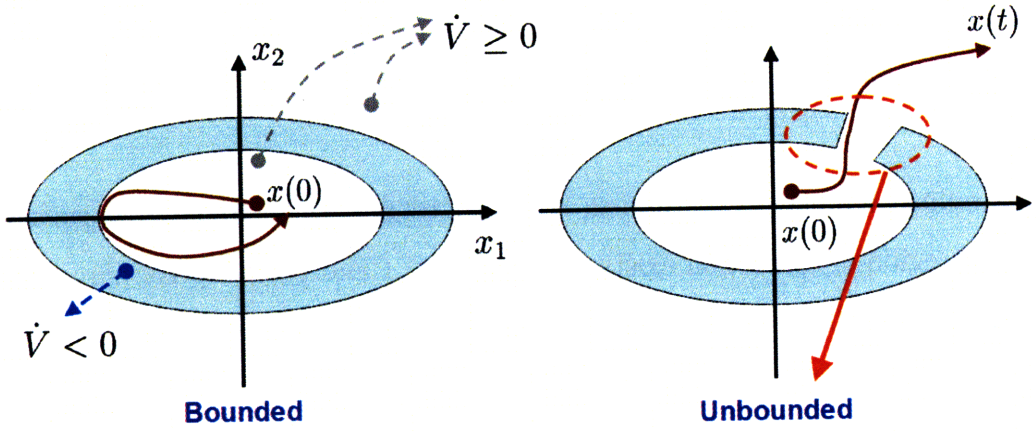

Figure 5-7: Bounded (left) and unbounded (right) sets of attraction.

when the region of attraction is not guaranteed since the state variables can grow in an unbounded fashion for small perturbations. For $\gamma = 0.5$ and $\sigma = 0.5$, the result of this method is plotted in Figure 5-8. As shown in Figure 5-8, there exists a bounded region of attraction when $\tau = 0.081$. However, the region of attraction becomes unbounded as τ is increased to 0.082. Therefore, we claim that the analytic margin is $\tau_m = 0.081$.

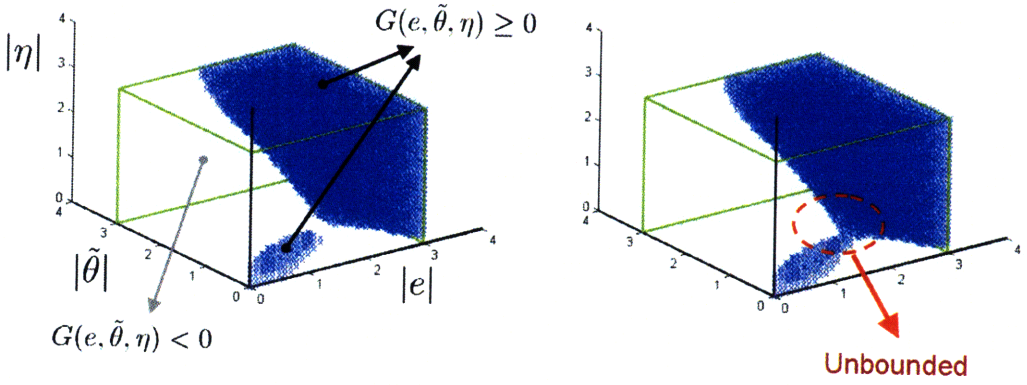

Figure 5-8: The region where $G(e, \tilde{\theta}, \eta) \geq 0$ is shaded in blue. A bounded set of attraction exists when $\tau = 0.081$ (left) but there is no bounded set for $\tau = 0.082$.

Method 3 Search on $\dot{V}$

The third method is to directly search $\dot{V}$ in (5.72) over the (e, $\tilde{\theta}$, η) space. This method is able to reduce the gap between the analytic and simulation-based margins more compared to Method 2. In order to evaluate $\dot{V}$ in (5.72), it is required to know the value of $x_m(t)$. Assuming that $r(t) = c, \ \forall t \geq t_0$ and $x_m(t_0) = c$, we obtain that

$$x_m(t) = c, \ \forall t \geq t_0. \tag{5.85}$$

In a similiar manner to Method 2, we need to find the maximum τ such that a bounded region of attraction exists. When $r(t) = 1$ and the adaptive parameters are $\gamma = 0.5$ and $\sigma = 0.5$, the search results are plotted in (5-9). The figure shows that a

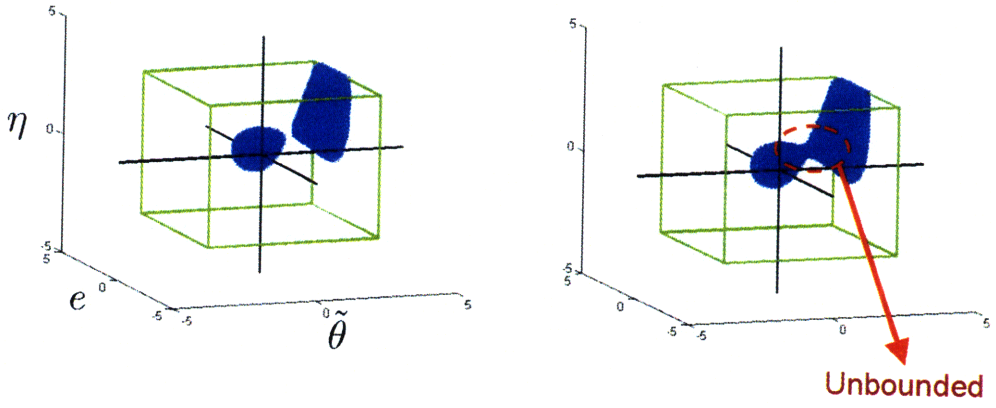

Figure 5-9: The region where $\dot{V}(e, \tilde{\theta}, \eta) \geq 0$ is shaded in blue. A bounded set of attraction exists when $\tau = 0.15$ (left) but there is no bounded set for $\tau = 0.16$.

bounded region of attraction exists when $\tau = 0.15$ but as τ increases, the region of attraction becomes unbounded. Using Method 3, we can reduce the analytic margin to $\tau_m = 0.15$.

We utilize Method 1, 2, and 3 to reduce the conservatism in the analytic margins for the first order plant in (5.67). For comparison purpose, we find simulation-based margins where all the signals in the simulation result are bounded. Table 5.1 compares the margins from analytic methods and simulation study for $\gamma = 0.5,\ 1,\ 2,\ 5$ and $\sigma = 0.5$. As seen in the table, the margins decrease in both analysis and simulation

Adaptive rate (γ)	0.5	1	2	5
Analytic Margin	0.039	0.012	0.0035	0.00061
Method 1	0.040	0.029	0.023	0.011
Method 2	0.081	0.064	0.049	0.032
Method 3	0.15	0.11	0.079	0.047
Simulation-based Margin	0.45	0.40	0.38	0.30

Table 5.1: Analytic and simulation-based margins for the first order plant when $\gamma = 0.5,\ 1,\ 2,\ 5$ and $\sigma = 0.5$.

as the adaptive gain (γ) increases. As we use Method 1, 2, and 3 in the analytic margin, we can reduce the gap between analytic and simulation-based margins and with Method 3, they are finally in the same order of magnitude when $\gamma = 0.5$.

5.4.3 Time delay and the Pade approximations

Time-delay ($e^{-\tau s}$) can be approximated only in a limited range of frequency as shown in Figure 5-10. Figure 5-10 compares the phase plots of the time delay and the first, second, and third order Pade approximations. As the order of the approximation increases, the frequency range where the approximation is relevant also increases. Therefore, in order to approximate the input-output relation of $e^{-\tau s}$ with the Pade approximations, it is required to investigate the frequency range in the control input signal. When the maximum frequency of the control input remains in the frequency

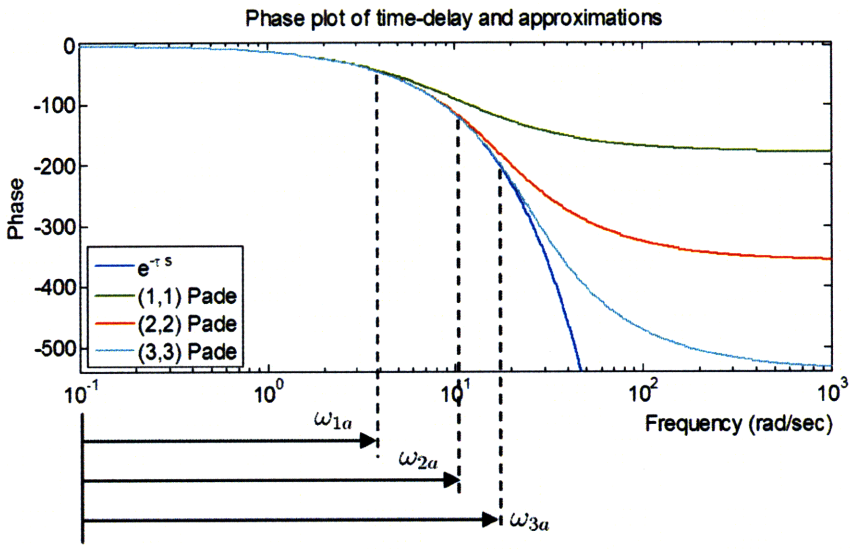

Figure 5-10: Phase plot of time-delay and the Pade approximations.

range where $e^{-\tau s}$ is properly approximated, it is appropriate to replace $e^{-\tau s}$ with the approximation. Then τ_m which is obtained based on the Lyapunov analysis can be claimed as an analytic margin. However, we need to use more precise approximations when the control input signal has frequencies where the time-delay and the approximation do not match. Then the order of the approximation needs to be increased until the frequency condition is met. The following is the pseudo code to compute the analytic margin.

SET n to zero
REPEAT
    COMPUTE the analytic margin τ_m with (n, n) Pade approximation
    COMPUTE the frequency ω^* where $e^{-\tau s}$ and (n, n) Pade approximation depart
    SIMULATE with time-delay τ_m
    COMPUTE the frequency of control input signal ω_s
UNTIL $\omega_s \leq \omega^*$

One may argue that this loop can run infinitely. However, as we witnessed in the previous computation, the analytic margin, τ_m, decreases with the order of Pade approximation. With the increased order, the range of frequency where the time-delay

and its approximation match widen while the control input becomes less oscillatory. This guarantees the convergence of the loop in the above code.

We use the first order adaptive system from (5.67) to (5.70) to justify the replacement of time-delay with the Pade approximations. When the adaptive parameters are given as $\gamma = 0.5$, $\sigma = 0.5$, we obtain the analytic margin as $\tau_m = 0.15$. For this τ_m, we can draw the phase plots of the time-delay and $(1,1)$ Pade approximation as shown in Figure 5-11. When the frequency of the control input is less than $5.13 rad/sec$,

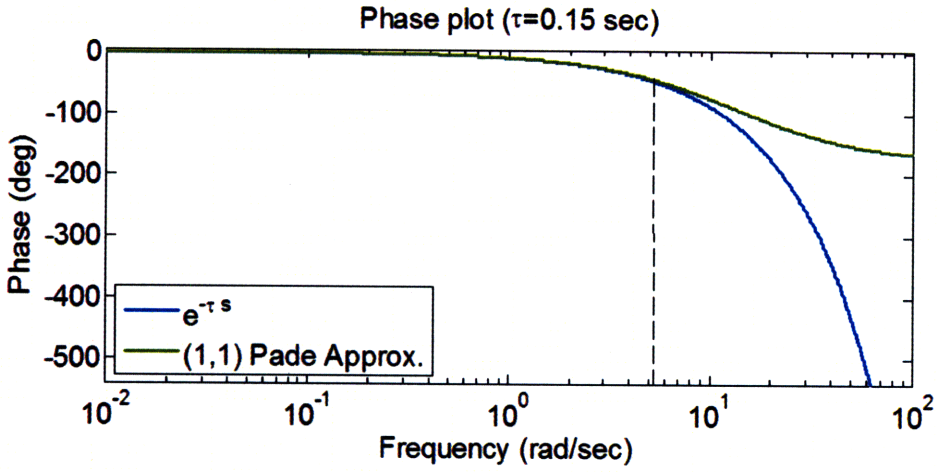

Figure 5-11: Phase plot of time-delay and $(1,1)$ Pade approximation ($\tau = 0.15$).

then the phase difference between the delay and the first order Pade approximation is less than 2°. Then we simulate in the presence of the time delay with $\tau = 0.15$ and obtain the control input signal to check if its dominant frequency is within the range of $5.13 rad/sec$ where the delay is properly approximated.

As we can see in Figure 5-12, the amplitude spectrum of the control input signal becomes negligible when the frequency is beyond $1 rad/sec$. From the result in Figure 5-12, we can conclude that $(1,1)$ Pade approximation can replicate the time-delay for the given adaptive parameters. Therefore, stability of the closed-loop system with adaptive control is guaranteed when $\tau < 0.15$. Furthermore, we compute the frequencies of control inputs for various adaptive parameters to check if they are within the range where the time-delay is properly approximated. Results are tabulated in Table 5.2. As shown in Table 5.2, the dominant frequencies in control inputs are less than

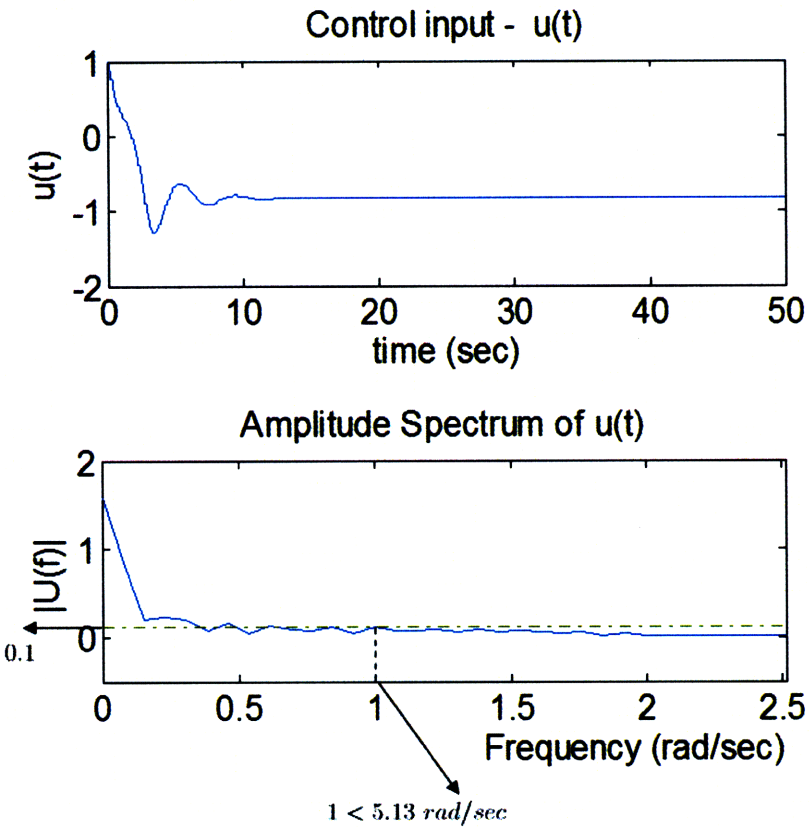

Figure 5-12: Control input signal (above) with the delay ($\tau = 0.15$) and the amplitude spectrum of the control input (below)

Adaptive rate (γ)	0.5	1	2	5
Method 3	0.15	0.11	0.079	0.047
Departing frequency (ω^*)	5.13	7.00	9.74	16.38
Dominant frequency in control inputs(ω_s)	1.00	0.63	0.59	0.28
Order of the Pade approximation (n)	1	1	1	1

Table 5.2: Analytic margins with the Pade approximation. departing frequencies, and dominant frequencies in control input

the departing frequencies so that the $(1,1)$ Pade approximation is relevant.

5.4.4 Delay Margins in a Generic Transport Model (GTM)

One instance which mandates to develop stability margins in adaptive control is that a technical tool to estimate its robustness is required to transition adaptive control to safety critical application such as a passenger aircraft. As an extended study of the first order plant in Section 5.4.2, we find the analytic margins with the GTM. To investigate the analytic margin, we employ a C-5A (Galaxy) aircraft as the model and compute the margins. The planform of a C-5A aircraft is given in Figure 5-13. The short period dynamics of the C-5A in [11] is given in the presence of uncertainties

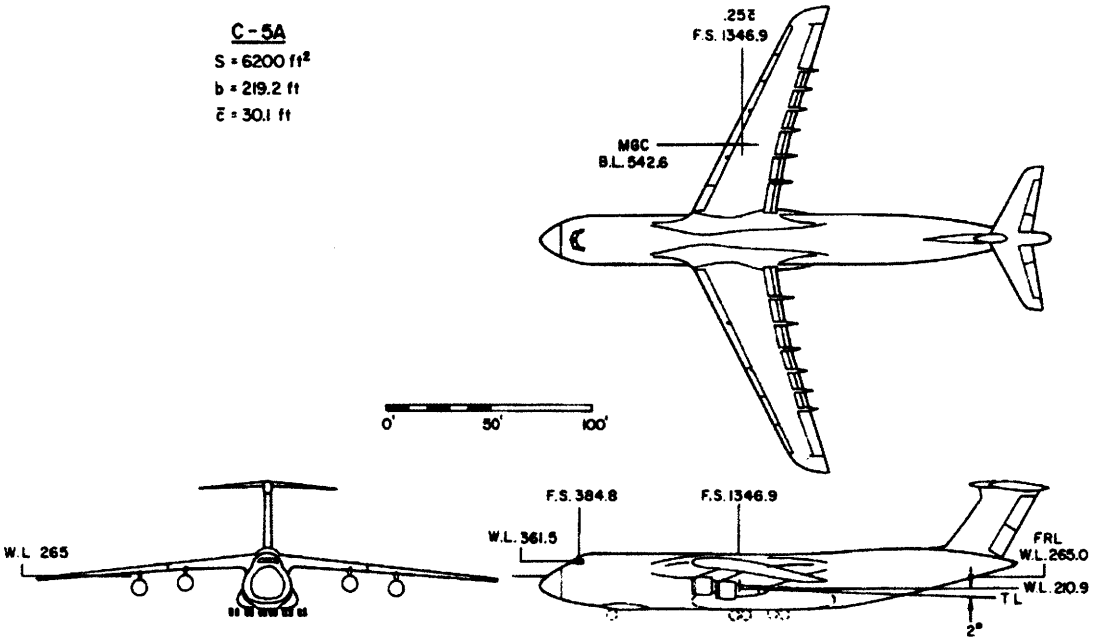

Figure 5-13: Planform of the C-5A aircraft [11]

and time-delay in the form of

$$\underbrace{\begin{bmatrix} \dot{\alpha} \\ \dot{q} \\ \dot{e}_\alpha \end{bmatrix}}_{\dot{x}_p} = \underbrace{\begin{bmatrix} Z_\alpha & 1 & 0 \\ \lambda_\alpha M_\alpha & \lambda_q M_q & 0 \\ 1 & 0 & 0 \end{bmatrix}}_{A_{p\lambda}} \underbrace{\begin{bmatrix} \alpha \\ q \\ e_\alpha \end{bmatrix}}_{x_p} + \underbrace{\begin{bmatrix} 0 \\ M_u \\ 0 \end{bmatrix}}_{b_{p_1}} \lambda e^{-\tau s} u + \underbrace{\begin{bmatrix} 0 \\ 0 \\ -1 \end{bmatrix}}_{b_{p_2}} r \qquad (5.86)$$

where λ_α, λ_q, and λ are uncertainties and τ is an unknown time-delay. For nominal control, we design LQR PI controller based on the known part of the plant and then we build a reference model to be tracked by the adaptive controller. With the error between the plant and the reference model, the adaptive controller is designed in an augmentation with the nominal LQR PI controller.

The analytic margins of the C-5A are obtained by Method 1 and 2 introduced in Section 5.4.2. For given uncertainties as $\lambda = 0.8$, $\lambda_\alpha = -0.2$, and $\lambda_q = 1$, the analytic margins are computed for the case where $\sigma = 0.5$ and γ is set to 2, 3, 4, 5, and 10. Results of the analytic and simulation-based margins are shown in Table 5.3. When the analytic margins are obtained from Method 1, its margin is more

Adaptive rate (γ)	2	3	4	5	10	Computation Time
Method 1	0.0077	0.0069	0.0062	0.0051	0.0040	11.6 sec
Method 2	0.0089	0.0082	0.0076	0.0071	0.0059	1 hr 43 sec
Simulation Margin	0.29	0.27	0.24	0.20	0.16	

Table 5.3: Analytic and simulation-based margins for the short period dynamics of C-5A when $\gamma = 2,\ 3,\ 4,\ 5,\ 10$ and $\sigma = 0.5$.

conservative but it can be computed more efficiently. When we use Method 2, i.e. evaluate $G(e, \tilde{\theta}, \eta)$ and search a bounded region of attraction, analytic margins are less conservative whereas computational workloads become high.

5.5 Summary

In this chapter, we derived the delay margins of the proposed adaptive controller for linear plants whose states are accessible. In particular, semi-global boundedness of states is established with respect to the amount of time-delay, using the general (n, n) Pade approximation. The delay margins derived theoretically are validated with the NASA X-15 aircraft and they are compared with margins from simulation studies. We also investigate the effect of adaptive parameters on the margins. In order to

reduce the gap between analytic and simulation-based margins, we proposed three methods which are shown to be useful by the first order plant. These methods are finally validated by a generic transport model aircraft.

Chapter 6

Summary and Future Work

6.1 Summary

In order to deploy adaptive control to safety critical applications such as flight control, a unified framework needs to be developed to design and analyze adaptive control in the presence of both parametric and nonparametric uncertainties, control failures, multi-input saturation, and perturbations such as time-delay. In particular, analytical tools to measure its robustness with respect to perturbations are of paramount importance since absence of those tools has been one of critical obstacles to utilize the adaptive controller. In addition, a formal stability analysis is provided to combine adaptive control with a gain-scheduling nominal controller for a general nonlinear system and this analysis has a critical value in a sense that most of physical systems are represented by nonlinear dynamics.

The importance of compensating multi-input saturation is highlighted in Chapter 3. In this chapter, we develop an extension of the approach used in [19] to multi-input systems. First of all, to utilize the characteristic of direction-preserving in its constrained inputs, we introduce an artificial elliptical multi-input saturation and provide stability analysis while the proposed adaptive controller is in an augmentation with the nominal PI controller. This result is naturally extended to the case where inputs are constrained in magnitude with a realistic multi-input saturation. Then we derive sufficient conditions for boundedness of the closed-loop system, showing that stability

result is semi-global with respect to the level of saturation. In other words, boundedness is globally guaranteed without input saturation while locally guaranteed with input saturation and its region of attraction is determined by the degree of saturation. Through the simulation studies based on the nonlinear 6–DoF model of NASA X–15 hypersonic aircraft, we demonstrate the proposed adaptive controller follows the desired model even when actuator anomalies are present. Simulation studies also show that the compensating method for magnitude saturation prevents input signals from being excessively oscillatory and then being susceptible to structural failure.

In Chapter 4, we discussed design, stability analysis, and assessment of the proposed adaptive controller when it is augmented with gain-scheduling algorithm to control nonlinear systems. Under the assumption that the underlying nonlinear systems are composed of multi-rate state variables, the approach taken in the control design consists of two steps; the outer-loop controller is designed to control the slow state variables and the inner-loop counterpart is designed to regulate the fast state variables. The adaptive controller is combined with the gain-scheduling controller and is proposed as the inner-loop controller. A non-adaptive controller is designed in the outer-loop. The adaptive law is built such that global boundedness of state variables and adaptive parameters are guaranteed based on Lyapunov stability theory. The nonlinear 6–DoF model of NASA X–15 hypersonic aircraft is utilized to demonstrate the control design. To accomplish gain-scheduling, multiple trim points are chosen over the large flight envelope based on gain-scheduling variables and a fixed gain controller is designed as the inner-loop controller at each frozen trim point. Then the inner-loop controller is implemented to vary with the current values of gain-scheduling variables. Augmented with the inner-loop gain-scheduling controller, the adaptive controller is designed to cope with uncertainties. Simulations results show that the augmented adaptive controller with the gain-scheduling nominal controller is capable of stabilizing in the presence of uncertainties while instability cannot be overcome only with the nominal controller. Though non-augmented adaptive controller can stabilize the closed-loop system, it causes state variables to have undesirable high frequency signals.

As we see in the previous results, the adaptive controller promises its ability to change control parameters on-line in order to guarantee safety and reliability during various maneuvers when uncertainties are present. While stability of adaptive control systems and their robustness to disturbances, unmodeled dynamics, and time-delays have been extensively analyzed for last three decades, what is missing is the development of margins that explicitly quantifies the extent of these perturbations that the adaptive controller can withstand. We make an attempt to quantify theoretically the robustness of adaptive controllers to time-delays and unmodeled dynamics. To develop analytical margins, a formal stability analysis is conducted which results in semi-global boundedness with respect to the perturbations. The margins derived analytically are validated using a generic transport model (GTM). For given adaptive parameters, we first compute the analytical margins and compare with margins that we obtain from simulation studies. It should be worth noting that both margins are reduced when the adaptation rate (γ) is increased. In order to reduce the gap between the simulation-based margin and the analytic margin, we utilize numerical methods which provide less conservative margins but require more computational workloads.

6.2 Future Work

In this section, we introduce the future work associated with this thesis. These include rate saturation in the adaptive control inputs, robust adaptive control in a linear time-varying system, and numerically efficient stability / robustness analysis tools.

Inputs in flight control applications are generally constrained in both magnitude and rate. From simulation studies, we found that the same compensation algorithm for rate saturation also works efficiently as well as for magnitude saturation. Furthermore, the combined constraints in both magnitude and rate can be compensated with the similar algorithm discussed in Chapter 3. Though results from simulation studies are convincing, there is no formal stability analysis for the case when the rates of inputs are saturated. Once such an analysis is completed, the theoretical gaps between

adaptive control theory and its application can be reduced and the usage of adaptive control will be expedited.

To control a nonlinear plant over a large flight envelope, adaptive control is augmented with the gain-scheduling nominal controller. To provide rigorous stability analysis, we use a robust adaptive controller in [21] where the adaptive law is modified to prevent adaptive control parameters from diverging due to disturbances. It is well known that the adaptive law should be robustified when there are disturbances in state variables [28]. However, the closed-loop system with adaptive control in Chapter 4 has bounded disturbances in adaptive parameters not in state variables. It is mainly due to the matching conditions of linear time-varying (LTV) systems. When the underlying plant is represented by a linear time-invariant (LTI) system, ideal adaptive parameters (θ^*) are obtained as constants from the matching condition. When it comes to a LTV system, ideal adaptive parameters become bounded functions of time. This, in turn, implies that there exist disturbances in adaptive parameters. Since adaptive control is capable of coping with parameter variations, it is certain that stability can be guaranteed without robust adaptive control. This is also observed in simulation studies but there is no formal stability analysis yet. The value of this work will be critical because there is no formal method even in designing linear controllers to guarantee stability for a general LTV system.

In addition to the analytic margin developed in the previous chapter, it is necessary to develop numerically efficient techniques to estimate stability / robustness boundaries for a given system with an adaptive controller and a pre-specified set of uncertainties. Since thorough computation studies require high workload but are necessary in practice, stability / robustness analysis tools should be numerically efficient. This will contribute to Verification and Validation (V&V) techniques for general adaptive systems. Utilizing the proposed numerical tools, it is hoped that the worst case uncertainties that the adaptive controller can withstand will be determined theoretically for a given controller design.

The research topics introduced above are under development and they will contribute to improve adaptive control to one of the enabling technologies for safety

critical applications such as aircraft, spacecraft, automobiles, and underwater vehicles. Particularly in flight control applications, adaptive control is designed for high performance aircraft such as the X-43 hypersonic aircraft and it will be flight-tested in the near future under the circumstances where there are numerous unknown uncertainties. For examples, it is highly expected that adaptive control can mitigate the effect of shock waves on the control surface effectiveness as the aircraft flies faster than than the speed of sound. With success on unmanned aerial vehicles, adaptive control will be transition to passenger jet aircraft where safety is one of the most critical issues in control design. This will trigger the development of more precise and numerically efficient tools for validation and verification (V&V).

Appendix A

NASA X-15 Hypersonic Aircraft

In order to evaluate the performance of the proposed adaptive controller, a nonlinear 6-DoF flight dynamics model is constructed based on NASA X-15's aerodynamic data. In this chapter, we introduce NASA X-15 hypersonic aircraft with a brief review of its history and discuss the formulation of its nonlinear flight dynamics model.

A.1 History

The X-15 was designed for a hypersonic research aircraft and had the first flight in 1959. The X-15 fuselage was long and cylindrical as shown in Figure A-1 and it was a missile shaped vehicle with an wedge-shaped vertical tail powered by a rocket engine. The X-15 was designed to be carried aloft under the wing of a B-52 bomber plane like other experimental aircraft. Three NASA X-15s were built and they were flown over a period of nearly 10 years - from 1959 to 1968 with making a total of 199 flights. The X-15 program successfully contributed to investigate various aspects of manned hypersonic aircraft and information gained from this program was later used to design the space shuttle.

Unfortunately, there was only one fatal accident during the entire X-15 program. On November 15th 1967, the third X-15 aircraft was launched in Nevada and an electrical disturbance degraded the aircraft's controllability while climbing. The aircraft began a slow drift in heading, which soon became a spin. Through some combination

Figure A-1: NASA X-15 hypersonic aircraft [3]

of pilot technique and basic aerodynamic stability, the pilot recovered from the spin and entered an inverted Mach 4.7 dive. As the X-15 plummeted into the increasingly thicker atmosphere, "so called" adaptive flight control system caused the vehicle to begin oscillating. As the pitching motion increased, aerodynamic forces finally broke the aircraft into several pieces.

A.2 X-15 Flight Dynamics Model

The X-15 flight dynamics is modeled using five components as shown in Figure A-2. These include the equations of motion, aerodynamics data, actuator dynamics, actuator saturation, and sensor dynamics. Each of these components is discussed in discussed in subsequent sections.

A.2.1 Equations of Flight Dynamics

In order to derive the equation of motion, state and input variables are introduced in Table A.1 as well as constants relating to aircraft specifications and geometry.

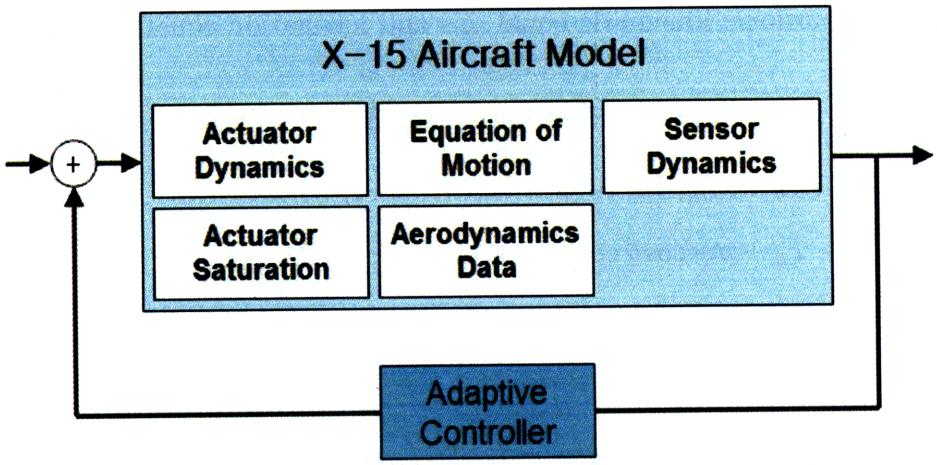

Figure A-2: The full nonlinear X-15 aircraft model

Table A.1: Nomenclature

N	Aircraft position (North)	M_x	Aerodynamic Moment (x-axis)
E	Aircraft position (East)	M_y	Aerodynamic Moment (y-axis)
D	Aircraft position (Down)	M_y	Aerodynamic Moment (z-axis)
α	Angle-of-Attack	δ_{th}	Thrust
β	Sideslip angle	δ_{Left}	Left elevon deflection
p	Roll rate	δ_{Right}	Right elevon deflection
q	Pitch rate	δ_r	Rudder deflection
r	Yaw rate	δ_e	Elevator deflection
V_T	True Airspeed	δ_a	Aileron deflection
ϕ	Roll angle	b_{ref}	Aircraft wingspan
θ	Pitch angle	c_{ref}	Mean aerodynamic chord
ψ	Heading angle	S	Wing surface area
u	Aircraft velocity (x-direction)	W	Aircraft gross weight
v	Aircraft velocity (y-direction)	I_{xx}	Moment of Inertia (x-axis)
w	Aircraft velocity (z-direction)	I_{yy}	Moment of Inertia (y-axis)
h	Altitude	I_{zz}	Moment of Inertia (z-axis)
F_x	Aerodynamic Forces (x-direction)	I_{xz}	Product of Inertia (xz-plane)
F_y	Aerodynamic Forces (y-direction)		
F_z	Aerodynamic Forces (z-direction)		

With given notations in Table A.1, the standard equations of motion can be formulated based on conservation laws. These includes linear momentum and angular momentum equations, kinematic equations and navigation equations as

$$
\begin{aligned}
F_x - mg\sin\theta &= m(\dot{u} + qw - ru) \\
F_y + mg\cos\theta\sin\phi &= m(\dot{v} + ru - pw) \\
F_z + mg\cos\theta\cos\phi &= m(\dot{u} + qw - ru)
\end{aligned}
$$

$$
\begin{aligned}
M_x &= I_{xz}\dot{p} - I_{xz}\dot{r} + qr(I_{zz} - I_{yy}) - I_{xz}pq \\
M_y &= I_{yy}\dot{q} + rq(I_{xx} - I_{zz}) + I_{xz}(p^2 - r^2) \\
M_z &= -I_{xz}\dot{p} + I_{zz}\dot{r} + pq(I_{yy} - I_{xx}) + I_{xz}qr
\end{aligned}
$$

$$
\begin{aligned}
\dot{\theta} &= q\cos\phi - r\sin\phi \\
\dot{\phi} &= p + q\sin\phi\tan\theta + r\cos\phi\tan\theta \\
\dot{\psi} &= (qsin\phi + r\cos\phi)\sec\theta
\end{aligned}
\tag{A.1}
$$

$$
\begin{aligned}
\dot{N} &= u\cos\theta\cos\psi + v(-\cos\phi\sin\psi + \sin\phi\sin\theta\cos\psi) \\
&+ w(\sin\phi\sin\psi + \cos\phi\sin\theta\cos\psi), \\
\dot{E} &= u\cos\theta\sin\psi + v(\cos\phi\cos\psi + \sin\phi\sin\theta\sin\psi) \\
&+ w(-\sin\phi\cos\psi + \cos\phi\sin\theta\sin\psi), \\
\dot{h} &= u\sin\theta - v\sin\phi\cos\theta - w\cos\phi\cos\theta.
\end{aligned}
$$

A.2.2 Aerodynamic Data

The aerodynamic forces and moments acting on the aircraft are generally written with non-dimensional force and moments coefficients multiplied by dynamic pressure and geometric constants [37]. Forces acting on the aircraft body can be computed by transforming aerodynamics forces such as lift and drag in stability axes to those in

body axes. Forces and moments are described by

$$\begin{bmatrix} F_x \\ F_y \\ F_z \end{bmatrix} = \bar{q}S \begin{bmatrix} \cos\alpha & 0 & -\sin\alpha \\ 0 & 1 & 0 \\ \sin\alpha & 0 & \cos\alpha \end{bmatrix} \begin{bmatrix} -C_D \\ C_Y \\ -C_L \end{bmatrix}, \quad \begin{bmatrix} M_x \\ M_y \\ M_z \end{bmatrix} = \bar{q}S \begin{bmatrix} b_{ref}C_l \\ c_{ref}C_m \\ b_{ref}C_n \end{bmatrix} \tag{A.2}$$

where C_L, C_D, and C_Y are lift, drag, and side-force coefficients respectively and C_l, C_m, and C_n are the moment coefficients. These coefficients are functions of state variables and inputs. The X-15 totally has four control inputs: one thrust (δ_{th}) and three control surfaces (Figure A-3). A rudder (δ_r) is designed for yaw control, and roll and pitch are controlled by elevons (δ_{Left}, δ_{Right}) which combines functions of the elevator and the aileron. From the deflection of elevons, the elevator and the aileron inputs can be computed as

$$\delta_e = \frac{\delta_{Left} + \delta_{Right}}{2}, \ \delta_a = \frac{\delta_{Left} - \delta_{Right}}{2}. \tag{A.3}$$

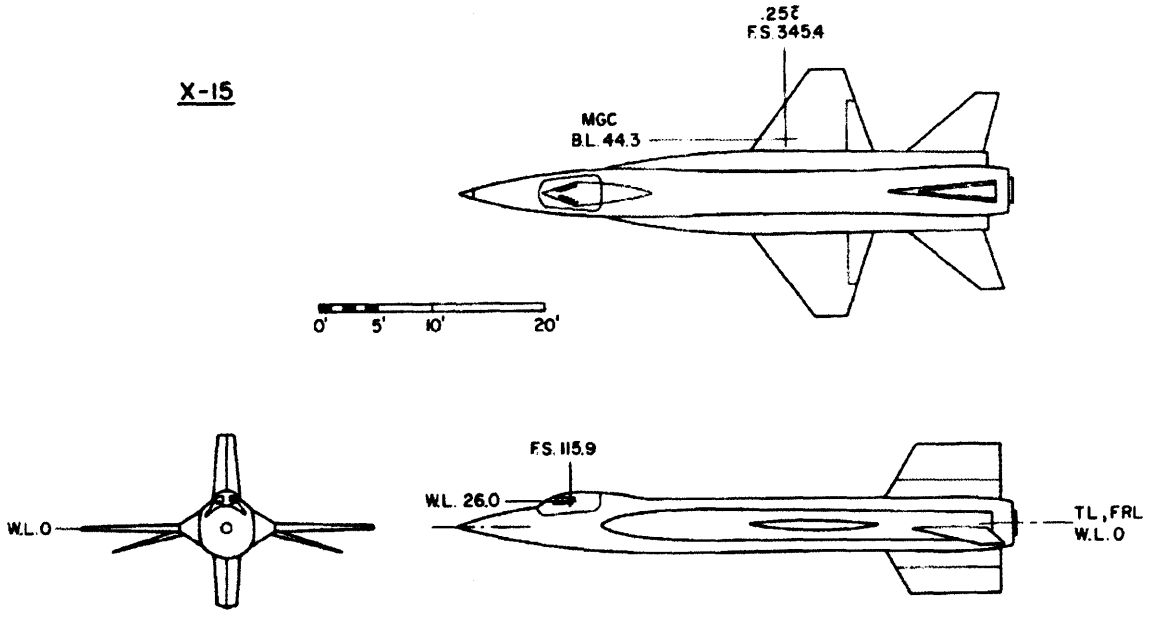

Figure A-3: Planfrom of the X-15 hypersonic aircraft [12].

With the above control inputs, the force and moment coefficients are written in

the following form:

$$
\begin{aligned}
C_L &= C_{L_{wing-body}} + C_{L_{\delta_e}}\delta_e \\
C_D &= C_{D_{wing-body}} + C_{D_{\delta_e}}\delta_e + C_{D_{\delta_{SB}}}\delta_{SB} \\
C_Y &= C_{Y_\beta}\beta + C_{Y_p}p\frac{b_{ref}}{2V_T} + (C_{Y_r} - C_{Y_{\dot\beta}})(r - \dot\beta)\frac{b_{ref}}{2V_T} + C_{Y_{\delta_a}}\delta_a + C_{Y_{\delta_r}}\delta_r \\
C_l &= C_{l_\beta}\beta + C_{l_p}p\frac{b_{ref}}{2V_t} + (C_{l_r} - C_{l_{\dot\beta}})(r - \dot\beta)\frac{b_{ref}}{2V_T} + C_{l_{\delta_a}}\delta_a + C_{l_{\delta_r}}\delta_r \\
C_m &= C_{m_{wing-body}} + (C_{m_q} + C_{m_{\dot\alpha}})(q - \dot\alpha)\frac{c_{ref}}{2V_T} + C_{m_{\delta_e}}\delta_e + C_{m_{\delta_{SB}}}\delta_{SB} \\
C_n &= C_{n_\beta}\beta + C_{n_p}p\frac{b_{ref}}{2V_t} + (C_{n_r} - C_{n_{\dot\beta}})(r - \dot\beta)\frac{b_{ref}}{2V_T} + C_{n_{\delta_a}}\delta_a + C_{n_{\delta_r}}\delta_r
\end{aligned}
\tag{A.4}
$$

$C_{L_{wing-body}}$, $C_{D_{wing-body}}$, and $C_{m_{wing-body}}$ are the coefficients of lift, drag, and pitching moment with respect to the wing and the body. $C_{D_{\delta_{SB}}}$ and $C_{m_{\delta_{SB}}}$ are the coefficients of drag and pitching moment with respect to the speed brakes. Though they are included in the aircraft to increase drag and pitching moment, it is not modeled in the simulation setup. All other aerodynamic coefficients in (A.4) are non-dimensional derivatives which are found by wind tunnel tests, flight tests, and theoretical studies [40, 42, 43]. These derivative (shown in Figure A-4) are transformed to lookup tables based on Mach number and angle of attack. Equations from (A.1) to (A.4) construct the model of NASA X-15 hypersonic aircraft.

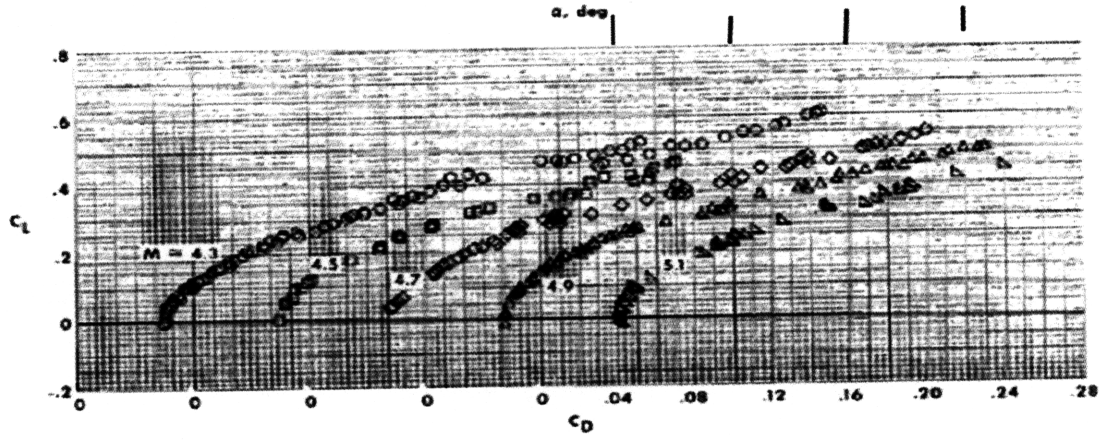

Figure A-4: Lift and drag coefficients [13].

A.2.3 Actuators and Sensors

The control input deflections on the X-15 aircraft were actuated by hydraulic actuators. The dynamics of these actuators can be modeled as second order systems with transfer functions described by

$$G_{actuator}(s) = \frac{\omega_n^2}{s^2 + 2\zeta\omega_n + \omega_n^2} \tag{A.5}$$

where the damping ratio $\zeta = 0.7$ and natural frequency $\omega_n = 90$ Hz for the elevons and $\omega_n = 70$ Hz for the rudder. The actuator saturation limits were imposed to be $\pm 15°$ for the elevons and $\pm 30°$ the rudder. The rates of the aircraft p, q, and r were measured by rate gyroscopes, however the dynamics of these sensors were neglected for simulation studies.

Appendix B

Proofs and Constants

B.1 Proof of Proposition 4.1

Proof. We define a compact set S such that

$$(X_{g,i},\ X(X_{g,i}),\ U_1(X_{g,i})) \in S, \quad i = 1,\ 2,\ \cdots, k. \tag{B.1}$$

This implies S covers all operating points of the nonlinear plant in (4.1). For simplicity, we also define

$$H(X,\ X_g,\ U_1) = f(X,\ X_g) + g(X,\ X_g)U_1. \tag{B.2}$$

When $h_c(X_g, X_{g,cmd})$ is designed, X_g follows $X_{g,cmd}$ in a bounded manner so that $X^*(t)$ and $U_1^*(t)$ are bounded from the definitions in (4.8). Then, there exist Lipschitz constants, L, L_g, and L_u, such that

$$\begin{aligned} &\left\| H(X^*(t), X_g(t), U_1^*(t)) - H(X(X_{g,i}), X_{g,i}, U_1(X_{g,i})) \right\| \\ &\leq L \left\| X^*(t) - X(X_{g,i}) \right\| + L_g \left\| X_g(t) - X_{g,i} \right\| + L_u \left\| U_1^*(t) - U_1(X_{g,i}) \right\|. \end{aligned} \tag{B.3}$$

From (4.8), (B.3) can be written as

$$\begin{aligned} &\left\| H(X^*(t), X_g(t), U_1^*(t) - H(X(X_{g,i}), X_{g,i}, U_1(X_{g,i})) \right\| \\ &\leq (L_p M + L_g + L_u N) \left\| X_g(t) - X_{g,i} \right\| \end{aligned} \tag{B.4}$$

where $M = \max_{1 \leq i \leq k} \|M_i\|$ and $N = \max_{1 \leq i \leq k} \|N_i\|$. From Assumption 2, (B.4) is rewritten as

$$\begin{aligned} &\left\| H(X^*(t), X_g(t), U_1^*(t)) - H(X(X_{g,i}), X_{g,i}, U_1(X_{g,i})) \right\| \\ &\leq (L_p M + L_g + L_u N) \, \epsilon_2. \end{aligned} \tag{B.5}$$

The higher order term, $O(x_p^2)$, can be neglected and by differentiating both sides in (4.8) and using Assumption 1, the following inequality is obtained:

$$\left\| \dot{X}^*(t) \right\| < M \epsilon_1. \tag{B.6}$$

Finally, it is shown that $\epsilon_x(t)$ is uniformly bounded and its bound has dependency on ϵ_1 and ϵ_2 as

$$\|\epsilon_x(t)\| \leq M \epsilon_1 + (L_p M + L_g + L_u N) \, \epsilon_2. \tag{B.7}$$

□

B.2 Constants for Theorem 5.2

$$
\begin{aligned}
C_{4,0,0} &= \gamma|\lambda||c_\eta^\top b_\tau|\|b_{p_1}^\top P\|^2 \\
C_{3,0,1} &= \gamma a_0\|c_\eta c_\eta^\top + 2R\|\|b_\tau\|\|b_{p_1}^\top P\| \\
C_{2,2,0} &= a_0|c_\eta^\top b_\tau| \\
C_{1,2,1} &= |\lambda|a_0\|c_\eta c_\eta^\top + 2R\|\|b_\tau\|\|b_{p_1}\| \\
C_{3,0,0} &= 2\gamma|\lambda|c_0 r_0|c_\eta^\top b_\tau|\|b_{p_1}^\top P\|^2 \\
C_{2,1,0} &= |c_\eta^\top b_\tau|\Big[|\lambda|\|b_{p_1}^\top P\|\,(\sigma + \|A_m\|) + a_0\|k + \theta_x^*\|\Big] + |\lambda|\|b_{p_1}^\top P\| \\
C_{2,0,1} &= 2\gamma a_0 c_0 r_0\|c_\eta c_\eta^\top + 2R\|\|b_\tau\|\|b_{p_1}^\top P\| \\
C_{1,2,0} &= a_0|c_\eta^\top b_\tau|(c_0 r_0 + 1) \\
C_{1,1,1} &= a_0\left[|c_\eta^\top b_\tau| + \|c_\eta c_\eta^\top + 2R\|\|b_\tau\|\big(\sigma + \|A_m\| + |\lambda|\|b_{p_1}\|\|k + \theta_x^*\|\big) + \|c_\eta\|\right] \\
C_{0,2,1} &= |\lambda|a_0\|c_\eta c_\eta^\top + 2R\|\|b_\tau\|\|b_{p_1}\|(c_0 r_0 + 1) \\
C_{0,1,2} &= |\lambda|a_0\|c_\eta c_\eta^\top + 2R\|\|b_\tau\|\|b_{p_1}\| \\
C_{2,0,0} &= |\lambda||c_\eta^\top b_\tau|\|b_{p_1}^\top P\|\Big[\gamma\|b_{p_1}^\top P\|(c_0^2 r_0^2 + 1) + \sigma\|\theta^*\| + \|k + \theta_x^*\|\|A_m\|\Big] - \frac{q_{\min}}{2} \\
C_{1,1,0} &= |c_\eta^\top b_\tau|\Big\{|\lambda|\|b_{p_1}^\top P\|\Big[\sigma(c_0 r_0 + 1) + (\|A_m\|c_0 + \|b_m\|)r_0\Big] \\
&\quad + a_0(c_0 r_0 + 1)\|k + \theta_x^*\|\Big\} + |\lambda|\|b_{p_1}^\top P\|(c_0 r_0 + 1) \\
C_{1,0,1} &= a_0|c_\eta^\top b_\tau|\|k + \theta_x^*\| + a_0\|c_\eta c_\eta^\top + 2R\|\|b_\tau\|\Big[\gamma\|b_{p_1}^\top P\|(c_0^2 r_0^2 + 1) + \sigma\|\theta^*\| \\
&\quad + \|k + \theta_x^*\|\|A_m\|\Big] + |\lambda|\|b_{p_1}^\top P\| + |\lambda|\|c_\eta\|\|b_{p_1}^\top P\|\|A_m\| \\
C_{0,1,1} &= a_0\|c_\eta c_\eta^\top + 2R\|\|b_\tau\|\Big[(c_0 r_0 + 1)(\sigma + |\lambda|\|b_{p_1}\|\|k + \theta_x^*\|) \\
&\quad + (\|A_m\|c_0 + \|b_m\|)r_0\Big] + a_0\|c_\eta\|(c_0 r_0 + 1) \\
C_{0,0,2} &= |\lambda|a_0\|c_\eta c_\eta^\top + 2R\|\|b_\tau\|\|b_{p_1}\|\|k + \theta_x^*\| + a_0\|c_\eta\| \\
C_{1,0,0} &= |\lambda|\|b_{p_1}^\top P\||c_\eta^\top b_\tau|\Big[\sigma(c_0 r_0 + 1)\|\theta^*\| + \|k + \theta_x^*\|(\|A_m\|c_0 + \|b_m\|)r_0\Big] \\
C_{0,0,1} &= a_0\|c_\eta c_\eta^\top + 2R\|\|b_\tau\|\Big[\sigma(c_0 r_0 + 1)\|\theta^*\| + \|k + \theta_x^*\|(\|A_m\|c_0 + \|b_m\|)r_0\Big].
\end{aligned}
\tag{B.8}
$$

Bibliography

[1] Karl J. Astrom and Bjorn Wittenmark. *Adaptive Control.* Addison-Wesley, Reading, MA, 2nd edition, 1996.

[2] Marc Bodson and William A. Pohlchuck. Command limiting in reconfigurable flight control. *Journal of Guidance, Control, and Dynamics*, 21(4):639 – 646, 1998.

[3] NASA Dryden Research Center. http://www.dfrc.nasa.gov/gallery/photo/X-15/.

[4] NASA Dryden Research Center. http://www.dfrc.nasa.gov/gallery/photo/X-43A/.

[5] J.-Y. John Cheng and Yi-Ming Wang. *Adaptive Control of Nonsmooth Dynamic Systems*, Chapter 12. Adaptive Control for Systems with Input Constraints - A Survey, pages 311–332. edited by Gang Tao and Frank L. Lewis. Springer, London, 2001.

[6] Aniruddha Datta and Petros A. Ioannou. Robustness analysis of commonly used adaptive control structures. In *Proceedings of the 29th Conference of Decision and Control*, Honolulu, Hawaii, 1990.

[7] Jonh Van de Vegte. *Feedback Control Systems.* Prentice Hall, Eagelwood, New Jersey, third edition, 1994.

[8] Zachary T. Dydek, Himani Jain, Jinho Jang, Anuradha M. Annaswamy, and Eugene Lavretsky. Theoretically verifiable stability margins for an adaptive controller. In *Proceedings of AIAA Guidance, Navigation, and Control Conference*, Keystone, CO, 2006.

[9] David G. Ward et al. Flight test results of an adaptive guidance system for reusable launch vehicles. In *Proceedings of 2nd AIAA Unmanned Unlimited Systems Systems, Technologies, and Operations – Aerospace, Land, and Sea Conference and Workshop & Exhibit*, 2003.

[10] Gene F. Franklin, J. David Powell, and Abbas Emami-Naeini. *Feedback Control of Dynamic Systems.* Addison-Wesley, Reading, MA, 3rd edition, 1995.

[11] Robert K. Heffley and Wayne F. Jewell. Aircraft handling qualities data. Contractor's Report CR-2144, NASA, Systems Technology, Inc. Hawthorne, CA 90250, December 1972.

[12] Robert K. Heffley and Wayne F. Jewell. Aircraft handling qualities data. Contractor's Report CR-2144, NASA, Systems Technology, Inc. Hawthorne, CA 90250, December 1972. Available at ntrs.nasa.gov.

[13] Euclid. C. Holleman. Summary of high-altitude and entry flight control experience with the X-15 airplane. Technical Note D-3386, NASA, Flight Research Center, Edwards, California, April 1966.

[14] Petros A. Ioannou and Petar V. Kokotovic. Instability analysis and the improvement of robustness of adaptive control. *Automatica*, 20(5):583–594, 1984.

[15] Petros A. Ioannou and Jing Sun. *Robust Adaptive Control.* Prentice-Hall, Upper Saddle River, NJ, 1995.

[16] Alberto Isidori. *Nonlinear Control Systems.* Springer, London, UK, 3rd edition, 1995.

[17] Eric N. Johnson and Anthony J. Calise. Neural network adaptive control of systems with input saturation. In *Proceedings of the American Control Conference*, volume 5, pages 3527 – 3532, Arlington, VA, 2001.

[18] Isaac Kaminer, Antonio M. Pascoal, Pramod P. Khargonekar, and Edward E. Coleman. A velocity algorithm for the implementation of gain-scheduled controllers. *Automatica*, 31(8):1185–1191, 1995.

[19] Steingrimur P. Karason and Anuradha M. Annaswamy. Adaptive control in the presence of input constraints. *IEEE Transactions on Automatic Control*, 39(11):2325–30, 1994.

[20] Hassan K. Khalil. *Nonlinear Systems.* Prentice-Hall, Upper Saddle River, NJ, 3rd edition, 2002.

[21] Gerhard Kreisselmeier and Kumpati S. Narendra. Stable model reference adaptive control in the presence of bounded disturbances. *IEEE Transactions on Automatic Control*, 27(6):1169–1175, 1982.

[22] Miroslav Krstić, Ioannis Kanellakopoulos, and Petar V. Kokotovic. *Nonlinear and Adaptive Control Design.* John Wiley & Sons, New York, NY, 1995.

[23] Ioan D. Landau. *Adaptive Control: The Model Reference Approach.* Marcel Dekker, New York, NY, 1979.

[24] Eugene Lavretsky and Naira Hovakimyan. Stable adaptation in the presence of actuator constraints with flight control applications. *Journal of Guidance, Control, and Dynamics*, 30(2):337 – 345, 2007.

[25] Douglas J. Leith and William E. Leithead. Appropriate realisation of gain-scheduled controllers with application to wind turbine regulation. *International Journal of Control*, 65(2):223–248, 1996.

[26] Douglas J. Leith and William E. Leithead. Survey of gain-scheduling analysis and design. *International Journal of Control*, 73(11):1001–1025, 2000.

[27] Kumpati S. Narendra. *Adaptive and Learning Systems.* Plenum Press, New York, NY, 1986.

[28] Kumpati S. Narendra and Anuradha M. Annaswamy. *Stable Adaptive Systems.* Prentice-Hall, Englewood Cliffs, NJ, 1989.

[29] Robert A. Nichols, Robert T. Reichert, and Wilson J. Rugh. Gain scheduling for h_∞ controllers: a flight control example. *IEEE Transactions on Control System Technology*, 1(2):69–78, 1993.

[30] S. Joe Qin and Guy Borders. Multi-region fuzzy logic control system with auxiliary variables. *IEEE Transactions on Fuzzy Systems*, 2(1):74–89, 1994.

[31] Willson J. Rugh. Analytical framework for gain-scheduling. *IEEE Control Systems Magazine*, 11(1):79–84, 1995.

[32] Wilson J. Rugh and Jeff S. Shamma. Research on gain scheduling. *Automatica*, 36(10):1401–1425, 2000.

[33] Shankar Sastry and Marc Bodson. *Adaptive Control: Stability, Convergence, and Robustness.* Prentice-Hall, Englewood Cliffs, NJ, 1989.

[34] Mac Schwager and Anuradha M. Annaswamy. Direct adaptive control of multi-input plants with magnitude saturation constraints. In *Proceedings of the 44th IEEE Conference on Decision and Control, and the European Control Conference, CDC-ECC '05*, Seville, Spain, 2005.

[35] Jeff S. Shamma and Michael Athens. Analysis of nonlinear gain scheduled control systems. *IEEE Transactions on Automatic Control*, 35(8):898–907, 1990.

[36] Jean-Jacques E. Slotine and Weiping Li. *Applied Nonlinear Control.* Prentice-Hall, Eagle Wood Cliffs, NJ, 1991.

[37] Brian L. Stevens and Frank L. Lewis. *Aircraft Control and Simulation.* John Willey & Sons, Hoboken, NJ, 2nd edition, 2003.

[38] Dionisio A. Suarez-Cerda and Rogelio Lozano. *Adaptive Control of Nonsmooth Dynamic Systems*, Chapter 14. Adaptive Control of Linear Systems with Poles in the Closed LHP with Constrained Inputs, pages 349–359. edited by Gang Tao and Frank L. Lewis. Springer, London, 2001.

[39] Konstantinos S. Tsakalis and Petros A. Ioannou. *Linear Time-Varying Systems: Control and Adaptation.* Prentice-Hall, Englewood Cliffs, NJ, 1992.

[40] Harold J. Walker and Chester H. Wolowicz. Theoretical stability derivatives for the X-15 research airplane at supersonic and hypersonic speeds including a comparison with wind tunnel results. Technical Memorandum X-287, NASA, Flight Research Center, Edwards, California, August 1960.

[41] Kevin A. Wise, Joseph S. Brinker, Anthony J. Calise, Dale F. Enns, Michael R. Elgersma, and Petros Voulgaris. Direct adaptive reconfigurable flight control for a tailless advanced fighter aircraft. *International Journal of Robust and Nonlinear Control*, (14):999–1012, 1999.

[42] Roxanah B. Yancey. Flight measurements of stability and control derivatives of the X-15 research airplane to a mach number of 6.02 and an angle of attack of 25°. Technical Note D-2532, NASA, Flight Research Center, Edwards, California, January 1964.

[43] Roxanah B. Yancey, Herman A. Rediess, and Glenn H. Robinson. Aerodynamic derivative characteristics of the X-15 research airplane as determined from flight tests for mach numbers from 0.6 to 3.4. Technical Note D-1060, NASA, Flight Research Center, Edwards, California, January 1962.